Aus dem Institut für Medizinische Genetik und Humangenetik
der Medizinischen Fakultät Charité – Universitätsmedizin Berlin

DISSERTATION

# Genetic Factors Regulating Bone Mass

zur Erlangung des akademischen Grades
Doctor medicinae (Dr. med.)

vorgelegt der Medizinischen Fakultät
Charité – Universitätsmedizin Berlin

von

Antonia Elsa Elisabeth Howaldt

aus Frankfurt am Main

Datum der Promotion: 17.09.2021

für meine Eltern

# Inhaltsverzeichnis

# 1 Table of Abbreviations

| | |
|---|---|
| AD | Autosomal dominant |
| ADO | Autosomal Dominant Osteopetrosis |
| ALP | Alkaline phosphatase activity |
| ALX1 | ALX Homeobox 1 |
| AR | Autosomal recessive |
| ARO | Autosomal Recessive Osteopetrosis |
| BLAST | Basic Local Alignment Search Tool |
| BLAT | BLAST-Like Alignment Tool |
| BM | Bone marrow |
| BMD | Bone mineral density |
| BMI | Body mass index |
| BMP | Bone Morphogenetic Protein |
| BMU | Bone multicellular unit |
| BWA | Burrows-Wheeler Aligner |
| CAII | Carbonic anhydrase II |
| cDNA | Complementary DNA |
| CFNS | Craniofrontonasal Syndrome |
| CLCN7 | Chloride Voltage-Gated Channel 7 |
| CNCC | Cranial neural crest cell |
| CTSK | Cathepsin K |
| DNA | Deoxyribonucleic acid |
| DOS | Dysosteosclerosis |
| EFNB1 | Ephrin-B1 |
| FGF | Fibroblast growth factor |
| HSCT | Hematopoietic stem cell transplantation |
| IKBKG | Inhibitor of kappa light polypeptide gene enhancer in B cells, kinase gamma |
| IL-1 | Interleukin-1 |
| IL-6 | Interleukin-6 |
| LPIN2 | Lipin 2 |
| LRP5 | Lipoprotein receptor-related protein 5 |
| LRRK1 | Leucine-Rich Repeat Kinase 1 |
| M-CSF | Macrophage colony-stimulating factor |

| | |
|---|---|
| MRONJ | Medication-related necrosis of the jaw |
| MSC | Mesenchymal stem cell |
| NCC | Neural crest cell |
| NEMO | NF-kappa B Essential Modulator |
| NGS | Next-generation sequencing |
| OB | Osteoblast |
| OC | Osteoclast |
| OL-EDA-ID | Lymphedema-anhidrotic ectodermal dysplasia with immunodeficiency |
| OMIM | Online Mendelian Inheritance in Man, online compendium of genes and genetic disorders |
| ONJ | Osteonecrosis of the jaws |
| OPG | Osteoprotegerin |
| OPPG | Osteoporosis pseudoglioma syndrome |
| ORN | Osteoradionecrosis |
| OSMD | Osteometaphyseal Dysplasia |
| OSMT1 | Osteopetrosis-associated transmembrane protein 1 |
| PAX3 | Paired box 3 protein |
| PBMC | Peripheral blood mononucleated cell |
| PBS | Phosphate-buffered saline |
| PLEKHM1 | Pleckstrin homology domain-containing family M member 1 |
| PTH | Parathyroid hormone |
| RANK | Receptor activator of nuclear factor kappa-B |
| RANKL | Receptor activator of nuclear factor kappa-B ligand |
| RIPA | Radioimmunoprecipitation assay |
| RNA | Ribonucleic acid |
| RT-PCR | Reverse transcription-polymerase chain reaction |
| RTA | Renal tubular acidosis |
| SD | Standard deviation |
| SHH | Sonic Hedgehog |
| SLC29A3 | Solute Carrier Family 29 Member 3 |
| SNX10 | Sorting-nexin 10 |
| SOST | Sclerostin |
| TCIRG1 | T-Cell Immune Regulator 1 |

| | |
|---|---|
| TGFβ | Transforming growth factor beta |
| TNF | Tumor necrosis factor |
| TNFRSF11A | Tumor necrosis factor Receptor Superfamily Member 11a |
| TNFSF11 | Tumor necrosis factor ligand superfamily member 11 |
| TRAP | Tartrate-resistant acid phosphatase |
| vcf | Variant call format |
| WES | Whole exome sequencing |
| WGS | Whole-genome sequencing |
| WT | wild-type |
| XL | X-linked |

# 2 List of Tables

# 3 Abstract [English]

**Objective:** To evaluate factors regulating craniofacial morphologies and bone mass by investigating high bone mass disorders (eg. autosomal recessive osteopetrosis, dysosteosclerosis, craniofrontonasal syndrome, and osteosclerotic metaphyseal dysplasia) and their genetic defects on a molecular level.

**Methods:** Next Generation Sequencing was performed on patient DNA, bioinformatic filtering was used to decipher new disease-causing mutations in a group of patients. Sanger sequencing was used to confirm the variants. Patient cells – osteoclasts, mesenchymal stem cells, and osteoblasts – were grown in cell culture. Protein and RNA were extracted with Radioimmunoprecipitation assay (RIPA) buffer and Trizol lysis respectively. Immunoblot assays, cDNA sequencing, and reverse transcription-polymerase chain reaction (RT-PCR) were performed to analyze the effect of the mutation on protein- and RNA levels. Osteoclasts were grown, stained for Tartrate-resistant acid phosphatase (TRAP), and visualized by fluorescence microscopy. A resorption assay was performed to illustrate the resorption behavior of mutated osteoclasts.

**Results:** Two novel mutations in the Solute Carrier Family 29 Member 3 *(SLC29A3)* gene and one new splice-site mutation in the T-Cell Immune Regulator 1 *(TCIRG1)* gene were found in patients with moderate autosomal-recessive osteopetrosis. Four new mutations in the Ephrin-B1 *(EFNB1)* gene were depicted in an Indian cohort of non-consanguineous individuals with craniofrontonasal syndrome. In a patient suffering from osteopetrosis and severe osteonecrosis of the jaws, we described the fourth mutation in the Leucine-Rich Repeat Kinase 1 *(LRRK1)* gene known to date. LRRK1-mutated osteoclasts showed shallow resorption pits and ineffective bone resorption.

**Conclusion:** We could broaden the spectrum of high bone mass disorders as well as of the disease entity of craniofrontonasal syndrome by the detection of new disease-causing mutations and the description of the resulting molecular effects. In the future, this can facilitate diagnosis and reveal new potential molecular targets for the therapy of osteoporosis.

# 4 Abstract [German]

**Fragestellung:** Analyse von genetischen Einflüssen auf Skelettentwicklung und -homöostase durch Untersuchung der seltenen genetischen Erkrankungen kraniofrontonasale Dysplasie, autosomal-rezessive Osteopetrose, Dysosteosklerose und osteosklerotische metaphysäre Dysplasie. Darstellung der Auswirkungen der gefundenen genetischen Veränderungen auf zellulärer und molekularer Ebene.

**Methoden:** Patienten-DNA wurde mittels Next Generation Sequencing dechiffriert und bioinformatische Filtermethoden wurden verwendet, um neue krankheitsbedingende Mutationen bei Patienten mit den verschiedenen Erkrankungen mit erhöhter Knochendichte zu detektieren. Mittels Sanger Sequenzierung wurden die Varianten bestätigt. Patientenzellen – Osteoklasten, mesenchymale Stammzellen, und Osteoblasten – wurden in der Zellkultur gezüchtet. Protein- und RNA-Extraktionen wurden mit RIPA-Puffer bzw. Trizol durchgeführt. Durch funktionelle Analysen mit Western Blots, cDNA-Sequenzierungen und RT-PCR wurden die Effekte der Mutationen auf Protein-, cDNA- und RNA-Ebene analysiert. Osteoklasten wurden aus perpipheren mononukleären Zellen differenziert, mittels tartartresistenter saurer Phosphatase (TRAP)-Aktivität angefärbt und durch Fluoreszenzmikroskopie visualisiert. Ein Resorptionsassay wurde durchgeführt, um das Resorptionsverhalten von Osteoklasten darzustellen.

**Ergebnisse:** Zwei neue Mutationen in dem für den Nukleosidtransporter 3 kodierenden Solute Carrier Family 29 Member 3 *(SLC29A3)* Gen und eine neue splice-site Mutation in dem T-Zell-Immunregulator 1 Gen *(TCIRG1)* wurden bei Patient*innen mit moderater autosomal-rezessiver Osteopetrose gefunden. Bei vier nicht-konsanguinen indischen Patientinnen mit kraniofrontonasaler Dysplasie konnten vier neue Mutationen Ephrin B1 Gen *(EFNB1)* bestätigt werden. In einem unter Osteopetrose und schweren rezidivierenden Kiefernekrosen leidenden Patienten haben wir die vierte weltweit beschriebene Mutation in dem Leucin-rich repeat kinase 1 *(LRRK1)* Gen nachgewiesen. *LRRK1*-mutierte Osteoklasten zeigten abgeschwächtes Resorptionsverhalten, flachere Resorptionspits und eine ineffektive Knochenresorption.

**Schlussfolgerung:** Im Rahmen des Spektrums von Erkrankungen mit erhöhter Knochenmasse und des Krankheitsbildes der kraniofrontonasalen Dysplasie konnten wir neue krankheitsbedingende Mutationen finden und die Effekte auf molekularer Ebene darstellen. Zukünftig kann dies die Diagnostik von seltenen Erkrankungen mit erhöhter Knochendichte erleichtern und langfristig neue molekulare Ansatzpunkte für die Osteoporosetherapie aufzeigen.

# 5 Introduction

Bone is metabolically active tissue and a central part of the human body serving as protection for vital organs, a site for hematopoiesis, and as a reservoir for minerals. It shapes the human body and facial appearance, serves as a muscle insertion point for muscles, and thus enables locomotion [1]. Its microarchitecture is subject to lifelong remodeling [2]. Bone cells – namely osteoclasts, osteoblasts, and osteocytes – shape the plastic tissue of bone and orchestrate an equilibrium between bone formation and bone resorption.

The skeleton originates from different cell lineages and can be categorized into three different types – the craniofacial, axial, and appendicular skeleton [3].

The craniofacial skeleton can be regarded as the most sophisticated part of the skeleton in terms of the differentiation process and postnatal modification. When traced back in history, the craniofacial skeleton seems to have evolved before the axial and appendicular skeleton. The skull consists of 22 different bones and 20 deciduous teeth, later replaced by 32 permanent teeth. It can be subdivided into the neurocranium and the viscerocranium [4]. The bones of the neurocranium – the frontal, parietal, temporal, sphenoid, occipital, and ethmoid bones – encompass and protect the brain. The viscerocranium consists of bones (maxilla, mandible; nasal, lacrimal, palatine, zygomatic, and auditory bones) that shape the appearance of the face. During neurulation and the formation of a neural tube, the neural crest forms as a transient structure. From the dorsal edges of the neural tube, neural crest cells (NCCs) arise and migrate extensively and differentiate into a variety of different cell types (i.e. neurons, glia, skin, smooth muscle, glands) [5]. Cranial neural crest cells (CNCCs) are located at the cranial part of the neural tube and contribute to a large extent to the formation of the craniofacial skeleton. They migrate to the pharyngeal arches and differentiate into bone, cartilage, connective tissue, and neuroglia located at the anterior part of the skull [4]. The migration is organized by modification of Hox-gene expression [6]. Not only NCCs but also mesodermal cells contribute to the formation of the craniofacial skeleton. Bone and cartilage of the posterior part of the skull are formed by prechordal mesodermal cells [7]. Signaling pathways crucial for cranial neural crest and cranial development include the Bone Morphogenetic Protein (BMP), fibroblast growth factor (FGF) receptor gene family, Wnt/β-Catenin, and Sonic Hedgehog (SHH) pathways [8-10]. When disturbed, various craniofacial syndromes result, e.g. cleft lip and palate, craniosynostosis, and holoprosencephaly.

Craniofrontonasal Syndrome (CFNS) is a disorder of skeletal patterning with X-linked transmission caused by mutations in the Ephrin-B1 *(EFNB1)* gene [11]. The Ephrin-B1 protein is necessary for neural crest cell migration, patterning of somites and rhombencephalon, growth as well as the development of the nervous system and blood vessels. The involvement of the axial skeleton has also been described, e.g. the pairing of ribs in ephrinB1 deficient mutatant mice [12-14].

The axial skeleton derives from the somites, the paraxial mesoderm located at the sides of the neural tube, that forms the vertebrae and the dorsal part of the ribs. Crucial signaling pathways include the SHH and the BMP inhibitor Noggin [3]. The appendicular skeleton derives from the lateral plate mesodermal cells and forms the limbs by FGF-, SHH-, and WNT-signaling amongst others [7]. Altered or disturbed Hedgehog signaling for instance can result in polydactyly [3].

Bone is a plastic and dynamic tissue capable of adapting its structure in response to mechanical loading or diverse remodeling stimuli. It is mainly composed of hydroxyapatite, collagen I, osteonectin, fibronectin, and osteopontin [15]. Bone resorption and bone formation are regulated by osteoblasts, osteoclasts, and osteocytes.

Osteoclasts are multinucleated cells of hematopoietic origin that resorb bone by the secretion of proteases and collagenases. Osteoblasts are cells of mesenchymal origin capable of secreting an unmineralized bone matrix that eventually makes bone (intramembranous bone formation). Mesenchymal cells can also differentiate into chondrocytes to form cartilage which can then be transformed into bone (enchondral bone formation). Osteocytes, osteoblast-derived cells entrapped in the bone matrix, sense mechanical strain and adapt bone formation accordingly, eg. by secreting growth factors [16]. Osteoclasts differentiate when the receptor activator of nuclear factor kappa-B ligand (RANKL) and the macrophage colony-stimulating factor (M-CSF) are released by osteoblasts or osteocytes. RANKL interacts with the receptor activator of nuclear factor kappa-B (RANK) which results in the downstream activation of signaling molecules [17]. Osteoprotegerin (OPG) released by osteoblast cells can bind to RANKL and inhibit further osteoclast differentiation [18]. The process of bone remodeling is located in the bone multicellular units (BMUs) [19]. Osteoblasts and osteoclasts are known to communicate by cell-cell contact, diffusible paracrine factors as well as cell-bone matrix interactions to ensure the physiologic bone homeostasis, eg. RANKL, RANK, M-CSF (level is increased by the secretion of Interleukin-1 (IL-1) and Tumor necrosis factor (TNF), antagonized by estrogen), OPG, Calcitonin, Parathyroid hormone (PTH), 1,25-Dihydroxyvitamin D3, and Transforming growth factor beta (TGFβ) [3, 20].

When the equilibrium of bone homeostasis is distorted, there can either be a surplus or shortage of bone mass, both of which cause bone to break more easily and bring about more adverse effects.

Table 1 Classification of clinical pictures described in this thesis and comparative presentation of related clinical pictures modified from a publication by *Stark et al.* [21]

| **Classification & Type of Malformation** | **Disease entity** | | **Trans-mission** | **Gene** | **Onset** | **Severity** |
|---|---|---|---|---|---|---|
| **Disorder of Homeostasis - Malformation of the axial skeleton** | **Autosomal Recessive Osteopetrosis (ARO)** | Classic | AR | *TCIRG1* | perinatal | severe |
| | | Neurono-pathic | AR | *CLCN7, OSTM1* | perinatal | severe |
| | | ARO with RTA | AR | *CAII* | infancy | moderate |
| | **X-linked Osteopetrosis** | | XL | *IKBKG (NEMO)* | infancy | severe |
| | **Intermediate Osteopetrosis** | | AR | *CLCN7, PLEKHM1, TCIRG1* | childhood | mild to moderate |
| | **Autosomal Dominant Osteopetrosis (ADO)** | | AD | *CLCN7* | adulthood | mild to moderate, rarely severe |
| | **Hyperostosis** | | AD | *LRP5* | adulthood | mild |
| | **Osteometaphyseal Dysplasia (OSMD)** | | AR | *LRRK1* | adulthood | moderate |
| **Disorder of Skeletal Patterning - Malformation of the craniofa-cial skeleton** | **Craniofrontonasal Syndrome (CFNS)** | | XL | *EFNB1* | perinatal | moderate, rarely severe |

The rare genetic setting of a surplus in bone referred to as osteopetrosis is caused by changes in osteoclast or osteoblast function. Deficient osteoclast differentiation or defective pathways which – in a physiologic state – orchestrate bone formation can lead to deficient bone resorption. It can

clinically be distinguished between mild, moderate, and severe osteopetrosis and also be classified by the manner of genetic inheritance, namely recessive, dominant, or X-linked transmission [22]. Genetic skeletal dysplasias are summarized in the *"Nosology and classification of genetic skeletal disorders: 2019 revision"* [23]. Table 1, modified from a publication by *Stark et al.* [21], provides an overview of the different disease entities discussed in the publications summarized in this thesis. Table 2 provides a summary of the clinical and radiographic findings in the conditions discussed in this work.

Autosomal recessive osteopetrosis (ARO) is a rare disease entity that can be divided into different sub-forms.

A) In the osteoclast-rich forms of ARO, osteoclasts are present in an abundant manner but exhibit reduced function and diminished bone resorption capacity due to an altered sealing zone [22].
   I. Classic ARO
   II. Neuronopathic ARO
   III. ARO with renal tubular acidosis (RTA)
   IV. Intermediate ARO

B) The osteoclast-poor forms are suggested to contribute to less than 10% of ARO cases. Mutations in *TNFSF11* encoding for RANKL and *TNFRSF11A* encoding for RANK lead to ineffective differentiation of osteoclasts from hematopoietic stem cells [24, 25].

Infantile malignant autosomal recessive osteopetrosis Type 1 (ARO, Online Mendelian Inheritance in Man database (OMIM) #259700) caused by mutations in the T-cell immune regulator 1 *(TCIRG1)* gene is a severe disorder which often has an infantile malignant course leading to death within the first decade of life [22]. Thickened bone can obliterate the bone marrow cavity, causing pancytopenia, detrimental infections, and extramedullary hematopoiesis with splenomegaly and hepatomegaly. Also, cranial nerve compression can result from an enhanced bone density and reduced diameter of the osseous foramina. To date, allogeneic hematopoietic stem cell transplantation (HSCT) is the only curative treatment method that comes with known risk factors such as graft rejection, graft failure, or infections amongst others [26]. Mutations in the Chloride Voltage-Gated Channel 7 gene *(CLCN7)* with a loss-of-function effect result in ARO Type 4 (OMIM #611490) but mutations in *CLCN7* can also lead to autosomal dominant or intermediate autosomal recessive forms of osteopetrosis [27, 28].

Neuronopathic ARO caused by mutations in the osteopetrosis-associated transmembrane protein 1 *(OSMT1)* gene, also referred to as ARO Type 5 (OMIM #607649), is the most severe type of ARO leading to a severely reduced life expectancy in affected individuals. Apart from an increased bone mass, it involves neurologic manifestations such as cerebral atrophy, reduced myelinization, hydrocephaly, microcephaly, seizures, blindness, and deafness [29].

ARO with renal tubular acidosis (OMIM #259730) is caused by homozygous or compound heterozygous mutations in the carbonic anhydrase II *(CAII)* gene. It is a less severe form and involves intracranial calcifications, fractures, short stature, cranial nerve compression, and developmental delay [30, 31]. Intermediate ARO (OMIM # 259710) has been described in patients carrying homozygous or compound heterozygous mutations in *CLCN7* [32], in the Pleckstrin homology domain-containing family M member 1 gene *(PLEKHM1)* [33], and the Sorting-nexin 10 gene *(SNX10)* [34, 35]. Recently, an intronic *TCIGR1* mutation has been identified in a case of intermediate ARO [36].

Autosomal dominant osteopetrosis (ADO, OMIM #607634) is more common with a prevalence of 1:20,000 births and has a milder course than ARO, though the clinical course is very variable [37, 38]. It can be divided into two subtypes.

Autosomal dominant osteopetrosis Type II (ADO II), first described by Albers Schönberg in 1904 and also known as Albers-Schönberg disease, typically involves sclerosis of the spine, pelvis, and skull base, as well as an increased fracture rate [39]. It is caused by mutations in the *CLCN7* [28]. Physiologically, this chloride channel contributes to the acidification of resorption lacunae at the ruffled border membrane of osteoclasts [40]. *CLCN7* mutations with a loss-of-function effect result in a defective bone resorption and an increased bone mineral density. Extra-skeletal manifestations involve visual impairment, osteomyelitis, bone marrow failure, and hepatosplenomegaly [37]. Through a *CLCN7* mouse model investigating the mutation *CLCN7* p.G213R, it has recently been suggested that extra-skeletal manifestations also involve perivascular fibrosis with an increased macrophage count and lymphoid infiltrates. Lung, kidney, brain, and muscle tissue also revealed alterations [41].

Lipoprotein receptor-related protein 5 gene (*LRP5)*-induced hyperostosis, in literature sometimes referred to as Autosomal dominant osteopetrosis Type I (ADO I), typically involves generalized

Table 2 Overview of disease entities and their corresponding clinical characteristics.

| Disease entity | Skeletal characteristics | Clinical Characteristics<br>Special Radiographic findings |
|---|---|---|
| **Classic ARO** | elevated bone density,<br>osteosclerosis,<br>pathologic fractures,<br>modeling defects (predominantly of the metaphyses),<br>osteomyelitis,<br>dental abnormalities | death within the first decade of life, pancytopenia,<br>infections, extramedullary hematopoiesis, hepatosplenomegaly, cranial nerve compression, hydrocephalus, hypocalcemia;<br>*radiographic findings:* the obliteration of the bone marrow cavity and cranial foramina |
| **Neuronopathic ARO** | | in addition to classic ARO: neurodegenerative, eg. retinal atrophy, blindness, hearing loss;<br>*radiographic findings:* microcephaly, cerebral atrophy, craniosynostosis, Type I Chiari malformation |
| **ARO with RTA** | | mental retardation, renal tubular acidosis, developmental delay, cranial nerve compression, rarely bone marrow impairment;<br>*radiographic findings*: cerebral calcification |
| **X-linked Osteopetrosis** | | severe immunodeficiency<br>ectodermal dysplasia like features |
| **Intermediate Osteopetrosis** | | anemia, extramedullary hematopoiesis<br>occasional optic nerve compression |
| **Autosomal Dominant Osteopetrosis (ADO)** | | moderate hematological failure, cranial nerve compression;<br>*radiographic findings:* sandwich vertebrae |
| **Osteometaphyseal Dysplasia (OSMD)** | | osteonecrosis of the jaws as a new rare trait [42] |
| **Hyperostosis** | increased bone mass, predominantly of the skull | enlarged mandible |
| **Craniofrontonasal Syndrome (CFNS)** | hypertelorism, depressed nasal bridge coronal synostosis, cleft lip, and palate | diaphragmatic hernias,<br>*radiographic findings:* corpus callosum agenesis or dysgenesis |

increased thickness of cortical bone, predominantly at the skull vault. It is the only form of increased bone mass with high mechanical stability. The condition is not associated with an increased fracture risk [3]. *LRP5* usually regulates osteoblast differentiation and mutations with a gain-of-function effect in *LRP5* induce an increase in bone mineral density. Patients are often asymptomatic or have minor symptoms such as back pain. Also, an association with osteoarthritis has been described [43, 44]. Loss of function of *LRP5* has been shown to cause a diminished bone mass and was linked to the autosomal recessive osteoporosis pseudoglioma syndrome (OPPG, OMIM #259770) [45]. Although sometimes referred to as "benign osteopetrosis", more than 50% of ADO patients exhibit clinical symptoms.

X-linked recessive osteopetrosis and lymphedema-anhidrotic ectodermal dysplasia with immunodeficiency (OL-EDA-ID) caused by mutations in the Inhibitor of kappa light polypeptide gene enhancer in B cells kinase gamma *(IKBKG)* gene involve osteopetrosis, lymphedema, and a predisposition for severe, life-threatening infections due to suppression of NF-κB activation [46, 47]. Dysosteosclerosis (DOS) is another sclerosing bone dysplasia with autosomal recessive inheritance characterized by osteosclerosis and platyspondyly, caused by mutations in *SLC29A3, TCIRG1,* and *TNFRSF11A*. There is a great spectrum of disease severity and in some cases, a reduced life expectancy has been observed [48]. Pycnodysostosis is a disease with an autosomal recessive mode of inheritance due to homozygous or compound heterozygous *CTSK* mutations. Cathepsin K is an acidic protease secreted by osteoclasts which cleave and hence degrade bone matrix, predominantly composed of collagen type I. In the setting of a *CTSK* mutation, osteoclasts only insufficiently cleave collagen. This culminates in the phenotype of short stature, fragile bones, skull deformity, and clavicle hypoplasia [49, 50].

Osteoporosis is defined as a condition of low bone mineral density (BMD), defined as a T-score less than or equal to -2,5 standard deviation (SD), and disrupted bone microarchitecture leading to mechanical instability and an increased fracture rate. It significantly increases mortality and morbidity and represents a major healthcare problem and economic burden in today's world. In the EU, 22 million women and 5,5 million men suffer from osteoporosis [51]. With the demographic change and the increase in longevity, the number of affected individuals is expected to increase even more in the next years. According to *Hernlund et al.*, the prevalence of osteoporosis is expected to rise from 28 million in 2010 to 34 million in 2025 [51]. The prevalence of osteoporotic vertebral fractures worldwide ranges between 9 – 26%. In Europe, it is highest in Scandinavia (24%) and lowest in Eastern Europe (16%), whereas in the female North American population >50

years, a prevalence of 24% is noted with the white complexion being 1.6 times more affected than the black complexion. In Latin America, a lower prevalence of 11-19% is noted [52].

There are various causes of osteoporosis. General risk factors for osteoporosis include female sex, advanced age, estrogen deficiency, pre-existing illness, and genetic defects amongst others. In females, the disease entity can be subdivided into pre- and postmenopausal osteoporosis. Postmenopausal osteoporosis is majorly caused by estrogen deficiency. Premenopausal osteoporosis can be caused by hypo- and hypergonadotropic hypogonadism, gastrointestinal malabsorption, renal disease, and other causes of calcium loss, eg. hypercalciuria, liver disease, hematologic disorders, hyperthyroidism, hyperparathyroidism, Cushing's syndrome, history of glucocorticoid treatment or other drugs, e.g. immunosuppressants, anticonvulsive medications, and proton-pump inhibitors, Vitamin D and calcium deficiency, alcohol abuse, and anorexia nervosa [53-56]. In men, hypogonadism, gastrointestinal disease, and steroid treatment are the most common causes of osteoporosis [57, 58]. Other lifestyle factors accounting for an increased risk for osteoporosis are similar to those observed in women, e.g. Vitamin D deficiency, smoking, alcohol abuse, and low Body mass index (BMI) amongst others. Men tend to be underscreened [59]. Drugs for the treatment of osteoporosis either inhibit osteoclast activity or fuel osteoblast activity. Bisphosphonates have evolved to the standard treatment option tackling osteoporosis. Side effects include medication-related necrosis of the jaw (MRONJ) occurring in 0,1 % of cases in otherwise healthy individuals and approximately 2,09% - 5,16% of cases in patients with different types of underlying malignant diseases [60]. Existing treatment options for osteoporosis are unsatisfying and can be further improved.

The final aim of this project is to acquire a more profound understanding of the molecular background of different types of osteopetrosis. This can potentially open new perspectives for the development of osteoanabolic drugs to treat and prevent osteoporosis.

# 6 Material and Methods

The here cited experiments have been conducted at the Institute of Human Genetics, Charité University Medicine Berlin, in the research group of Prof. Dr. rer. nat. Uwe Kornak. Most of the materials and methods have already been described in the three papers summarized below [36, 61, 62].

## 6.1 Next-Generation Sequencing (NGS) – Gene Panel and Whole Exome Sequencing

Depending on the case, we decided on gene panel sequencing or whole-exome sequencing (WES). Alexej Knaus assisted in teaching the methods of NGS and bioinformatic evaluation. He was also involved in the evaluation of the NGS data set of the case later published in the Journal of Bone and Mineral Research (JBMR).

### *6.1.1 Gene Panel Sequencing*

Gene panels allow for the sequencing of a defined set of genes that are most commonly mutated in the setting of a particular disease entity. A customized bone mass panel containing 70 genes known or suggested to cause alterations in bone mineral density was run on DNA of patients discussed in the here cited publication "*Sclerosing bone dysplasias with hallmarks of dysosteosclerosis in four patients carrying mutations in SLC29A3 and TCIRG1*" [36]. The coding regions of the genes were enriched and then run on a high-throughput sequencer. To ensure a correct statistic representation of variants, the percentage of target regions covered by a minimum of 20 reads was noted. The patient NGS data were mapped to the reference genome (hg19) with Burrows-Wheeler Aligner (BWA) to enable a comparison of the sequencing data to healthy controls.

### *6.1.2 Whole Exome Sequencing (WES)*

In WES, the entirety of all exons, the exome, is sequenced. Compared to whole-genome sequencing (WGS), this is a more cost-efficient and timesaving way of sequencing DNA probes that can deliver the data covering the majority of disease-causing mutations. The SureSelect targeted Enrichment system is a method to enrich the genomic DNA of interest by hybridization that is then captured with magnetic beads and subsequently sequenced on an Illumina sequencer [63]. In a here delineated publication, WES was performed on the DNA of Patients 3 and 4 and then mapped to the reference genome (hg19) with BWA [36].

## 6.2 Bioinformatic Filtering of Variants and Evaluation of the pathogenic potential of Mutations

Bioinformatic filtering via the GeneTalk platform was used to break down the abundance of variants of an NGS data set to a manageable amount, which was then further evaluated by Sanger sequencing. A variant call format (vcf)-file was uploaded to the GeneTalk platform, filtered according to measures of function (effect on protein level), linkage, quality (quality and coverage of reads), and genotype frequency [64]. The pathogenic potential of individual candidate variants was evaluated by MutationTaster [65]. Literature was reviewed to check for genes and the corresponding protein function of feasible candidates.

## 6.3 Polymerase Chain Reaction

PCR primers were designed using Primer 3 Plus [66]. Primers were compared to a wild-type homo sapiens reference with the Ensembl BLAST/BLAT search to check for specificity. DNA concentration and purity were measured using the NanoDrop system (ThermoFisher Scientific). Approximately 10ng of DNA was loaded onto a single well and DNA amplification was achieved with 5x FIREPol Master Mix (Solis BioDyne).

## 6.4 Sanger-Sequencing

Before initiating NGS and as a method to validate mutations depicted by NGS, Sanger sequencing was performed. Respective exons and exon-intron boundaries of genes of interest were amplified using oligonucleotide primers and sequenced on an ABI3730xl DNA Analyzer (Applied Biosystems). Sequencing data were evaluated using the Geneious platform (https://www.geneious.com). In this way, the actual sequence of a certain gene was deciphered.

## 6.5 Cell culture

### *6.5.1 Mesenchymal Stem Cells*

The differentiation of patient-derived mesenchymal stem cells (MSCs) and osteoblasts was performed by the research group of Dr.-Ing. Sven Geissler at the Berlin Institute of Health (BIH) Center for regenerative medicine, Berlin. Patient bone marrow (BM) was harvested during a planned operation the patient underwent due to recurrent osteonecrosis of the jaws and served as a source for the isolation of MSCs [42]. Density centrifugation was used to isolate MSCs from the BM specimen. Cells were cultured in Dulbecco's modified Eagle's medium (DMEM Low Glucose; Gibco, Grand Island, NY, USA) with 10% fetal calf serum (Biochrom, Berlin, Germany), 5 mM

L-alanyl-l-glutamine (Gibco, Grand Island, NY, USA), 100 U/ml penicillin plus 100 µg/ml streptomycin (Biochrom, Berlin, Germany). Successful differentiation into MSCs was investigated by checking for cell phenotype and differentiation potential according to the protocol published by the International Society for Cellular Therapy [67].

#### *6.5.2 Osteoblasts*

To isolate osteoblasts, pieces of cancellous bone were washed with Phosphate-buffered saline (PBS) multiple times, manually dissected with a scalpel, and subsequently grown in a culture flask in the above-mentioned medium used to differentiate MSCs (Dulbecco's modified Eagle's medium (DMEM Low Glucose; Gibco, Grand Island, NY, USA) with 10% fetal calf serum (Biochrom, Berlin, Germany), 5 mM L-alanyl-l-glutamine (Gibco, Grand Island, NY, USA), 100 U/ml penicillin plus 100 µg/ml streptomycin (Biochrom, Berlin, Germany)). At an 80% confluency achieved after 3-4 weeks, Alizarin staining and alkaline phosphatase activity (ALP) were conducted to check for the osteogenic potential of the cells [68].

#### *6.5.3 Osteoclast differentiation*

The differentiation of patient-derived osteoclasts was performed under the supervision of Anna Floriane Hennig and Uta Rössler. Human osteoclasts were generated from peripheral blood mononucleated cells (PBMCs). Heparinized blood samples (30ml) were collected from the index patient and a healthy control. Density gradient centrifugation was performed to isolate PBMCs, with a bottom layer of Biocoll Separating Solution Ficoll (1,077g/ml; Biochrom) and a top layer of Buffy Coat solution (1:2 dilution with PBS (brand)). PBMCs were seeded out at a density of $3x10^5$ cells per 24-well and grown in medium composed of DEMEM + 10%FCS + 1% Ultraglutamine, 1% Pen/Streptomycin + 15ng/ml rhM-CSF (R&D Systems #216-MCC), which was changed every 2-3 days. On day 3, rhRANKL (PeproTech #310-01) was first added to the medium at a concentration of 50ng/ml. Differentiation success was tracked daily by light microscopic evaluation.

### 6.6 Osteoclast staining

*In-vitro* differentiated osteoclasts (OCs) were stained to confirm successful osteoclast differentiation by the analysis of their function and morphology. OCs were fixed with 4% paraformaldehyde (PFA) at day 14, permeabilized with 0,1% Saponin, and stained for 15min at room temperature for tartrate-resistant acid phosphatase (TRAP) activity. Overnight staining with fluorescent-labeled phalloidin was followed by staining with 4',6-diamidino-2-phenylindole (DAPI) to visualize

the nuclei. OCs were visualized using the Olympus BX60 fluorescence microscope (Olympus, Waltham, MA, USA).

### 6.7 Osteoclast resorption pit assay

*In-vitro* osteoclast-mediated bone resorption was quantified by measuring the resorption capacity of osteoclasts that had previously been seeded onto dentin chips or bone slices at a defined density. Resorption events were marked by a 0,25% Toluidine blue stain and visualized by a Laser Scanning Confocal Microscope LSM 700.

### 6.8 Immunoblot (Western Blot)

The published immunoblot is a work of lab member and co-author Nina Stelzer. Human osteoclasts (hOCs), human osteoblasts (hOBs), human MSCs (hMSCs) cultured to a confluent state were lysed using 100-200µl ice-cold RIPA buffer (150mM NaCl, 50mM Tris, 5mM EDTA, 1% Triton X-100, 0,25% Desoxycholate, 0,1% SDS). Protein concentration and quality were assessed using the Pierce BCA-assay Kit (Thermo Fisher Scientific). Protein lysates were primed for immunoblotting by loading with a dye and denatured by heating the probes on a heat block to up to 70°C.

### 6.9 RNA

Trizol-based (Life Technology) RNA isolation of different cell lines (hMSCs, hOBs, hOCs) was performed with the Direct-zol RNA kit (Zymo Research). RNA concentration and quality were measured by the NanoDrop system (Thermo Fisher Science).

### 6.10 cDNA Sequencing

Reverse transcription was performed with the RevertAid First Strand cDNA Synthesis Kit (Thermo Fisher Scientific) to transcribe RNA into cDNA. Oligonucleotide primers were designed with Primer 3 plus [66], the cDNA of interest was amplified using PCR, and the PCR product was then sequenced on an ABI3730xl DNA Analyzer (Applied Biosystems).

# 7 Results

In families and individuals with rare monogenic high bone mass disorders, hitherto undescribed mutations in different genes were detected by NGS and their molecular effects were described.

## 5.1 Novel mutations identified in four patients with craniofrontonasal syndrome (CFNS)

In four unrelated, female patients from four Indian families, the clinical diagnosis of Craniofrontonasal Syndrome (CFNS) was made. As the clinical picture was characteristic if not pathognomonic for CFNS caused by mutations in *EFNB1*, only specific testing by Sanger sequencing was performed. Through Sanger sequencing, four previously unknown *EFNB1* mutations were detected. The newly found mutations EFNB1 c.186_188delCAT (p.Ile63del), c.404_405insTACATTAC (p.Ser136Thrfs*26), c.196_197insC (p.Arg66Profs*9), and c.42_43delG (p.Ala15Argfs*31) accumulated in exons 1 and 2 [61]. All patients exhibited characteristic and mainly facial features of CFNS. Three out of four mutations were predicted to alter splicing.

## 5.2 Analysis of five patients with osteopetrosis of intermediate severity and unusual manifestations

In all osteopetrosis cases, the clinical picture prompted the testing strategy. Before genetic testing, the clinical picture was analyzed in detail including the assessment of the past medical history, X-ray images or CT scans, and laboratory results. First, mutations in *CLCN7* were excluded as the most likely candidate.

Four patients from three different families with osteosclerosis, platyspondyly, and long bone modeling defects suggesting the diagnosis of intermediate autosomal recessive osteopetrosis (ARO) or dysosteosclerosis (DOS) were found to carry mutations in *SLC29A3* and *TCIRG1*. The radiologic phenotype encompassed sandwich vertebrae and osteosclerosis of long tubular bones (femur, humerus, radius, and ulna), the phalanges, and ribs [36]. In two patients of Turkish descent, a high bone mass gene panel was run and two homozygous mutations in *SLC29A3* were found – c.302_303insCTACTTTGAGAGCTACCT (p.Asn101delinsAsnTyrPheGluSerTyrLeu) in Patient 1, both parents carrying the mutation in a heterozygous state, and c.1172C>A (p.Pro391His) in Patient 2. All mutations were confirmed by Sanger sequencing. WES was performed in two individuals from one Indian family. Two *TCIRG1* variants were detected, one frameshift variant, c.1732_1733delCT (p.Ala796fs*34), and one splice site variant c.117+4A>C. Sanger sequencing confirmed the compound heterozygous transmission of the two *TCIRG1* variants.

Osteosclerotic metaphyseal dysplasia (OSMD) to some extent resembles subtypes of ARO (dysosteosclerosis, intermediate ARO) [42]. In a 34-year-old male of Bulgarian origin who presented with sandwich vertebrae, platyspondyly, osteosclerosis of the tubular bones, pathologic fractures, and anemia, we have linked the homozygous splice-site mutation c.261G>A in *LRRK1* to the OSMD-phenotype and his severe form of osteonecrosis of the jaws. Trio-based exome sequencing, bioinformatic filtering, and Sanger sequencing detected the disease-causing mutation that is predicted to affect splicing. cDNA sequencing confirmed altered splicing as the entire exon 3 was skipped, leading to a frameshift and premature stop codon (p.Ala34Profs*33). Further investigations depicted the molecular effects of this osteoclast-rich type of osteopetrosis. The histologic analysis of an iliac crest biopsy revealed hypermineralized cartilage remnants, oversized multinucleated osteoclasts with abnormal morphology, and insufficient bone resorption. Osteoclasts isolated from whole peripheral blood via PBMCs and RANKL-induced differentiation grew at a faster pace and into larger osteoclasts compared to a wild-type (WT) control. A resorption pit assay showed an ineffective bone resorption behavior with more shallow resorption pits. An immunoblot on protein derived from patient osteoclasts, osteoblasts, and mesenchymal stem cells displayed a significantly reduced phosphorylation of L-Plastin at position Ser5, visualizing a loss of function of the altered LRRK1 kinase protein [42].

# 8 Discussion

## 8.1 Comparison of phenotypes characterized in this work

Craniofrontonasal Syndrome – a defect of skeletal patterning

Patients described in the publication "*Four novel mutations in EFNB1 in Indian patients with craniofrontonasal syndrome (CFNS)"* make up an individual cohort with pathognomonic facial features and alterations of the appendicular skeleton, eg. syndactyly and brachydactyly [61]. In comparison to the patients and disease entities discussed in the other here delineated papers, CFNS is a defect of skeletal patterning, not of bone homeostasis. Frontonasal dysplasia (FND, OMIM #136760) is an autosomal-recessive syndrome resembling CNFS. It is caused by mutations in the ALX Homeobox 1 *(ALX1)* gene and involves the clinical picture of hypertelorism, wide nasal bridge, microphthalmia, cleft palate, and low-set ears [69]. Also assigned to the group of skeletal patterning defects, it is a severe disease entity exhibiting similarities to the pathomechanism of CNFS. Recently, ALX1 was shown to regulate the Paired box 3 transcription factor (PAX3), which is a transcription factor that enables cranial neural crest development during craniofacial development [70].

Osteosclerotic metaphyseal dysplasia – a defect of bone homeostasis

Osteosclerotic metaphyseal dysplasia (OSMD) and severe osteonecrosis of the jaws (ONJ) are distinct features of the Bulgarian patient carrying an *LRRK1* splice-site mutation described in the publication *"Adult Osteosclerotic Metaphyseal Dysplasia with Progressive Osteonecrosis of the Jaws and Abnormal Bone Resorption Pattern Due to a LRRK1 Splice Site Mutation"* [42]. OSMD is a defect of bone homeostasis due to defective osteoclasts. Platyspondyly, sandwich vertebrae, diaphyseal thickening, and metaphyseal modeling defects occur as a result.

The patient discussed in the above-mentioned publication also suffered from recurrent ONJ and is the first patient reported to suffer from OSMD paired with severe, non medication-related ONJ. It has been observed that in the setting of osteonecrosis, there is decreased bone turnover due to inactivated osteoclasts. In medication-related necrosis of the jaw (MRONJ), giant multinucleated and inactive osteoclasts (reduced number of TRAP-positive OCs) were depicted [71]. When assessing a patient suffering from ONJ, the following differentials should be considered. MRONJ as the most prevalent cause is triggered by antiresorptive or antiangiogenic drugs such as bisphos-

phonates and RANKL-inhibitors which are often prescribed in oncologic patients with bone metastases or the setting of osteoporosis [72-74]. ONJ can also be triggered by intravenous drug abuse. Especially the intake of krokodil, a semi-synthetic type of heroin used as a cheap heroin substitute, has been reported to cause ONJ as an unwanted side effect [75]. Diffuse sclerosing osteomyelitis (DSO) is a rare disease of unknown etiology that can also cause an ONJ resembling phenotype [76]. Another differential is osteoradionecrosis (ORN) which is an unintended side effect of irradiation to the head and neck region used as a curative or adjuvant oncologic therapy for head and neck cancer [77]. Genetic causes of ONJ are less common and should be considered after excluding the above-mentioned risk factors for ONJ. Further evidence of a genetic cause can be found by taking a family history, evaluating x-ray images, and performing genetic testing. Chronic recurrent multifocal osteonecrosis (CRMO; OMIM #259680) is an autoinflammatory condition characterized by sterile bone inflammation which in the majority of cases occurs sporadically and often is recurrent [78]. There also is an autosomal recessive form known as Majeed syndrome, which has been linked to mutations in the Lipin 2 *(LPIN2)* gene [79].

Osteopetrosis cases

All patients delineated in this work have a monogenetic disease affecting bone. They share similar clinical features and show distinct findings.

Patients described in the publications "*Sclerosing bone dysplasias with hallmarks of dysosteosclerosis in four patients carrying mutations in SLC29A3 and TCIRG1*" and *"Adult osteosclerotic metaphyseal dysplasia with progressive osteonecrosis of the jaws and abnormal bone resorption pattern due to a LRRK1 splice-site mutation*" share the diagnosis of osteopetrosis with autosomal recessive inheritance [36, 42]. Each patient involved in the above-mentioned publications can be assigned to the osteopetrosis subtypes dysosteosclerosis, intermediated ARO, or OSMD. They exhibit similar features and have differences that make each subgroup and each patient distinct. Commonalities include a high bone mass detectable by X-ray images or CT scans. In comparison to a healthy individual, an elevated cortical bone density and altered bone shape (sandwich vertebrae, platyspondyly, slightly broadened femur, or severe Erlenmeyer flask deformity) were present. The altered bone architecture and poor quality in terms of stability resulted in fractures representing another key common trait.

Dysosteosclerois (DOS) and osteopetrosis can be challenging to discriminate and it is being discussed, whether listing the aforementioned disorders as distinct disease entities are reasonable due to their great commonalities. The patient with DOS described in the above-mentioned publication

carried a *SLC29A3* mutation. Clinical features that can facilitate the diagnosis of DOS were platyspondyly and a more pronounced tubular modeling defect.

Another commonality of the described genetic defects is the osteoclast function as all disease entities are osteoclast-rich with reduced osteoclast function. The described compound-heterozygous *TCIRG1* and homozygous *LRRK1* mutations are hypomorphic, exhibiting a reduced but not diminished gene function. Hence, not the picture of a complete loss of function effect is depicted here. Due to the mode of inheritance (recessive in our cohort) and the absence of RTA or severe neurologic manifestations, only differentials with autosomal recessive transmission were considered.

## 8.2 The road to the diagnosis

With a trained eye, fast visual diagnoses can be made in some genetic disease entities. CFNS for instance involves certain cranial stigmata that are pathognomonic for the disease. In this setting, targeted Sanger sequencing can be performed rather than more costly NGS. There are also cases in which a genetic cause of a disease is suspected but the road to the final genetic diagnosis can demand multiple efforts. The process until the disease-causing mutation in a patient or cohort is deciphered can then be challenging – as it has been the case of the patient suffering from *LRRK1*-induced OSMD [42]. This is due to genetic heterogeneity as different genetic defects can cause similar forms of osteoclast impairment.

## 8.3 Splicing in genetic diseases

Amongst genetic experts, it is widely known that splicing is a key genetic element that is vulnerable to impairment through mutations. The abundance of mutations affecting splicing and their effects are most likely underestimated. Alternative splicing is susceptible for and known to play an important role in the development of the human body and many disease entities, eg. in the development of the cerebral cortex and hence in brain malformations, prostate cancer, and cardiovascular disease amongst others [80-83]. *In-vitro* tools like the Human Splicing Finder describe the probability that a mutation has an effect on splicing [84]. The tool can make predictions on the severity of alternative splicing in certain cases, but only when a single request is inserted. So far, no tool allows for general screening for splicing events. Additionally, deep intronic or deep exonic variants and synonymous mutations that could affect splicing are not well annotated. Usually, more than one tool needs to be used to be able to comment on the most probable splicing effect. The lack of appropriate tools to reliably screen for implications on splicing can partially explain

why splicing is underrated in research thus far. This can serve as an incentive to work on the development of new *in-vitro* splicing tools that can predict the effects a mutation has on splicing. More extensive screening for splicing could benefit genetic research and contribute to a more profound understanding of the disease. New experiments could be conducted that deduce the putative effects certain mutations have on a donor or acceptor site from a vcf-file.

### 8.4 Impact on future research

Future therapies for the effective treatment of osteoporosis are continuously sought after. In the past 15-20 years, osteoporosis treatment has advanced significantly.

Containment of bone resorption on the one side was approached by bisphosphonates, estrogen, the selective estrogen receptor modulator Raloxifene, the humanized RANKL inhibitor Denosumab, and the selective Cathepsin K inhibitor Odanacatib [85, 86]. Osteoanabolic drugs on the contrary are human Parathyroid hormone (hPTH), and human PTH-related protein (hPTHrP) analogs [87]. A dual effect of increased bone formation and decreased bone resorption concurred in the monoclonal antibody against sclerostin Romosozumab [88].

A positive example of the successful invention and implementation of a drug can be illustrated by the sclerostin *(SOST)* gene, which was identified through investigating the very rare high bone mass disorders Van Buchem disease and sclerosteosis [89]. Sclerostin is a glycoprotein most commonly expressed by osteocytes. Excess sclerostin had been proven to cause diminished bone strength and bone degradation. Inactivation of sclerostin by mutations or anti-sclerostin antibodies leads to an increase in bone formation and was successfully used as an anabolic treatment for osteoporosis. Monoclonal antibodies to sclerostin were reported to prevent an increase in bone formation [90]. Low levels of extra-skeletal or other undesired effects were observed [91]. In a phase 3, multicenter, randomized, double-blind trial, the combination of Romosozumab treatment and subsequent treatment with the bisphosphonate alendronate was shown to reduce the fracture risk in postmenopausal osteoporosis compared to single treatment with alendronate [92].

The Cathepsin K inhibitor Odanacatib was long considered a promising candidate for an osteoclast-inhibiting therapy to tackle low BMD in osteoporosis. Cathepsin K is a cysteine protease highly expressed in osteoclasts [93]. Within OCs, it resides along the OC-bone resorptive area, in the endosomal/lysosomal system, and in cytoplasmic vesicles [94, 95]. Homozygous or compound

heterozygous mutations in the cathepsin K *(CTSK)* gene were found in patients with pycnodysostosis, which is a rare autosomal recessive lysosomal storage disorder (OMIM #265800) with elevated bone mass [96]. A lack of functional enzyme resulted in impaired bone/ collagen I resorption capacity and elevated BMD [97]. The Cathepsin K inhibitor Odanacatib disables matrix dissolution and decreases bone resorption. A multinational randomized, double-blind phase III study of Odanacatib was conducted in postmenopausal women. Clinical trials and further development of the drug were withdrawn due to an increased risk for cerebrovascular accidents in the verum group [85, 98].

LRRK1 has been discussed as a potential drug target for osteoanabolic treatment for osteoporosis. A small molecule inhibiting LRRK1 has been shown to effectively decrease osteoclast activity by blocking the LRRK1 kinase domain and preventing ATP binding without affecting osteoclast formation [99]. Although being a potential new drug target for osteoporosis, our study suggests that ONJ needs to be considered as a potential side-effect of anti-LRRK1 treatment.

# 9 Conclusion

In the past years, research on autosomal recessive forms of osteopetrosis has experienced notable progress. The reduced costs for NGS and the facilitated scientific exchange across the world have enabled the detection of more disease-causing variants and further analysis of the molecular effects.

In summary, the here delineated studies have dealt with mutations causing different types of osteopetrosis and bone disease. We have analyzed the mutation effects in a detailed manner. Four new *EFNB1* mutations were described in CFNS patients. We reported on a rare case of intermediate autosomal recessive osteopetrosis due to a *TCIRG1* variant and outlined undescribed *SLC29A3* mutations in dysosteosclerosis patients. The *LRRK1* mutation we described is the fourth known mutation in this gene that causes OSMD. *LRRK1* has previously been considered as a potential drug target for osteoporosis and our study raises concerns that the implementation of LRRK1-antibodies might cause ONJ as an undesired side effect. In sum, this work broadens the spectrum of high bone mass disease pathology and sheds light on the potential risks and benefits of using LRRK1 as a target for osteoporosis treatment.

# 10 Literature


1. Buck, D.W., 2nd and G.A. Dumanian, *Bone biology and physiology: Part I. The fundamentals.* Plast Reconstr Surg, 2012. **129**(6): p. 1314-20.
2. Sims, N.A. and J.H. Gooi, *Bone remodeling: Multiple cellular interactions required for coupling of bone formation and resorption.* Semin Cell Dev Biol, 2008. **19**(5): p. 444-51.
3. Kornak, U. and S. Mundlos, *Genetic disorders of the skeleton: a developmental approach.* Am J Hum Genet, 2003. **73**(3): p. 447-74.
4. Wilkie, A.O. and G.M. Morriss-Kay, *Genetics of craniofacial development and malformation.* Nat Rev Genet, 2001. **2**(6): p. 458-68.
5. Bhatt, S., R. Diaz, and P.A. Trainor, *Signals and switches in Mammalian neural crest cell differentiation.* Cold Spring Harb Perspect Biol, 2013. **5**(2).
6. Alexander, C., S. Piloto, P. Le Pabic, and T.F. Schilling, *Wnt signaling interacts with bmp and edn1 to regulate dorsal-ventral patterning and growth of the craniofacial skeleton.* PLoS Genet, 2014. **10**(7): p. e1004479.
7. Berendsen, A.D. and B.R. Olsen, *Bone development.* Bone, 2015. **80**: p. 14-18.
8. Graf, D., Z. Malik, S. Hayano, and Y. Mishina, *Common mechanisms in development and disease: BMP signaling in craniofacial development.* Cytokine Growth Factor Rev, 2016. **27**: p. 129-39.
9. Duan, P. and L.F. Bonewald, *The role of the wnt/β-catenin signaling pathway in formation and maintenance of bone and teeth.* Int J Biochem Cell Biol, 2016. **77**(Pt A): p. 23-29.
10. Prochazkova, M., J. Prochazka, P. Marangoni, and O.D. Klein, *Bones, Glands, Ears and More: The Multiple Roles of FGF10 in Craniofacial Development.* Front Genet, 2018. **9**: p. 542.
11. Wieland, I., S. Jakubiczka, P. Muschke, M. Cohen, H. Thiele, K.L. Gerlach, R.H. Adams, and P. Wieacker, *Mutations of the ephrin-B1 gene cause craniofrontonasal syndrome.* Am J Hum Genet, 2004. **74**(6): p. 1209-15.
12. Compagni, A., M. Logan, R. Klein, and R.H. Adams, *Control of skeletal patterning by ephrinB1-EphB interactions.* Dev Cell, 2003. **5**(2): p. 217-30.
13. Kullander, K. and R. Klein, *Mechanisms and functions of Eph and ephrin signalling.* Nat Rev Mol Cell Biol, 2002. **3**(7): p. 475-86.
14. Batlle, E., J.T. Henderson, H. Beghtel, M.M. van den Born, E. Sancho, G. Huls, J. Meeldijk, J. Robertson, M. van de Wetering, T. Pawson, and H. Clevers, *Beta-catenin and TCF mediate cell positioning in the intestinal epithelium by controlling the expression of EphB/ephrinB.* Cell, 2002. **111**(2): p. 251-63.

15. Seeman, E. and P.D. Delmas, *Bone quality--the material and structural basis of bone strength and fragility.* N Engl J Med, 2006. **354**(21): p. 2250-61.

16. Robling, A.G., A.B. Castillo, and C.H. Turner, *Biomechanical and molecular regulation of bone remodeling.* Annu Rev Biomed Eng, 2006. **8**: p. 455-98.

17. Lacey, D.L., W.J. Boyle, W.S. Simonet, P.J. Kostenuik, W.C. Dougall, J.K. Sullivan, J. San Martin, and R. Dansey, *Bench to bedside: elucidation of the OPG-RANK-RANKL pathway and the development of denosumab.* Nat Rev Drug Discov, 2012. **11**(5): p. 401-19.

18. Charles, J.F. and A.O. Aliprantis, *Osteoclasts: more than 'bone eaters'.* Trends Mol Med, 2014. **20**(8): p. 449-59.

19. Martin, T.J. and N.A. Sims, *Osteoclast-derived activity in the coupling of bone formation to resorption.* Trends Mol Med, 2005. **11**(2): p. 76-81.

20. Matsuo, K. and N. Irie, *Osteoclast-osteoblast communication.* Arch Biochem Biophys, 2008. **473**(2): p. 201-9.

21. Stark, Z. and R. Savarirayan, *Osteopetrosis.* Orphanet J Rare Dis, 2009. **4**: p. 5.

22. Tolar, J., S.L. Teitelbaum, and P.J. Orchard, *Osteopetrosis.* N Engl J Med, 2004. **351**(27): p. 2839-49.

23. Mortier, G.R., D.H. Cohn, V. Cormier-Daire, C. Hall, D. Krakow, S. Mundlos, G. Nishimura, S. Robertson, L. Sangiorgi, R. Savarirayan, D. Sillence, A. Superti-Furga, S. Unger, and M.L. Warman, *Nosology and classification of genetic skeletal disorders: 2019 revision.* Am J Med Genet A, 2019. **179**(12): p. 2393-2419.

24. Pangrazio, A., B. Cassani, M.M. Guerrini, J.C. Crockett, V. Marrella, L. Zammataro, D. Strina, A. Schulz, C. Schlack, U. Kornak, D.J. Mellis, A. Duthie, M.H. Helfrich, A. Durandy, D. Moshous, A. Vellodi, R. Chiesa, P. Veys, N. Lo Iacono, P. Vezzoni, A. Fischer, A. Villa, and C. Sobacchi, *RANK-dependent autosomal recessive osteopetrosis: characterization of five new cases with novel mutations.* J Bone Miner Res, 2012. **27**(2): p. 342-51.

25. Guerrini, M.M., C. Sobacchi, B. Cassani, M. Abinun, S.S. Kilic, A. Pangrazio, D. Moratto, E. Mazzolari, J. Clayton-Smith, P. Orchard, F.P. Coxon, M.H. Helfrich, J.C. Crockett, D. Mellis, A. Vellodi, I. Tezcan, L.D. Notarangelo, M.J. Rogers, P. Vezzoni, A. Villa, and A. Frattini, *Human osteoclast-poor osteopetrosis with hypogammaglobulinemia due to TNFRSF11A (RANK) mutations.* Am J Hum Genet, 2008. **83**(1): p. 64-76.

26. Orchard, P.J., A.L. Fasth, J. Le Rademacher, W. He, J.J. Boelens, E.M. Horwitz, A. Al-Seraihy, M. Ayas, C.M. Bonfim, F. Boulad, T. Lund, D.K. Buchbinder, N. Kapoor, T.A. O'Brien, M.A. Perez, P.A. Veys, and M. Eapen, *Hematopoietic stem cell transplantation for infantile osteopetrosis.* Blood, 2015. **126**(2): p. 270-6.

27. Li, L., S.S. Lv, C. Wang, H. Yue, and Z.L. Zhang, *Novel CLCN7 mutations cause autosomal dominant osteopetrosis type II and intermediate autosomal recessive osteopetrosis.* Mol Med Rep, 2019. **19**(6): p. 5030-5038.

28. Kornak, U., D. Kasper, M.R. Bösl, E. Kaiser, M. Schweizer, A. Schulz, W. Friedrich, G. Delling, and T.J. Jentsch, *Loss of the ClC-7 chloride channel leads to osteopetrosis in mice and man.* Cell, 2001. **104**(2): p. 205-15.

29. Ott, C.E., B. Fischer, P. Schröter, R. Richter, N. Gupta, N. Verma, M. Kabra, S. Mundlos, A. Rajab, H. Neitzel, and U. Kornak, *Severe neuronopathic autosomal recessive osteopetrosis due to homozygous deletions affecting OSTM1.* Bone, 2013. **55**(2): p. 292-7.

30. Ohlsson, A., G. Stark, and N. Sakati, *Marble brain disease: recessive osteopetrosis, renal tubular acidosis and cerebral calcification in three Saudi Arabian families.* Dev Med Child Neurol, 1980. **22**(1): p. 72-84.

31. Sly, W.S., M.P. Whyte, V. Sundaram, R.E. Tashian, D. Hewett-Emmett, P. Guibaud, M. Vainsel, H.J. Baluarte, A. Gruskin, M. Al-Mosawi, and et al., *Carbonic anhydrase II deficiency in 12 families with the autosomal recessive syndrome of osteopetrosis with renal tubular acidosis and cerebral calcification.* N Engl J Med, 1985. **313**(3): p. 139-45.

32. Campos-Xavier, A.B., J.M. Saraiva, L.M. Ribeiro, A. Munnich, and V. Cormier-Daire, *Chloride channel 7 (CLCN7) gene mutations in intermediate autosomal recessive osteopetrosis.* Hum Genet, 2003. **112**(2): p. 186-9.

33. Van Wesenbeeck, L., P.R. Odgren, F.P. Coxon, A. Frattini, P. Moens, B. Perdu, C.A. MacKay, E. Van Hul, J.P. Timmermans, F. Vanhoenacker, R. Jacobs, B. Peruzzi, A. Teti, M.H. Helfrich, M.J. Rogers, A. Villa, and W. Van Hul, *Involvement of PLEKHM1 in osteoclastic vesicular transport and osteopetrosis in incisors absent rats and humans.* J Clin Invest, 2007. **117**(4): p. 919-30.

34. Pangrazio, A., A. Fasth, A. Sbardellati, P.J. Orchard, K.A. Kasow, J. Raza, C. Albayrak, D. Albayrak, O.M. Vanakker, B. De Moerloose, A. Vellodi, L.D. Notarangelo, C. Schlack, G. Strauss, J.S. Kühl, E. Caldana, N. Lo Iacono, L. Susani, U. Kornak, A. Schulz, P. Vezzoni, A. Villa, and C. Sobacchi, *SNX10 mutations define a subgroup of human autosomal recessive osteopetrosis with variable clinical severity.* J Bone Miner Res, 2013. **28**(5): p. 1041-9.

35. Baer, S., É. Schaefer, C. Michot, M. Fischbach, G. Morelle, M. Bendavid, M. Castelle, D. Moshous, and C. Collet, *Intermediate autosomal recessive osteopetrosis with a large noncoding deletion in SNX10: A case report.* Pediatr Blood Cancer, 2019. **66**(7): p. e27751.

36. Howaldt, A., S. Nampoothiri, L.M. Quell, A. Ozden, B. Fischer-Zirnsak, C. Collet, M.C. de Vernejoul, H. Doneray, H. Kayserili, and U. Kornak, *Sclerosing bone dysplasias with hallmarks*

*of dysosteosclerosis in four patients carrying mutations in SLC29A3 and TCIRG1.* Bone, 2019. **120**: p. 495-503.

37. Waguespack, S.G., S.L. Hui, L.A. Dimeglio, and M.J. Econs, *Autosomal dominant osteopetrosis: clinical severity and natural history of 94 subjects with a chloride channel 7 gene mutation.* J Clin Endocrinol Metab, 2007. **92**(3): p. 771-8.

38. Bollerslev, J., K. Henriksen, M.F. Nielsen, K. Brixen, and W. Van Hul, *Autosomal dominant osteopetrosis revisited: lessons from recent studies.* Eur J Endocrinol, 2013. **169**(2): p. R39-57.

39. Benichou, O., E. Cleiren, J. Gram, J. Bollerslev, M.C. de Vernejoul, and W. Van Hul, *Mapping of autosomal dominant osteopetrosis type II (Albers-Schonberg disease) to chromosome 16p13.3.* Am J Hum Genet, 2001. **69**(3): p. 647-54.

40. Barvencik, F., I. Kurth, T. Koehne, T. Stauber, J. Zustin, K. Tsiakas, C.F. Ludwig, F.T. Beil, J.M. Pestka, M. Hahn, R. Santer, C. Supanchart, U. Kornak, A. Del Fattore, T.J. Jentsch, A. Teti, A. Schulz, T. Schinke, and M. Amling, *CLCN7 and TCIRG1 mutations differentially affect bone matrix mineralization in osteopetrotic individuals.* J Bone Miner Res, 2014. **29**(4): p. 982-91.

41. Maurizi, A., M. Capulli, A. Curle, R. Patel, A. Ucci, J.A. Cortes, H. Oxford, S.R. Lamande, J.F. Bateman, N. Rucci, and A. Teti, *Extra-skeletal manifestations in mice affected by Clcn7-dependent autosomal dominant osteopetrosis type 2 clinical and therapeutic implications.* Bone Res, 2019. **7**: p. 17.

42. Howaldt, A.H., AF.; Rösler, U.; Rolvien, T.; Stelzer,N.; Knaus, A.; Böttger, S.; Zustin, J.; Oheim, R.; Amling, M.; Geißler, S.; Howaldt, HP.; Kornak, U., *Adult osteosclerotic metaphyseal dysplasia with progressive osteonecrosis of the jaws and abnormal bone resorption pattern due to a LRRK1 splice site mutation.* Journal of Bone and Mineral Research 2020.

43. Van Hul, E., J. Gram, J. Bollerslev, L. Van Wesenbeeck, D. Mathysen, P.E. Andersen, F. Vanhoenacker, and W. Van Hul, *Localization of the gene causing autosomal dominant osteopetrosis type I to chromosome 11q12-13.* J Bone Miner Res, 2002. **17**(6): p. 1111-7.

44. Little, R.D., J.P. Carulli, R.G. Del Mastro, J. Dupuis, M. Osborne, C. Folz, S.P. Manning, P.M. Swain, S.C. Zhao, B. Eustace, M.M. Lappe, L. Spitzer, S. Zweier, K. Braunschweiger, Y. Benchekroun, X. Hu, R. Adair, L. Chee, M.G. FitzGerald, C. Tulig, A. Caruso, N. Tzellas, A. Bawa, B. Franklin, S. McGuire, X. Nogues, G. Gong, K.M. Allen, A. Anisowicz, A.J. Morales, P.T. Lomedico, S.M. Recker, P. Van Eerdewegh, R.R. Recker, and M.L. Johnson, *A mutation in the LDL receptor-related protein 5 gene results in the autosomal dominant high-bone-mass trait.* Am J Hum Genet, 2002. **70**(1): p. 11-9.

45. Boyden, L.M., J. Mao, J. Belsky, L. Mitzner, A. Farhi, M.A. Mitnick, D. Wu, K. Insogna, and R.P. Lifton, *High bone density due to a mutation in LDL-receptor-related protein 5.* N Engl J Med, 2002. **346**(20): p. 1513-21.

46. Döffinger, R., A. Smahi, C. Bessia, F. Geissmann, J. Feinberg, A. Durandy, C. Bodemer, S. Kenwrick, S. Dupuis-Girod, S. Blanche, P. Wood, S.H. Rabia, D.J. Headon, P.A. Overbeek, F. Le Deist, S.M. Holland, K. Belani, D.S. Kumararatne, A. Fischer, R. Shapiro, M.E. Conley, E. Reimund, H. Kalhoff, M. Abinun, A. Munnich, A. Israël, G. Courtois, and J.L. Casanova, *X-linked anhidrotic ectodermal dysplasia with immunodeficiency is caused by impaired NF-kappaB signaling.* Nat Genet, 2001. **27**(3): p. 277-85.

47. Ricci, S., F. Romano, F. Nieddu, C. Picard, and C. Azzari, *OL-EDA-ID Syndrome: a Novel Hypomorphic NEMO Mutation Associated with a Severe Clinical Presentation and Transient HLH.* J Clin Immunol, 2017. **37**(1): p. 7-11.

48. Lemire, E.G. and S. Wiebe, *Clinical and radiologic findings in an adult male with dysosteosclerosis.* Am J Med Genet A, 2008. **146a**(4): p. 474-8.

49. Gelb, B.D., G.P. Shi, H.A. Chapman, and R.J. Desnick, *Pycnodysostosis, a lysosomal disease caused by cathepsin K deficiency.* Science, 1996. **273**(5279): p. 1236-8.

50. Johnson, M.R., M.H. Polymeropoulos, H.L. Vos, R.I. Ortiz de Luna, and C.A. Francomano, *A nonsense mutation in the cathepsin K gene observed in a family with pycnodysostosis.* Genome Res, 1996. **6**(11): p. 1050-5.

51. Hernlund, E., A. Svedbom, M. Ivergard, J. Compston, C. Cooper, J. Stenmark, E.V. McCloskey, B. Jonsson, and J.A. Kanis, *Osteoporosis in the European Union: medical management, epidemiology and economic burden. A report prepared in collaboration with the International Osteoporosis Foundation (IOF) and the European Federation of Pharmaceutical Industry Associations (EFPIA).* Arch Osteoporos, 2013. **8**: p. 136.

52. Ballane, G., J.A. Cauley, M.M. Luckey, and G. El-Hajj Fuleihan, *Worldwide prevalence and incidence of osteoporotic vertebral fractures.* Osteoporos Int, 2017. **28**(5): p. 1531-1542.

53. Macdonald, H.M., S.A. New, M.K. Campbell, and D.M. Reid, *Influence of weight and weight change on bone loss in perimenopausal and early postmenopausal Scottish women.* Osteoporos Int, 2005. **16**(2): p. 163-71.

54. Uusi-Rasi, K., H. Sievänen, M. Pasanen, P. Oja, and I. Vuori, *Association of physical activity and calcium intake with the maintenance of bone mass in premenopausal women.* Osteoporos Int, 2002. **13**(3): p. 211-7.

55. Pivonello, R., A.M. Isidori, M.C. De Martino, J. Newell-Price, B.M. Biller, and A. Colao, *Complications of Cushing's syndrome: state of the art.* Lancet Diabetes Endocrinol, 2016. **4**(7): p. 611-29.

56. Insogna, K.L., *The effect of proton pump-inhibiting drugs on mineral metabolism.* Am J Gastroenterol, 2009. **104 Suppl 2**: p. S2-4.

57. Diamond, T., P. Smerdely, N. Kormas, R. Sekel, T. Vu, and P. Day, *Hip fracture in elderly men: the importance of subclinical vitamin D deficiency and hypogonadism.* Med J Aust, 1998. **169**(3): p. 138-41.

58. Gupta, S. and B. Shen, *Bone loss in patients with the ileostomy and ileal pouch for inflammatory bowel disease.* Gastroenterol Rep (Oxf), 2013. **1**(3): p. 159-65.

59. Jain, S., B. Bilori, A. Gupta, P. Spanos, and M. Singh, *Are Men at High Risk for Osteoporosis Underscreened? A Quality Improvement Project.* Perm J, 2016. **20**(1): p. 60-4.

60. Rugani, P., C. Walter, B. Kirnbauer, S. Acham, Y. Begus-Nahrman, and N. Jakse, *Prevalence of Medication-Related Osteonecrosis of the Jaw in Patients with Breast Cancer, Prostate Cancer, and Multiple Myeloma.* Dent J (Basel), 2016. **4**(4).

61. Howaldt, A., S. Nampoothiri, D. Yesodharan, S. Udayakumaran, P. Subash, and U. Kornak, *Four novel mutations in EFNB1 in Indian patients with craniofrontonasal syndrome.* J Hum Genet, 2019. **64**(9): p. 867-873.

62. Howaldt, A., A.F. Hennig, T. Rolvien, U. Rössler, N. Stelzer, A. Knaus, S. Böttger, J. Zustin, S. Geißler, R. Oheim, M. Amling, H.P. Howaldt, and U. Kornak, *Adult Osteosclerotic Metaphyseal Dysplasia With Progressive Osteonecrosis of the Jaws and Abnormal Bone Resorption Pattern Due to a LRRK1 Splice Site Mutation.* J Bone Miner Res, 2020. **35**(7): p. 1322-1332.

63. Cai, W., S. Nunziata, J. Rascoe, and M.J. Stulberg, *SureSelect targeted enrichment, a new cost effective method for the whole genome sequencing of Candidatus Liberibacter asiaticus.* Sci Rep, 2019. **9**(1): p. 18962.

64. Kamphans, T. and P.M. Krawitz, *GeneTalk: an expert exchange platform for assessing rare sequence variants in personal genomes.* Bioinformatics, 2012. **28**(19): p. 2515-6.

65. Schwarz, J.M., C. Rodelsperger, M. Schuelke, and D. Seelow, *MutationTaster evaluates disease-causing potential of sequence alterations.* Nat Methods, 2010. **7**(8): p. 575-6.

66. Untergasser, A., I. Cutcutache, T. Koressaar, J. Ye, B.C. Faircloth, M. Remm, and S.G. Rozen, *Primer3--new capabilities and interfaces.* Nucleic Acids Res, 2012. **40**(15): p. e115.

67. Dominici, M., K. Le Blanc, I. Mueller, I. Slaper-Cortenbach, F. Marini, D. Krause, R. Deans, A. Keating, D. Prockop, and E. Horwitz, *Minimal criteria for defining multipotent*

*mesenchymal stromal cells. The International Society for Cellular Therapy position statement.* Cytotherapy, 2006. **8**(4): p. 315-7.

68. Geissler, S., M. Textor, K. Schmidt-Bleek, O. Klein, M. Thiele, A. Ellinghaus, D. Jacobi, A. Ode, C. Perka, A. Dienelt, J. Klose, G. Kasper, G.N. Duda, and P. Strube, *In serum veritas-in serum sanitas? Cell non-autonomous aging compromises differentiation and survival of mesenchymal stromal cells via the oxidative stress pathway.* Cell Death Dis, 2013. **4**: p. e970.

69. Uz, E., Y. Alanay, D. Aktas, I. Vargel, S. Gucer, G. Tuncbilek, F. von Eggeling, E. Yilmaz, O. Deren, N. Posorski, H. Ozdag, T. Liehr, S. Balci, M. Alikasifoglu, B. Wollnik, and N.A. Akarsu, *Disruption of ALX1 causes extreme microphthalmia and severe facial clefting: expanding the spectrum of autosomal-recessive ALX-related frontonasal dysplasia.* Am J Hum Genet, 2010. **86**(5): p. 789-96.

70. Hu, Y., J. Pini, J. Kueper, B. Agnihotri, R. Maas, and E.C. Liao, *Abstract 105: ALX1 Regulates PAX3 to Enable Cranial Neural Crest Migration During Craniofacial Development.* 2019.

71. Gross, C., M. Weber, K. Creutzburg, P. Möbius, R. Preidl, K. Amann, and F. Wehrhan, *Osteoclast profile of medication-related osteonecrosis of the jaw secondary to bisphosphonate therapy: a comparison with osteoradionecrosis and osteomyelitis.* J Transl Med, 2017. **15**(1): p. 128.

72. Edwards, B.J., M. Gounder, J.M. McKoy, I. Boyd, M. Farrugia, C. Migliorati, R. Marx, S. Ruggiero, M. Dimopoulos, D.W. Raisch, S. Singhal, K. Carson, E. Obadina, S. Trifilio, D. West, J. Mehta, and C.L. Bennett, *Pharmacovigilance and reporting oversight in US FDA fast-track process: bisphosphonates and osteonecrosis of the jaw.* Lancet Oncol, 2008. **9**(12): p. 1166-72.

73. Hoff, A.O., B.B. Toth, K. Altundag, M.M. Johnson, C.L. Warneke, M. Hu, A. Nooka, G. Sayegh, V. Guarneri, K. Desrouleaux, J. Cui, A. Adamus, R.F. Gagel, and G.N. Hortobagyi, *Frequency and risk factors associated with osteonecrosis of the jaw in cancer patients treated with intravenous bisphosphonates.* J Bone Miner Res, 2008. **23**(6): p. 826-36.

74. Zervas, K., E. Verrou, Z. Teleioudis, K. Vahtsevanos, A. Banti, D. Mihou, D. Krikelis, and E. Terpos, *Incidence, risk factors and management of osteonecrosis of the jaw in patients with multiple myeloma: a single-centre experience in 303 patients.* Br J Haematol, 2006. **134**(6): p. 620-3.

75. van Kempen, E.E.J. and H.S. Brand, *Effects of krokodil (desomorphine) use on oral health - a systematic review.* Br Dent J, 2019. **227**(9): p. 806-812.

76. van de Meent, M.M., H. Meshkini, M. Fiocco, M.J.M. Wetselaar-Glas, N.M. Appelman-Dijkstra, and J.P.R. van Merkesteyn, *Conservative treatment of children with chronic diffuse*

*sclerosing osteomyelitis/tendoperiostitis of the mandible.* J Craniomaxillofac Surg, 2017. **45**(12): p. 1938-1943.

77. Sroussi, H.Y., J.B. Epstein, R.J. Bensadoun, D.P. Saunders, R.V. Lalla, C.A. Migliorati, N. Heaivilin, and Z.S. Zumsteg, *Common oral complications of head and neck cancer radiation therapy: mucositis, infections, saliva change, fibrosis, sensory dysfunctions, dental caries, periodontal disease, and osteoradionecrosis.* Cancer Med, 2017. **6**(12): p. 2918-2931.

78. Ferguson, P.J., X. Bing, M.A. Vasef, L.A. Ochoa, A. Mahgoub, T.J. Waldschmidt, L.T. Tygrett, A.J. Schlueter, and H. El-Shanti, *A missense mutation in pstpip2 is associated with the murine autoinflammatory disorder chronic multifocal osteomyelitis.* Bone, 2006. **38**(1): p. 41-7.

79. Cox, A.J., Y. Zhao, and P.J. Ferguson, *Chronic Recurrent Multifocal Osteomyelitis and Related Diseases-Update on Pathogenesis.* Curr Rheumatol Rep, 2017. **19**(4): p. 18.

80. Zhang, X., M.H. Chen, X. Wu, A. Kodani, J. Fan, R. Doan, M. Ozawa, J. Ma, N. Yoshida, J.F. Reiter, D.L. Black, P.V. Kharchenko, P.A. Sharp, and C.A. Walsh, *Cell-Type-Specific Alternative Splicing Governs Cell Fate in the Developing Cerebral Cortex.* Cell, 2016. **166**(5): p. 1147-1162.e15.

81. Munkley, J., K. Livermore, P. Rajan, and D.J. Elliott, *RNA splicing and splicing regulator changes in prostate cancer pathology.* Hum Genet, 2017. **136**(9): p. 1143-1154.

82. de Bruin, R.G., T.J. Rabelink, A.J. van Zonneveld, and E.P. van der Veer, *Emerging roles for RNA-binding proteins as effectors and regulators of cardiovascular disease.* Eur Heart J, 2017. **38**(18): p. 1380-1388.

83. van den Hoogenhof, M.M., Y.M. Pinto, and E.E. Creemers, *RNA Splicing: Regulation and Dysregulation in the Heart.* Circ Res, 2016. **118**(3): p. 454-68.

84. Desmet, F.O., D. Hamroun, M. Lalande, G. Collod-Beroud, M. Claustres, and C. Beroud, *Human Splicing Finder: an online bioinformatics tool to predict splicing signals.* Nucleic Acids Res, 2009. **37**(9): p. e67.

85. Drake, M.T., B.L. Clarke, M.J. Oursler, and S. Khosla, *Cathepsin K Inhibitors for Osteoporosis: Biology, Potential Clinical Utility, and Lessons Learned.* Endocr Rev, 2017. **38**(4): p. 325-350.

86. Khosla, S., M.J. Oursler, and D.G. Monroe, *Estrogen and the skeleton.* Trends Endocrinol Metab, 2012. **23**(11): p. 576-81.

87. Costa, S., H. Fairfield, and M.R. Reagan, *Inverse correlation between trabecular bone volume and bone marrow adipose tissue in rats treated with osteoanabolic agents.* Bone, 2019. **123**: p. 211-223.

88. Cosman, F., D.B. Crittenden, J.D. Adachi, N. Binkley, E. Czerwinski, S. Ferrari, L.C. Hofbauer, E. Lau, E.M. Lewiecki, A. Miyauchi, C.A. Zerbini, C.E. Milmont, L. Chen, J. Maddox, P.D. Meisner, C. Libanati, and A. Grauer, *Romosozumab Treatment in Postmenopausal Women with Osteoporosis.* N Engl J Med, 2016. **375**(16): p. 1532-1543.

89. Balemans, W., M. Ebeling, N. Patel, E. Van Hul, P. Olson, M. Dioszegi, C. Lacza, W. Wuyts, J. Van Den Ende, P. Willems, A.F. Paes-Alves, S. Hill, M. Bueno, F.J. Ramos, P. Tacconi, F.G. Dikkers, C. Stratakis, K. Lindpaintner, B. Vickery, D. Foernzler, and W. Van Hul, *Increased bone density in sclerosteosis is due to the deficiency of a novel secreted protein (SOST).* Hum Mol Genet, 2001. **10**(5): p. 537-43.

90. Honasoge, M., A.D. Rao, and S.D. Rao, *Sclerostin: recent advances and clinical implications.* Curr Opin Endocrinol Diabetes Obes, 2014. **21**(6): p. 437-46.

91. Yavropoulou, M.P., C. Xygonakis, M. Lolou, F. Karadimou, and J.G. Yovos, *The sclerostin story: from human genetics to the development of novel anabolic treatment for osteoporosis.* Hormones (Athens), 2014. **13**(4): p. 323-37.

92. Saag, K.G., J. Petersen, M.L. Brandi, A.C. Karaplis, M. Lorentzon, T. Thomas, J. Maddox, M. Fan, P.D. Meisner, and A. Grauer, *Romosozumab or Alendronate for Fracture Prevention in Women with Osteoporosis.* N Engl J Med, 2017. **377**(15): p. 1417-1427.

93. Dodds, R.A., I.E. James, D. Rieman, R. Ahern, S.M. Hwang, J.R. Connor, S.D. Thompson, D.F. Veber, F.H. Drake, S. Holmes, M.W. Lark, and M. Gowen, *Human osteoclast cathepsin K is processed intracellularly prior to attachment and bone resorption.* J Bone Miner Res, 2001. **16**(3): p. 478-86.

94. Brix, K., A. Dunkhorst, K. Mayer, and S. Jordans, *Cysteine cathepsins: cellular roadmap to different functions.* Biochimie, 2008. **90**(2): p. 194-207.

95. Littlewood-Evans, A., T. Kokubo, O. Ishibashi, T. Inaoka, B. Wlodarski, J.A. Gallagher, and G. Bilbe, *Localization of cathepsin K in human osteoclasts by in situ hybridization and immunohistochemistry.* Bone, 1997. **20**(2): p. 81-6.

96. Andren, L., J.F. Dymling, K.E. Hogeman, and B. Wendeberg, *Osteopetrosis acro-osteolytica. A syndrome of osteopetrosis, acro-osteolysis and open sutures of the skull.* Acta Chir Scand, 1962. **124**: p. 496-507.

97. Stroup, G.B., M.W. Lark, D.F. Veber, A. Bhattacharyya, S. Blake, L.C. Dare, K.F. Erhard, S.J. Hoffman, I.E. James, R.W. Marquis, Y. Ru, J.A. Vasko-Moser, B.R. Smith, T. Tomaszek, and M. Gowen, *Potent and selective inhibition of human cathepsin K leads to inhibition of bone resorption in vivo in a nonhuman primate.* J Bone Miner Res, 2001. **16**(10): p. 1739-46.

98. McClung, M.R., M.L. O'Donoghue, S.E. Papapoulos, H. Bone, B. Langdahl, K.G. Saag, I.R. Reid, D.P. Kiel, I. Cavallari, M.P. Bonaca, S.D. Wiviott, T. de Villiers, X. Ling, K. Lippuner, T. Nakamura, J.Y. Reginster, J.A. Rodriguez-Portales, C. Roux, J. Zanchetta, C.A.F. Zerbini, J.G. Park, K. Im, A. Cange, L.T. Grip, N. Heyden, C. DaSilva, D. Cohn, R. Massaad, B.B. Scott, N. Verbruggen, D. Gurner, D.L. Miller, M.L. Blair, A.B. Polis, S.A. Stoch, A. Santora, A. Lombardi, A.T. Leung, K.D. Kaufman, and M.S. Sabatine, *Odanacatib for the treatment of postmenopausal osteoporosis: results of the LOFT multicentre, randomised, double-blind, placebo-controlled trial and LOFT Extension study.* Lancet Diabetes Endocrinol, 2019. **7**(12): p. 899-911.

99. Si, M., C. Zeng, H. Goodluck, S. Shen, S. Mohan, and W. Xing, *A small molecular inhibitor of LRRK1 identified by homology modeling and virtual screening suppresses osteoclast function, but not osteoclast differentiation, in vitro.* Aging (Albany NY), 2019. **11**(10): p. 3250-3261.

# 11 Eidesstattliche Versicherung/ Anteilserklärung

„Ich, Antonia Howaldt, versichere an Eides statt durch meine eigenhändige Unterschrift, dass ich die vorgelegte Dissertation mit dem Thema: „Genetic Factors Regulating Bone Mass“ selbstständig und ohne nicht offengelegte Hilfe Dritter verfasst und keine anderen als die angegebenen Quellen und Hilfsmittel genutzt habe.
Alle Stellen, die wörtlich oder dem Sinne nach auf Publikationen oder Vorträgen anderer Autoren beruhen, sind als solche in korrekter Zitierung kenntlich gemacht. Die Abschnitte zu Methodik (insbesondere praktische Arbeiten, Laborbestimmungen, statistische Aufarbeitung) und Resultaten (insbesondere Abbildungen, Graphiken und Tabellen werden von mir verantwortet.

Meine Anteile an etwaigen Publikationen zu dieser Dissertation entsprechen denen, die in der untenstehenden gemeinsamen Erklärung mit dem/der Betreuer/in, angegeben sind. Für sämtliche im Rahmen der Dissertation entstandenen Publikationen wurden die Richtlinien des ICMJE (International Committee of Medical Journal Editors; www.icmje.og) zur Autorenschaft eingehalten. Ich erkläre ferner, dass mir die Satzung der Charité – Universitätsmedizin Berlin zur Sicherung Guter Wissenschaftlicher Praxis bekannt ist und ich mich zur Einhaltung dieser Satzung verpflichte.

Die Bedeutung dieser eidesstattlichen Versicherung und die strafrechtlichen Folgen einer unwahren eidesstattlichen Versicherung (§156,161 des Strafgesetzbuches) sind mir bekannt und bewusst.“

| | |
|---|---|
| ..... | ..... |
| Datum | Antonia Howaldt |

## Anteilserklärung an den erfolgten Publikationen

Antonia Howaldt hatte folgenden Anteil an den folgenden Publikationen:

Publikation 1:

**Howaldt, A.,** S. Nampoothiri, L.M. Quell, A. Ozden, B. Fischer-Zirnsak, C. Collet, M.C. de Vernejoul, H. Doneray, H. Kayserili, and U. Kornak, *Sclerosing bone dysplasias with hallmarks of dysosteosclerosis in four patients carrying mutations in SLC29A3 and TCIRG1.* Bone, 2019. **120**: p. 495-503.[36] (Impact factor: 4.31; Jahr 2019)

Anteilserklärung: Ich, Antonia Howaldt, habe das Exom der Patient*innen 3 und 4 bioinformatisch ausgewertet und die Validierung der *TCIRG1* Variante sowie die Segregationsanalyse im Labor durchgeführt (Sanger Sequenzierung von Index-Patient, Eltern und Geschwistern). Weiterhin habe ich die Mehrheit der Figures und das Manuskript maßgeblich entworfen. Dies betrifft insbesondere: Table 1, Figure 1, 2, 3, 4 A, B, und C, Figure 5 sowie die Supplementary (Suppl.) Figure 1, Suppl. Table 1 und Supple Table 2. Die *SLC29A3* Mutationen in Patientinnen 1 und 2 hat eine vorherige Doktorandin, Frau Dr. med Lisa-Marie Quell, gefunden, die auch Co-Autorin des Papers ist. Figure 4 D hat Prof. Dr. rer. nat. Uwe Kornak entworfen.

Publikation 2:

**Howaldt, A.,** S. Nampoothiri, D. Yesodharan, S. Udayakumaran, P. Subash, and U. Kornak, Four novel mutations in EFNB1 in Indian patients with craniofrontonasal syndrome. J Hum Genet, 2019. 64(9): p. 867-873. [61] (Impact factor 3.46; Jahr 2019)

Anteilserklärung: Ich, Antonia Howaldt, habe im Labor die Sanger Sequenzierung von *EFNB1* der DNA der vier Patientinnen und, sofern vorhanden, der Familienmitglieder durchgeführt. Ich habe die Ergebnisse ausgewertet, dabei bisher unbekannte Mutationen finden können und diese graphisch dargestellt. Weiterhin habe ich das Manuskript geschrieben sowie Table 1, Figure 1, 2, 4 und Suppl. Table 1 entworfen. Figure 3 hat Prof. Dr. rer. nat. Uwe Kornak entworfen.

Publikation 3:

**Howaldt, A.,** A.F. Hennig, T. Rolvien, U. Rössler, N. Stelzer, A. Knaus, S. Böttger, J. Zustin, S. Geißler, R. Oheim, M. Amling, H.P. Howaldt, and U. Kornak, *Adult Osteosclerotic Metaphyseal Dysplasia With Progressive Osteonecrosis of the Jaws and Abnormal Bone Resorption Pattern*

*Due to a LRRK1 Splice Site Mutation.* J Bone Miner Res, 2020. **35**(7): p. 1322-1332. [62] (Impact factor 5.46; Jahr 2019)

Anteilserklärung: Ich, Antonia Howaldt, habe Teile der Experimente für diese Veröffentlichung insbesondere die Immunoblot Analyse geplant und Vorarbeit für die molekularen Analysen geleistet. Ich habe per Sanger Sequenzierung der Familie des Patienten die in der Trio-Exom Analyse gefundene Mutation bestätigt, das Manuskript maßgeblich entworfen und dabei auch die Figures. 1, 2, 5A, und die Supporting Figure 1 erstellt. Die histologische Evaluation der Knochenschnitte wurde von Kollegen und Co-Autoren Zustin/Oheim/Amling am UKE Hamburg durchgeführt, die auch die Figure 3 und Figure 4 entworfen haben. Der Immunoblot wurde von Nina Stelzer durchgeführt, die Funktionsanalyse der Osteoklasten von Anna Floriane Hennig und Uta Rösler, welche ebenfalls Co-Autorinnen des Papers sind. Die klinische Analyse und die Behandlung wurden von Kollegen des Uniklinikums Gießen durchgeführt, die auch die Foto- und Röntgenaufnahmen gemacht haben. Diese sind Grundlage für Figure 1 und 2 der Publikation.

_____

Prof. Uwe Kornak (Unterschrift, Datum, Stempel)

_____

Antonia Howaldt

# 12 Druckexemplar der ausgewählten Publikationen

**Howaldt, A.,** S. Nampoothiri, L.M. Quell, A. Ozden, B. Fischer-Zirnsak, C. Collet, M.C. de Vernejoul, H. Doneray, H. Kayserili, and U. Kornak, **Sclerosing bone dysplasias with hallmarks of dysosteosclerosis in four patients carrying mutations in SLC29A3 and TCIRG1**. Bone, 2019. **120**: p. 495-503. [36]

https://doi.org/10.1016/j.bone.2018.12.002

Bone 120 (2019) 495–503

Contents lists available at ScienceDirect

Bone

journal homepage: www.elsevier.com/locate/bone

Full Length Article

# Sclerosing bone dysplasias with hallmarks of dysosteosclerosis in four patients carrying mutations in *SLC29A3* and *TCIRG1*

Antonia Howaldt[a], Sheela Nampoothiri[b], Lisa-Marie Quell[a], Ayse Ozden[c], Björn Fischer-Zirnsak[a], Corinne Collet[d], Marie-Christine de Vernejoul[e,f,g], Hakan Doneray[c], Hülya Kayserili[h], Uwe Kornak[a,i,j,*]

[a] *Institut für Medizinische Genetik und Humangenetik, Charité – Universitätsmedizin Berlin, corporate member of Freie Universität Berlin, Humboldt-Universität zu Berlin, and Berlin Institute of Health, Berlin, Germany*
[b] *Amrita Institute of Medical Sciences & Research Centre, Cochin, India*
[c] *Ataturk University Faculty of Medicine, Erzurum, Turkey*
[d] *Service de Biochimie et Biologie Moléculaire, CHU Paris-GH St-Louis Lariboisière F. Widal - Hôpital Lariboisière, Paris, France*
[e] *INSERM U1132 BIOSCAR, Hôpital Lariboisière, 75010 Paris, France*
[f] *University Paris Diderot, Sorbonne Paris Cité, Paris, France*
[g] *Service de Rhumatologie, GH Saint-Louis Lariboisière Fernand Widal, Paris, France*
[h] *Medical Genetics Department, Koç University School of Medicine (KUSOM), Istanbul, Turkey*
[i] *Max Planck Institute for Molecular Genetics, Berlin, Germany*
[j] *Berlin-Brandenburg Center for Regenerative Therapies, Charité – Universitätsmedizin Berlin, Freie Universität Berlin, Humboldt-Universität zu Berlin, and Berlin Institute of Health, Berlin, Germany*

ARTICLE INFO

*Keywords:*
TCIRG1
SLC29A3
Autosomal recessive osteopetrosis
Dysosteosclerosis
Platyspondyly
Next generation sequencing

ABSTRACT

The osteopetroses and related sclerosing bone dysplasias can have a broad range of manifestations. Especially in the milder forms, sandwich vertebrae are an easily recognizable and reliable radiological hallmark. We report on four patients from three families presenting with sandwich vertebrae and platyspondyly. The long bone phenotypes were discordant with one patient showing modeling defects and patchy osteosclerosis, while the second displayed only metaphyseal sclerotic bands, and the third and fourth had extreme metaphyseal flaring with uniform osteosclerosis. Two of the four patients had experienced pathological fractures, two had developmental delay, but none showed cranial nerve damage, hepatosplenomegaly, or bone marrow failure. According to these clinical features the diagnoses ranged between intermediate autosomal recessive osteopetrosis and dysosteosclerosis. After exclusion of mutations in *CLCN7* we performed gene panel and exome sequencing. Two novel mutations in *SLC29A3* were found in the first two patients. In the third family a *TCIRG1* C-terminal frameshift mutation in combination with a mutation at position +4 in intron 2 were detected. Our study adds two cases to the small group of individuals with *SLC29A3* mutations diagnosed with dysosteosclerosis, and expands the phenotypic variability. The finding that intermediate autosomal recessive osteopetrosis due to *TCIRG1* splice site mutations can also present with platyspondyly further increases the molecular heterogeneity of dysosteosclerosis-like sclerosing bone dysplasias.

## 1. Introduction

Sclerosing bone dysplasias can have a broad range of manifestations with autosomal recessive infantile malignant osteopetrosis at the one end and barely detectable bone mass alterations and/or absence of clinical signs in mild autosomal dominant osteopetrosis or osteomesopyknosis at the other end of the spectrum [12,24,30]. The underlying disease mechanism can be either increased activity of osteoblasts or decreased function of osteoclasts. The former case applies to the disease category hyperostosis with the craniotubular dysplasias as prominent examples, and the latter mechanism is at work in the case of the osteopetroses and related conditions like dysosteosclerosis

*Abbreviations:* ARO, autosomal recessive osteopetrosis; DOS, dysosteosclerosis; OP, osteopetrosis; TCIRG1, T-cell immune regulator 1; SLC29A3, solute carrier family 29 member 3; WES, whole exome sequencing

* Corresponding author at: Institute of Medical Genetics and Human Genetics, Charité-Universitaetsmedizin Berlin, Augustenburger Platz 1, 13353 Berlin, Germany.
*E-mail address:* uwe.kornak@charite.de (U. Kornak).

https://doi.org/10.1016/j.bone.2018.12.002
Received 24 September 2018; Received in revised form 1 December 2018; Accepted 6 December 2018
Available online 08 December 2018

[4,20]. An important indicator of impaired osteoclast function is sclerosis of the vertebral endplates due to non-resorbed mineralized cartilage leading to the radiological appearance of sandwich vertebrae.

Autosomal recessive osteopetrosis (ARO, OMIM #259700) is in the majority of cases caused by mutations in the T-cell immune regulator 1 (*TCIRG1*) gene and mostly has a lethal course if not timely treated by stem cell transplantation [33]. Due to the absence of a bone marrow cavity in ARO sandwich vertebrae are better seen in intermediate autosomal recessive osteopetrosis or autosomal dominant osteopetrosis type 2 (ADO2, OMIM #166600) that are mainly caused by biallelic or heterozygous mutations in *CLCN7*, respectively [3,5,7]. In rare cases, however, a similar phenotype can also be secondary to intronic mutations in *TCIRG1* [28,37].

Dysosteosclerosis (DOS, OMIM #244300), first described by Spranger et al., is also characterized by sandwich vertebrae and overlaps with intermediate ARO and ADO2 [34]. Additional features include platyspondyly, metaphyseal osteosclerosis and widening, sometimes reminiscent of Pyle's disease, short stature, pathological fractures, cranial nerve damage, hypodontia and impaired tooth calcification, and macular skin changes [4]. In two patients with this diagnosis biallelic mutations in *SLC29A3* were identified, encoding for the equilibrative nucleoside transporter 3 (ENT3), which transports nucleosides and free purine and pyrimidine bases across the lysosomal and mitochondrial membranes [15]. Mutations in *SLC29A3* are more often associated with histiocytosis-lymphadenopathy plus syndrome (OMIM #602782). Major features of this complex disease (generalized inflammation, histiocytic plaques, hepatosplenomegaly, lymphadenopathy) can be attributed to impaired macrophage function and increased proliferation [15]. In contrast, when monocytes from DOS patients were differentiated *in vitro* reduced osteoclast numbers were observed [4,36]. It is still debated whether dysosteosclerosis is an own disease entity or whether the osteosclerotic phenotype associated with *SLC29A3* mutations is just a special manifestation within the histiocytosis-lymphadenopathy disease spectrum. Moreover, in one patient diagnosed with DOS a homozygous intronic mutation in *TNFRSF11A* encoding RANK was identified, which increases the genetic heterogeneity of this phenotype [13]. We describe four patients from three families with sandwich vertebrae, variable platyspondyly, and metaphyseal flaring and sclerosis. We show the similarities between intermediate ARO caused by intronic *TCIRG1* mutations and DOS caused by *SLC29A3* mutations, compare these findings to the literature, and discuss the heterogeneity of dysosteosclerosis its role as a separate disease entity.

## 2. Material and methods

### 2.1. Next generation sequencing

Before next generation sequencing was initiated, mutations in *CLCN7* were excluded using Sanger sequencing. For Patients 1 and 2, a custom bone mass panel containing 70 genes known or suggested to cause alterations in bone mineral density was employed [27]. The enrichment of the coding regions of these genes was performed using SureSelect XT target enrichment system from Agilent or NEB-Next DNA Library Prep Master Mix Set from Illumina. Samples were run on an Illumina HiSeq1500 sequencer. On average 92–99% of the target region were covered by at least 20 reads. The resulting reads were mapped to the reference genome (hg19) with Burrows-Wheeler Aligner (BWA). PCR duplicates were removed using Picard and GATK [25] was used to perform realignment around indels and base score recalibrations. Variants were detected by Gene-Talk platform [16,35]. Variant analysis was restricted to all genes known at the time of analysis to cause high bone mass disorder. The pathogenic potential of individual candidate variants was evaluated by MutationTaster [31].

For Patients 3 and 4, libraries for whole exome sequencing (WES) were prepared using NEBNext DNA Library Prep Master Mix Set for Illumina (New England Biolabs). Enrichment of the target regions was done using the SureSelect Human Exome Kit V4 (Agilent Technologies) and run on a HiSeq 1500 Sequencer (Illumina). The average sequencing depth was above 40× and more than 90% of the exome target region was covered by more than 10 reads. Variants were detected with GATK toolkit version 2.6 and the exome genotyping accuracy was estimated to be above 0.9999 based on the variant calls. Variants were detected with SAMtools, annotated with ANNOVAR and finally analysed using the Gene-Talk platform [16]. The pathogenic potential of individual candidate variants was evaluated by MutationTaster [31].

### 2.2. Sanger sequencing

All 25 exons of the gene *CLCN7* were sequenced by the Sanger method as described before [19]. To validate the variants acquired by bioinformatic filtering of the gene-panel or WES sequencing data, the respective exons and exon–intron boundaries of *SLC29A3* (NM_001174098) and *TCIRG1* (NM_006019) were amplified using oligonucleotide primers (sequences available upon request) and sequenced on an ABI3730xl DNA Analyzer (Applied Biosystems). In this way, the gene regions of the mutations and adjacent regions were depicted and mutations verified, both in the index and family members whenever respective DNA was available.

## 3. Results

### 3.1. Clinical presentation of four individuals with sclerosing bone phenotypes

Four patients from three different families presented with osteosclerosis and long bone modeling defects suggesting the diagnosis intermediate autosomal recessive osteopetrosis or dysosteosclerosis (Table 1).

Patients 1 and 2 were of Turkish origin. Patient 1 was a 22-year-old female and the third child born to first-degree cousins. She had two healthy sisters and was the only one affected in the family. Patient 2 was a 11-year-old girl born to first-degree cousins. Her two elder sisters and parents had no phenotype suggestive for osteopetrosis. Patient 3 and 4 were siblings of Indian origin born to non-consanguineous parents. Patient 3 was a 15-year-old boy and his clinically affected 10-year-old sister is referred to as Patient 4. A brother and the parents had an unremarkable phenotype. Patient 1 had short stature (147 cm) and her arm span of 158 cm indicated truncal shortness. However, also the father (160 cm) and one healthy sibling (149 cm) were below the 3rd centile. Patient 2 was at the 3rd centile for height since early childhood. Patient 3 and 4 had clear short stature below the 3rd centile.

A mild global developmental delay and gross motor delay was described for Patients 2 and 3 and failure to thrive was noted in Patients 3 and 4. Skin signs like hypertrichosis or hyperpigmentation as well as macrocephaly, hydrocephaly, or optic nerve compression were absent in all patients. Neither observed were anemia, pancytopenia, hepatosplenomegaly, and recurrent infections.

### 3.2. Radiological phenotype

Since the radiological phenotype of the siblings Patient 3 and 4 is nearly identical only data for Patient 3 is shown while the existing X-rays for Patient 4 can be found in Supplementary Fig. 1. All four patients had similarly pronounced sandwich vertebrae (Fig. 1). However, platyspondyly was most pronounced in Patient 1 (Fig. 1A) and significantly weaker in Patients 2 to 4 (Fig. 1C, E). Moreover, only Patient

**Table 1**
Clinical presentation of four individuals with intermediate osteopetrosis and platyspondyly.

| | Pt 1 | Pt 2 | Pt 3 | Pt 4 | Campeau et al. | Whyte et al. |
|---|---|---|---|---|---|---|
| Gender | Female | Female | Male | Female | Female | Female |
| Age today | 22 y | 11 y and 2 months | 10 y | 5 y | n.d. | 10 y |
| Ethnicity | Turkish | Turkish | Indian | Indian | n.d. | Turkish |
| Consanguinity | Yes | Yes | No | No | Yes | No |
| Affected siblings | No | No | Yes | Yes | n.d. | No |
| Gene | **SLC29A3** | | **TCIRG1** | | | **SLC29A3** |
| Mutation(s) | c.302_303insCTACTTTGAGAGCTACCT (p.Asn101delins) | c.1172C > A (p.Pro391His) | c.117 + 4A > C (paternal) c.2380_2381delCT (p.Ala796fs*34) (maternal) | | (c.1346C > G) p.Thr449Arg | c.607T > C (p.Ser203Pro) c.1157G > A (p.Arg386Gln) |
| Zygosity | Homozygous | Homozygous | Compound heterozygous | | Homozygous | Compound heterozygous |
| *Clinical manifestations (HPO terms)* | | | | | | |
| Sandwich appearance of vertebral bodies (HP:0004618) | Yes | Yes | Yes | Yes | Yes | Yes |
| Flattened vertebrae (HP:0000926) | Yes | Yes | Yes | Yes | Yes | Yes |
| Erlenmeyer flask deformity of the femurs (HP:0004975) | No | No | Yes | Yes | Yes | Yes |
| Coxa vara (HP:0002812) | Yes | Yes | Yes | Yes | Yes | Yes |
| Fractures of the long bones (HP:0003084) | Yes (7 fractures femora) | No | No | Yes (clavicle) | Yes | Yes |
| Dense metaphyseal bands (HP:0100959) | Yes | Yes | Yes | Yes | Yes | Yes |
| Short stature (HP:0004322) | < 3rd centile | 3rd centile (borderline) | < 3rd centile | < 3rd centile | Yes | Yes |
| Thickened ribs (HP:0000900) | Yes | Yes | Yes | Yes | Yes | Yes |
| Osteosclerosis of the calvaria and base of the skull (HP:0005746) | Yes | Yes | Yes | Yes | Yes | Yes |
| Frontal bossing (HP: HP:0002007) | No | No | Yes | No | No | Yes |
| Prominent supraorbital ridges (HP:0000336) | Mild | Yes | No | No | n.d. | Yes |
| Narrow face (HP:0000275) | No | Yes | Yes | No | n.d. | Yes |
| Optic nerve compression (HP:0007807) | No | No | No | No | No | No |
| Failure to thrive (HP:0001508) | No | No | Yes | Yes | No | No |
| Motor delay (HP:0001270) | No | Yes | Yes | No | No | No |
| Mild global developmental delay (HP:0011342) | No | Yes | Yes | n.d. | No | No |
| Anemia (HP:0001903) | Yes (intermittent) | No | No | No | No | No |
| Hepatosplenomegaly (HP:0001433) | No | No | No | No | n.d. | n.d. |
| Abnormality of the teeth (HP:0000164) | Yes (poorly calcified) | Yes | No | No | No | Yes |
| Hyperpigmentation of the skin (HP:0000953) | No | No | No | No | No | Yes |
| Recurrent infections (HP:0002719) | No | No | No | No | Yes | Yes |

n.d. = not determined.

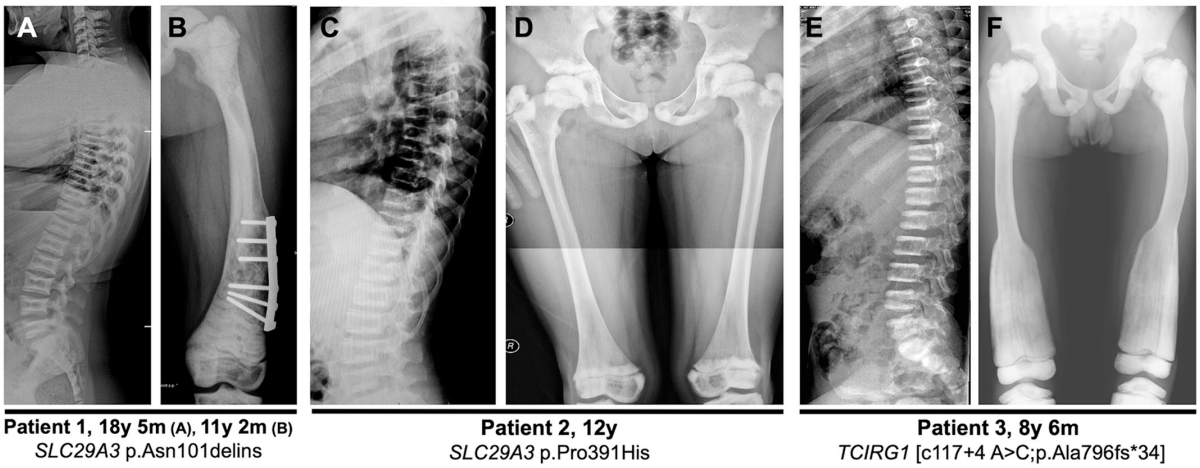


**Fig. 1.** Radiographs of spine and lower extremities. Patient 1 (A, B) presents with diffuse osteosclerosis, reduced translucency in the long bones and pathologic fractures (osteosynthesis material present). The shape of the femur is altered, it appears to be shortened and broadened. The vertebral endplates are dense and the vertebrae flattened. Patient 2 (C, D) reveals sclerosis of the proximal femur, the pelvis and vertebrae, which are mildly flattened. Patient 3 (E, F) presents with bilateral sclerosis of long bones in lower limbs, a modeling defect, Erlenmeyer flask shaped deformity of the tibia, metaphyseal flaring of tibia and femur, and flattened sandwich vertebrae.

1 showed an irregular concave vertebral shape and a bone-within-bone appearance. Thickened ribs were present in all four patients (Fig. 1A, C, E).

Sclerosis of the long bones was strikingly discordant among the four patients. Patient 1 showed patchy metaphyseal osteosclerosis of the femur, humerus, radius, and ulna (Figs. 1B, 2A). The phalanges showed doubled osteosclerotic bands that resulted in a bone-within-bone appearance (Fig. 2B). In Patient 2 narrow sclerotic bands below the growth plate of the proximal and distal femur and the proximal humerus were evident (Figs. 1D, 2C). The phalanges appeared opaque with only very faint metaphyseal sclerotic bands (Fig. 2D). Patients 3 and 4 presented with a rather uniform osteosclerosis of the femora, tibiae and fibulae (Fig. 1F), and prominent sclerotic bands in the metaphyses of metacarpals and phalanges (Fig. 2F). All patients displayed coxa vara (Fig. 1B, D, F). Fractures were reported in Patients 1 and 4. In Patient 1 the supracondylar region of the right femur was fractured at the age of two years. In the following she had in total seven fractures of both femurs, which were surgically treated three times, at the age of

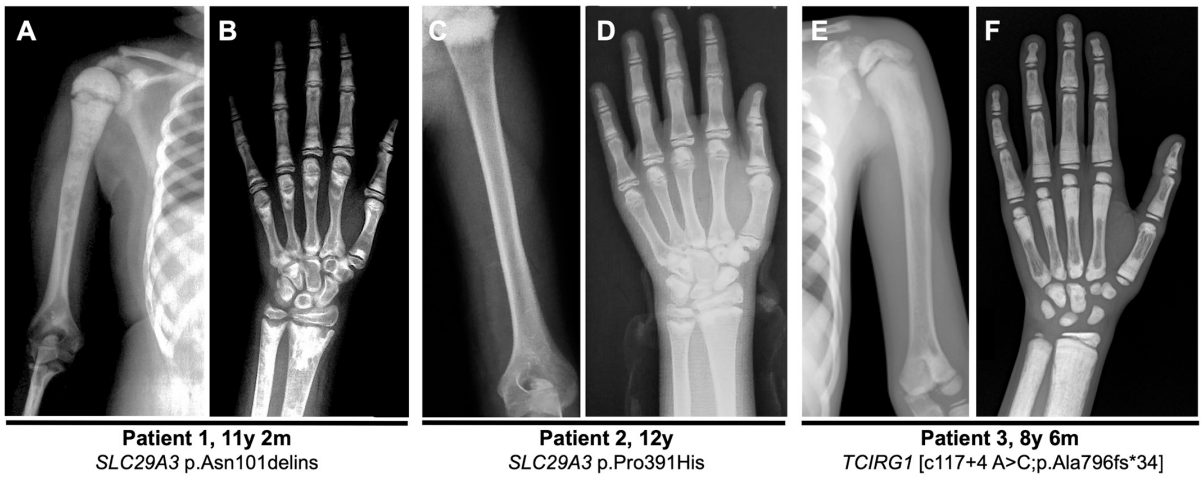


**Fig. 2.** Upper limb radiographs of Patient 1, 2 and 3. (A) Patient 1 presents with sclerotic foci of the humerus in the proximal two thirds and increased corticalis in the distal third of the humerus. The humerus appears slightly broadened and shortened. (B) Radii and ulnae reveal distinct osteosclerosis and a cloudy appearance. Osteosclerotic bands are predominantly present at the growth plates (C) Patient 2 presents with cortical thickening of the humeri and (D) diffuse sclerosis of the digiti, predominantly visible at methaphyseal regions. (E) In Patient 3, the proximal humerus reveals sclerosis and an abnormal curvature. (F) Strong sclerotic bands are present at distal radius and ulna, at the distal end of the metacarpals and the proximal ends of the phalanges.

eight, 12 and 13 years, respectively, with open reduction and internal fixation with plates and screws (Fig. 1B). Patient 4 experienced a fracture of the clavicle at the age of two years.

Long bone modeling defects were most prominent in Patients 3 and 4, who showed extreme metaphyseal flaring leading to Erlenmeyer shaped femora and broadening of the metaphyses of the upper limb bones and abnormal curvature of the humerus (Fig. 1F; Fig. 2E). In Patient 1 femoral shape appeared also altered with overall shortening and broadening in the presence of fractures which complicate the evaluation (Fig. 1B). A mild broadening and shortening was also evident in the humerus in absence of fractures (Fig. 2A). In Patient 2 no modeling defects were visible (Figs. 1D; 2C, D).

Sclerosis of the skull base was noted in all patients (Fig. 3A–E) (Supp. Fig. 1). Calvarial thickening was evident in Patients 2–4. Prominent supraorbital ridges and a narrow face were present in Patient 2 and 3; abnormalities of the teeth (not further specified) were only observed in Patient 2 (Table 1).

In the light of these clinical and radiological findings we speculated that Patient 2 might have autosomal dominant osteopetrosis type 2, whereas for the other patients the diagnoses intermediate autosomal recessive osteopetrosis or dysosteosclerosis seemed more likely.

### 3.3. Mutation analysis

After exclusion of mutations in *CLCN7* as the most likely candidate gene for intermediate and autosomal dominant osteopetrosis, gene panel or whole exome sequencing (WES) were carried out, respectively.

In Patient 1 the homozygous mutation *SLC29A3* c.302_303insCTA CTTTGAGAGCTACCT (p.Asn101delinsAsnTyrPheGluSerTyrLeu) was revealed by gene panel sequencing of the most common genes associated with pathological bone mass changes and confirmed by Sanger sequencing (Fig. 4A) [27]. The parents both carried the variant in a heterozygous state. One of the index' phenotypically unaffected sisters was a heterozygous carrier. Gene panel sequencing also detected the homozygous mutation *SLC29A3* c.1172C > A (p.Pro391His) in exon 6 in Patient 2 (Fig. 4B). No segregation analysis was possible due to absence of DNA samples from further family members. Both *SLC29A3* mutations have not been described before in literature. The insertion found in Patient 1 was neither annotated in ExAC nor in the 1000 Genomes project and ranked disease causing by MutationTaster. The missense mutation in Patient 2 was ranked disease-causing by MutationTaster, PolyPhen, and SIFT. The mutation occurred twice in ExAC in a heterozygous state and has not been detected in the 1000 Genome Project. In the ENT3/SLC29A3 topology model (Fig. 4C) the two mutations lie in the loop between transmembrane helices 1 and 2 and in transmembrane helix 9, respectively. A protein alignment shows complete evolutionary conservation of p.Pro391 (Fig. 4D).

In WES data of Patient 3, the compound heterozygous mutations *TCIRG1* c.117 + 4A > C and c.2380_2381delCT were identified. Segregation analysis confirmed a paternal origin of the c.117 + 4A > C change and a maternal origin for c.2380_2381delCT (Fig. 5 A). The same compound heterozygous mutations were detected in Patient 4 by Sanger Sequencing. In the unaffected sibling only the mutation c.117 + 4A > C was present. Both *TCIRG1* mutations have not been described before. However, the similar variant c.117 + 4A > T was shown to lead to a use of an upstream cryptic splice donor site [1,21]. According to *in silico* analysis with Human Splicing Finder both variants should have similar effects [8]. The deletion c.2380_2381delCT is predicted to cause a frameshift mutation (p.Ala796fs*34) potentially altering the C-terminus of the protein. The estimated location of the frameshift and splice site mutations are highlighted in the topology model of the a3 subunit of the V-ATPase according to Leng et al. [23] (Fig. 5B).


**Fig. 3.** Cranial radiographs of Patient 1 (A, B) and Patient 2 (C, D), and Patient 3 (E) in occipito-frontal (B), anterior-posterior (D), and lateral (A, C, E) exposure. In Patient 1, osteosclerosis of the skull base is revealed (A), but there is no clear evidence for calvarial thickening (B). Patient 2 shows a flat occiput and mild calvarial thickening (C,D). The skull base is mildly sclerotic. The most pronounced calvarial thickening is seen in Patient 3 (E), but sclerosis of the skull base is also rather mild.

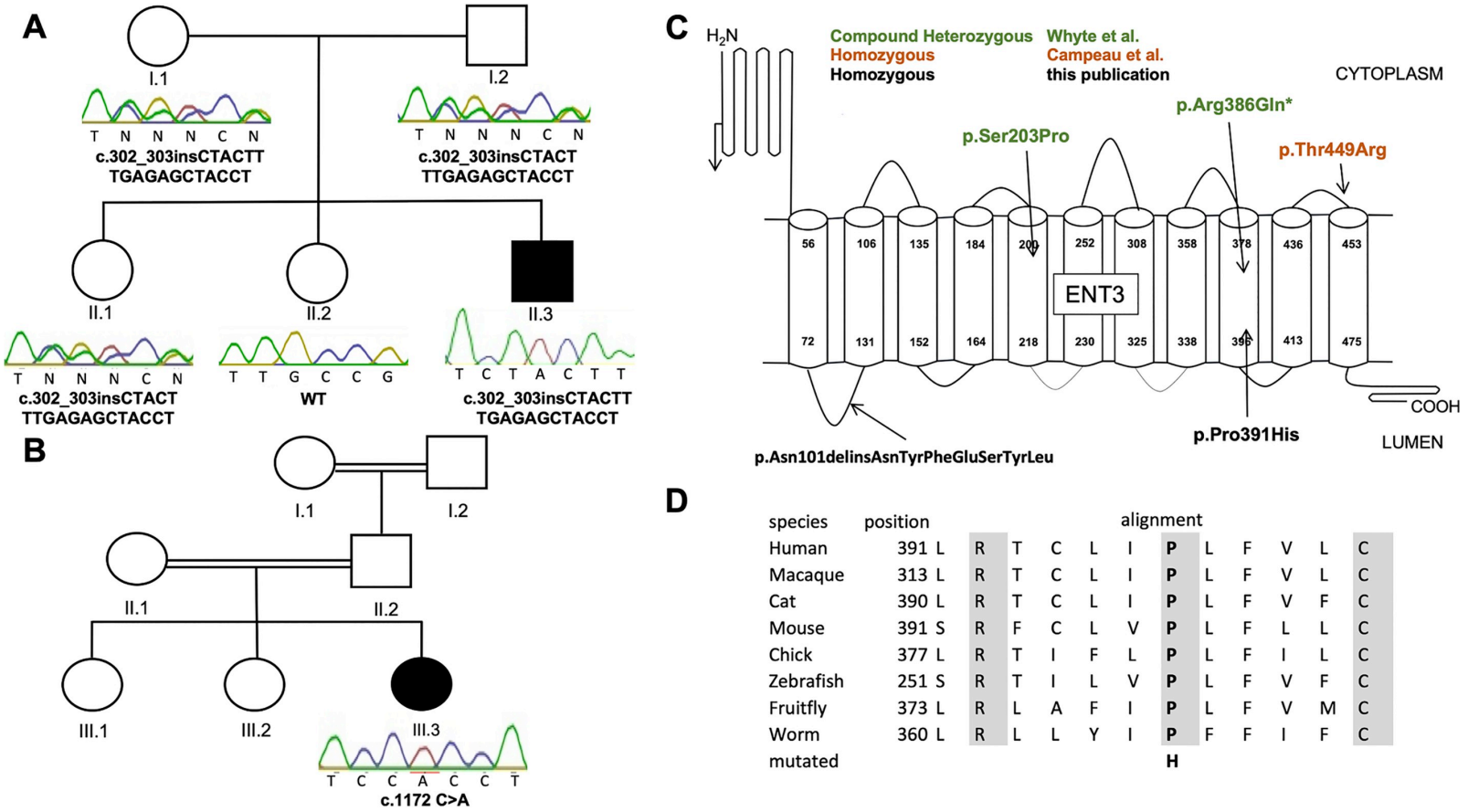


**Fig. 4.** Pedigrees and sequences of the *SLC29A3* mutations. (A) Pedigree of Patient 1. The index (II.3) with proven *SLC29A3* mutation is shown in black. The parents (I.1, II.2) and the youngest sibling of the index are heterozygous carrier of the mutation. (B) Pedigree of Patient 2. The Index (IV.3) is highlighted in black. Sanger Sequencing of *SLC29A3* confirmed the mutation c.1172 C > A, which is highlighted by an arrow. (C) Topology model of ENT3 encoded by *SLC29A3* consisting of 11 transmembrane helices delineating the effect of the mutations of Patients 1 and 2. Arrows mark the location of the mutations described in this paper and the mutations reported by Whyte et al. and Campeau et al.

## 4. Discussion

In this study, we describe two homozygous mutations in *SLC29A3* and two compound heterozygous mutations in *TCIRG1* in four individuals with sandwich vertebrae and different degrees of platyspondyly, sclerosis and modeling defects of long bones compatible with the diagnosis mild or intermediate ARO or DOS.

As shown in Table 1 the two patients with osteosclerotic phenotypes and *SLC29A3* mutations previously published by Whyte et al. and Campeau et al. resemble our Patients 1 and 2, although there are some differences [4,36]. The two patients we describe did not have a history of recurrent infections and no skin changes and Patient 2 neither presented with clear metaphyseal widening, nor with pathologic fractures. The absence of any significant skin findings, lymphadenopathy, or hepatosplenomegaly clearly separate Patients 1 and 2 from the histiocytosis-lymphadenopathy plus spectrum [26]. Only in a part of the reported DOS patients, and only in one of the two DOS patients with *SLC29A3* mutations, macular skin changes were found [4,36]. Therefore, our findings cast doubt on the relevance of this clinical feature for the diagnosis of DOS.

Except for Patient 1 with mild concave deformation of vertebrae, the vertebral shape of our patients is more regular and platyspondyly milder than in many described DOS patients [6,13,14,22,34]. The massive metaphyseal flaring present in Patient 3 and 4 is clearly different from the one found in Patients 1 and 2 and reminds of Pyle's disease (OMIM #265900), as already stated in the original description of DOS by Spranger et al. [34]. In contrast to the rather translucent metaphyses in Pyle's disease the flared metaphyses in Patients 3 and 4 are homogenously opaque. However, the intensity and distribution of bone sclerosis in DOS is high heterogeneous. It can strikingly change over time and metaphyses that were first opaque can become translucent after growth has stopped [14]. The DOS patient with the most similar massive metaphyseal flaring is case 1 reported by Elcioglu et al. [9]. The DOS patient depicted by Houston et al. and Lemire et al. displayed not only distal, but also proximal flaring of the femur leading to a widened femoral neck, which is also seen in Patients 1 and 3 [14,22]. The patient with a homozygous *TCIRG1* splice site mutation c.1941 + 5 G > A after exon 15 described by Sobacchi et al. seems very similar to our Patient 3 and 4, although no platyspondyly is explicitly mentioned [32].

Summarizing the findings in 17 patients diagnosed with DOS, Lemire et al. stressed that although the bone changes are not as severe as in infantile malignant osteopetrosis the clinical course also is aggressive and frequently leads to blindness, mental retardation, and even premature death, although bone marrow failure has never been noticed [22]. Two of our patients had evidence for a mild developmental delay, but in none of them vision was affected, which is also true for the two published DOS cases with *SLC29A3* mutations [4,36]. Recently, a patient with sandwich vertebrae, flattening and uneven shape of vertebrae, fractures, and severe long bone modeling defects was described to harbor a homozygous *TNFRSF11A* splice site mutation at position + 3 [13]. Taken together, defining DOS and separating it from the osteopetroses remains a challenge. *SLC29A3* mutations are not specific for DOS, but also cause histiocytosis-lymphadenopathy plus syndrome. Our Patient 2 indicates that sclerosing bone disorders caused by *SLC29A3* mutation do not always fulfill all criteria for DOS. Since also splice site mutations in *TNFRSF11A* and *TCIRG1* can cause flattened sandwich vertebrae and metaphyseal flaring *SLC29A3* mutations are no specific criterion for DOS. Although this suggests that mild mutations in ARO genes in general may cause this phenotype, it is worth noting that for unknown reasons in patients with biallelic *CLCN7* mutations and non-lethal ARO phenotype no platyspondyly has ever been observed [5,7,18]. The clinical features best distinguishing DOS from intermediate ARO is platyspondyly and a more pronounced tubular modeling defect. Since osteopetroses show a strong clinical variability and the therapeutic approach in severe cases is the same, probably no disadvantage would arise if DOS was lumped together with osteopetrosis.

The equilibrative nucleoside transporter 3 (ENT3) encoded by *SLC29A3* resides in lysosomes and mitochondria where it transports nucleosides and nucleotides when pH is acidic [2,29]. The mutation p.Asn101delinsAsnTyrPheGluSerTyrLeu found in Patient 1 is a novelty since no insertions in the coding region of *SLC29A3* have been described to date. It resides in the luminal loop between transmembrane domains 1 and 2, which plays a role in pH activation of ENT3 [29]. Given that the variant p.Met116Arg within this same loop is retained in the ER, it seems likely that this elongated mutant protein shares the same fate [17]. The mutation c.1172C > A (p.Pro391His) found in Patient 2 is nearest to the mutation p.Arg386Gln described in a subject with DOS [4]. Both missense mutations reside in transmembrane helix 9 of ENT3. The exchange of the completely conserved proline residue can be predicted to have severe functional consequences leading to lysosomal accumulation of nucleosides and nucleotides perturbing osteoclast differentiation or function. Our findings underline the great clinical heterogeneity of disorders caused by mutations in *SLC29A3* and the lack of a clear genotype-phenotype correlation. In fact, the mutation p.Arg386Gln (highlighted by * in Fig. 4C) was found in a homozygous state in a patient with histiocytosis-lymphadenopathy plus syndrome [10] and in a heterozygous state in a patient with DOS in combination with a second heterozygous missense mutation [36]. The germline knockout of *Slc29a3* in mice causes a histiocytosis phenotype [15]. Thus, it can be speculated that mutations leading to DOS do not entail a complete loss of ENT3 function. More mutations and functional investigations are needed to get a clearer picture.

*TCIRG1* encodes the a3 subunit that anchors the V-ATPase complex to the ruffled membrane of osteoclasts that shares many properties with the lysosomal membrane [33]. It is surprising that the previously published homozygous mutation c.117 + 4A > T causes classical infantile malignant ARO, whereas c.117 + 4A > C in combination with p.Ala796fs*34 entails intermediate ARO [21]. One explanation is increased residual expression of the wildtype transcript from the allele with the splice site alteration. Another explanation could be that p.Ala796fs*34 leads to a stable C-terminally altered protein with retained function. The most similar mutation is p.Glu791fs*27 described by Frattini et al. in a patient with classical ARO [11].

In summary, we add another two cases to the small group of patients with sandwich vertebrae and platyspondyly due to *SLC29A3* mutations. However, our findings also indicate that not all these patients fulfill the criteria for DOS. On the other hand, intermediate ARO due to *TCIRG1* splice site mutations can present with signs of dysosteosclerosis. This underlines the close phenotypic overlap of all osteosclerotic disorders caused by dysfunctional osteoclasts independent of the underlying genetic defect.

Supplementary data to this article can be found online at https://doi.org/10.1016/j.bone.2018.12.002.

## Conflicts of interest

None.

## Acknowledgments

We are grateful to the patients and family members whose cooperation made this study possible. This study was supported by the Berlin Institute of Health (BIH). This project has received funding from the European Community's Seventh Framework Programme under grant agreement no. 602300 (SYBIL) and the German Federal Ministry of Education and Research (BMBF) within the project “Detection and Individualized Management of Early Onset Osteoporosis (DIMEOS)”.

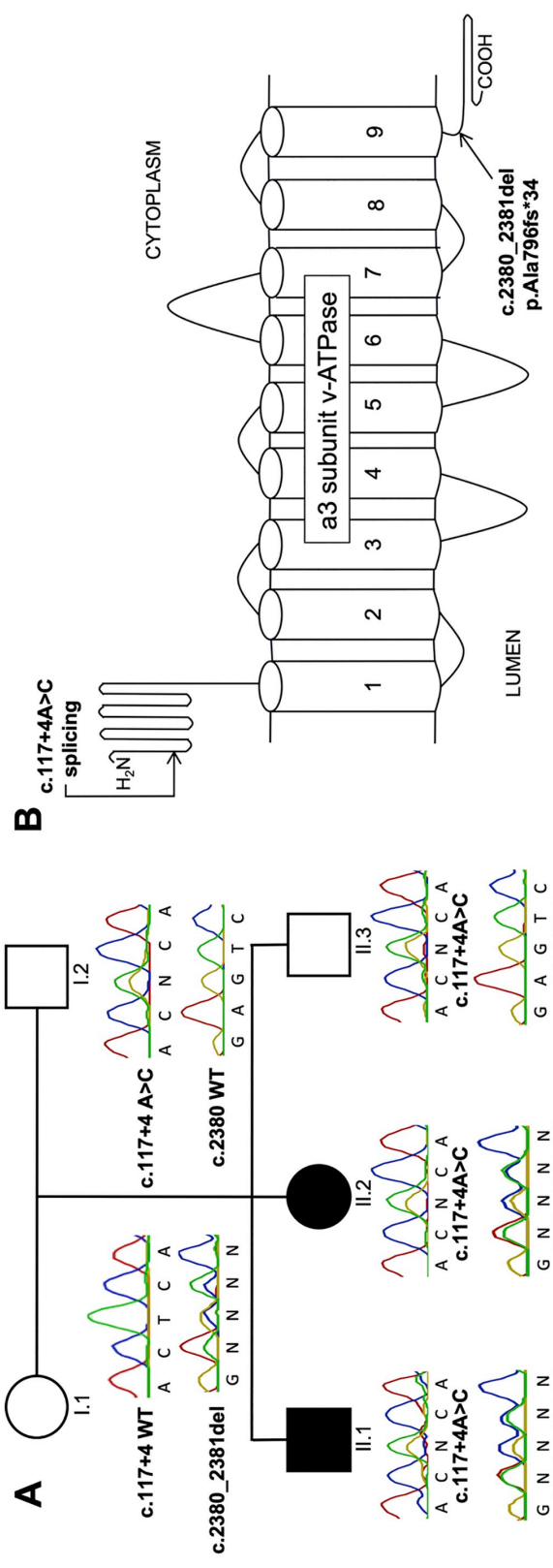


**Fig. 5.** Pedigree, sequences, topology model and splicing effect illustrating the impact of the *TCIRG1* mutations. (A) Pedigree of the family of patient 3 (II.1) and 4 (II.2). Affected individuals with mutations in *TCIRG1* are shown in black. (B) A model of the V-ATPase a3 subunit according to Leng et al. [9] with the estimated locations of the mutations.

## Web resources

The URLs for data presented herein are as follows:

Ensembl Genome Browser, http://www.emsembl.org

Exome Variant Server, NHLBI GO Exome Sequencing Project (ESP), Seattle, WA, http://evs.gs.washington.edu/EVS/

GeneTalk, http://www.gene-talk.de/

Mutation Taster, http://www.mutationtaster.org/

Online Mendelian Inheritance in Man (OMIM), http://www.ncbi.nlm.nih.gov/omim

PolyPhen2, http://genetics.bwh.harvard.edu/pph2/

SIFT, http://sift.jcvi.org/www/SIFT_enst_submit.html

Uniprot, www.uniprot.org

Human Spicing Finder, http://www.umd.be/HSF3/index.html

## References


[1] S.L. Anderson, C. Jalas, A. Fedick, K.F. Reid, T.O. Carpenter, D. Chirnomas, N.R. Treff, J. Ekstein, B.Y. Rubin, A founder mutation in the TCIRG1 gene causes osteopetrosis in the Ashkenazi Jewish population, Clin. Genet. 88 (2015) 74–79.

[2] S.A. Baldwin, S.Y. Yao, R.J. Hyde, A.M. Ng, S. Foppolo, K. Barnes, M.W. Ritzel, C.E. Cass, J.D. Young, Functional characterization of novel human and mouse equilibrative nucleoside transporters (hENT3 and mENT3) located in intracellular membranes, J. Biol. Chem. 280 (2005) 15880–15887.

[3] O.D. Benichou, J.D. Laredo, M.C. de Vernejoul, Type II autosomal dominant osteopetrosis (Albers-Schonberg disease): clinical and radiological manifestations in 42 patients, Bone 26 (2000) 87–93.

[4] P.M. Campeau, J.T. Lu, G. Sule, M.M. Jiang, Y. Bae, S. Madan, W. Hogler, N.J. Shaw, S. Mumm, R.A. Gibbs, M.P. Whyte, B.H. Lee, Whole-exome sequencing identifies mutations in the nucleoside transporter gene SLC29A3 in dysosteosclerosis, a form of osteopetrosis, Hum. Mol. Genet. 21 (2012) 4904–4909.

[5] A.B. Campos-Xavier, J.M. Saraiva, L.M. Ribeiro, A. Munnich, V. Cormier-Daire, Chloride channel 7 (CLCN7) gene mutations in intermediate autosomal recessive osteopetrosis, Hum. Genet. 112 (2003) 186–189.

[6] D. Chitayat, K. Silver, E.M. Azouz, Skeletal dysplasia, intracerebral calcifications, optic atrophy, hearing impairment, and mental retardation: nosology of dysosteosclerosis, Am. J. Med. Genet. 43 (1992) 517–523.

[7] E. Cleiren, O. Benichou, E. Van Hul, J. Gram, J. Bollerslev, F.R. Singer, K. Beaverson, A. Aledo, M.P. Whyte, T. Yoneyama, M.C. deVernejoul, W. Van Hul, Albers-Schonberg disease (autosomal dominant osteopetrosis, type II) results from mutations in the ClCN7 chloride channel gene, Hum. Mol. Genet. 10 (2001) 2861–2867.

[8] F.O. Desmet, D. Hamroun, M. Lalande, G. Collod-Beroud, M. Claustres, C. Beroud, Human Splicing Finder: an online bioinformatics tool to predict splicing signals, Nucleic Acids Res. 37 (2009) e67.

[9] N.H. Elcioglu, A. Vellodi, C.M. Hall, Dysosteosclerosis: a report of three new cases and evolution of the radiological findings, J. Med. Genet. 39 (2002) 603–607.

[10] M. Farooq, R.M. Moustafa, A. Fujimoto, H. Fujikawa, O. Abbas, A.G. Kibbi, M. Kurban, Y. Shimomura, Identification of two novel mutations in SLC29A3 encoding an equilibrative nucleoside transporter (hENT3) in two distinct Syrian families with H syndrome: expression studies of SLC29A3 (hENT3) in human skin, Dermatology 224 (2012) 277–284.

[11] A. Frattini, P.J. Orchard, C. Sobacchi, S. Giliani, M. Abinun, J.P. Mattsson, D.J. Keeling, A.K. Andersson, P. Wallbrandt, L. Zecca, L.D. Notarangelo, P. Vezzoni, A. Villa, Defects in TCIRG1 subunit of the vacuolar proton pump are responsible for a subset of human autosomal recessive osteopetrosis, Nat. Genet. 25 (2000) 343–346.

[12] A. Frattini, A. Pangrazio, L. Susani, C. Sobacchi, M. Mirolo, M. Abinun, M. Andolina, A. Flanagan, E.M. Horwitz, E. Mihci, L.D. Notarangelo, U. Ramenghi, A. Teti, J. Van Hove, D. Vujic, T. Young, A. Albertini, P.J. Orchard, P. Vezzoni, A. Villa, Chloride channel ClCN7 mutations are responsible for severe recessive, dominant, and intermediate osteopetrosis, J. Bone Miner. Res. 18 (2003) 1740–1747.

[13] L. Guo, N.H. Elcioglu, O.K. Karalar, M.O. Topkar, Z. Wang, Y. Sakamoto, N. Matsumoto, N. Miyake, G. Nishimura, S. Ikegawa, Dysosteosclerosis is also caused by TNFRSF11A mutation, J. Hum. Genet. 63 (2018) 769–774.

[14] C.S. Houston, J.W. Gerrard, E.J. Ives, Dysosteosclerosis, AJR Am. J. Roentgenol. 130 (1978) 988–991.

[15] C.L. Hsu, W. Lin, D. Seshasayee, Y.H. Chen, X. Ding, Z. Lin, E. Suto, Z. Huang, W.P. Lee, H. Park, M. Xu, M. Sun, L. Rangell, J.L. Lutman, S. Ulufatu, E. Stefanich, C. Chalouni, M. Sagolla, L. Diehl, P. Fielder, B. Dean, M. Balazs, F. Martin, Equilibrative nucleoside transporter 3 deficiency perturbs lysosome function and macrophage homeostasis, Science 335 (2012) 89–92.

[16] T. Kamphans, P.M. Krawitz, GeneTalk: an expert exchange platform for assessing rare sequence variants in personal genomes, Bioinformatics 28 (2012) 2515–2516.

[17] N. Kang, A.H. Jun, Y.D. Bhutia, N. Kannan, J.D. Unadkat, R. Govindarajan, Human equilibrative nucleoside transporter-3 (hENT3) spectrum disorder mutations impair nucleoside transport, protein localization, and stability, J. Biol. Chem. 285 (2010) 28343–28352.

[18] P.N. Kantaputra, S. Thawanaphong, W. Issarangporn, P. Klangsinsirikul, A. Ohazama, P. Sharpe, C. Supanchart, Long-term survival in infantile malignant autosomal recessive osteopetrosis secondary to homozygous p.Arg526Gln mutation in CLCN7, Am. J. Med. Genet. A 158A (2012) 909–916.

[19] U. Kornak, D. Kasper, M.R. Bosl, E. Kaiser, M. Schweizer, A. Schulz, W. Friedrich, G. Delling, T.J. Jentsch, Loss of the ClC-7 chloride channel leads to osteopetrosis in mice and man, Cell 104 (2001) 205–215.

[20] U. Kornak, S. Mundlos, Genetic disorders of the skeleton: a developmental approach, Am. J. Hum. Genet. 73 (2003) 447–474.

[21] U. Kornak, A. Schulz, W. Friedrich, S. Uhlhaas, B. Kremens, T. Voit, C. Hasan, U. Bode, T.J. Jentsch, C. Kubisch, Mutations in the a3 subunit of the vacuolar H(+)-ATPase cause infantile malignant osteopetrosis, Hum. Mol. Genet. 9 (2000) 2059–2063.

[22] E.G. Lemire, S. Wiebe, Clinical and radiologic findings in an adult male with dysosteosclerosis, Am. J. Med. Genet. A 146A (2008) 474–478.

[23] X.H. Leng, T. Nishi, M. Forgac, Transmembrane topography of the 100-kDa a subunit (Vph1p) of the yeast vacuolar proton-translocating ATPase, J. Biol. Chem. 274 (1999) 14655–14661.

[24] C. Letizia, A. Taranta, S. Migliaccio, C. Caliumi, D. Diacinti, E. Delfini, E. D'Erasmo, M. Iacobini, M. Roggini, O.M. Albagha, S.H. Ralston, A. Teti, Type II benign osteopetrosis (Albers-Schonberg disease) caused by a novel mutation in CLCN7 presenting with unusual clinical manifestations, Calcif. Tissue Int. 74 (2004) 42–46.

[25] A. McKenna, M. Hanna, E. Banks, A. Sivachenko, K. Cibulskis, A. Kernytsky, K. Garimella, D. Altshuler, S. Gabriel, M. Daly, M.A. DePristo, The Genome Analysis Toolkit: a MapReduce framework for analyzing next-generation DNA sequencing data, Genome Res. 20 (2010) 1297–1303.

[26] V. Molho-Pessach, I. Lerer, D. Abeliovich, Z. Agha, A. Abu Libdeh, V. Broshtilova, O. Elpeleg, A. Zlotogorski, The H syndrome is caused by mutations in the nucleoside transporter hENT3, Am. J. Hum. Genet. 83 (2008) 529–534.

[27] J. Mrosk, G.S. Bhavani, H. Shah, J. Hecht, U. Kruger, A. Shukla, U. Kornak, K.M. Girisha, Diagnostic strategies and genotype-phenotype correlation in a large Indian cohort of osteogenesis imperfecta, Bone 110 (2018) 368–377.

[28] E. Palagano, H.C. Blair, A. Pangrazio, I. Tourkova, D. Strina, A. Angius, G. Cuccuru, M. Oppo, P. Uva, W. Van Hul, E. Boudin, A. Superti-Furga, F. Faletra, A. Nocerino, M.C. Ferrari, G. Grappiolo, M. Monari, A. Montanelli, P. Vezzoni, A. Villa, C. Sobacchi, Buried in the middle but guilty: intronic mutations in the TCIRG1 gene cause human autosomal recessive osteopetrosis, J. Bone Miner. Res. 30 (2015) 1814–1821.

[29] M.F. Rahman, C. Askwith, R. Govindarajan, Molecular determinants of acidic pH-dependent transport of human equilibrative nucleoside transporter 3, J. Biol. Chem. 292 (2017) 14775–14785.

[30] B.M. Rashid, N.G. Rashid, A. Schulz, G. Lahr, B.F. Nore, A novel missense mutation in the CLCN7 gene linked to benign autosomal dominant osteopetrosis: a case series, J. Med. Case Rep. 7 (7) (2013).

[31] J.M. Schwarz, C. Rodelsperger, M. Schuelke, D. Seelow, MutationTaster evaluates disease-causing potential of sequence alterations, Nat. Methods 7 (2010) 575–576.

[32] C. Sobacchi, A. Pangrazio, A.G. Lopez, D.P. Gomez, M.E. Caldana, L. Susani, P. Vezzoni, A. Villa, As little as needed: the extraordinary case of a mild recessive osteopetrosis owing to a novel splicing hypomorphic mutation in the TCIRG1 gene, J. Bone Miner. Res. 29 (2014) 1646–1650.

[33] C. Sobacchi, A. Schulz, F.P. Coxon, A. Villa, M.H. Helfrich, Osteopetrosis: genetics, treatment and new insights into osteoclast function, Nat. Rev. Endocrinol. 9 (2013) 522–536.

[34] J. Spranger, C. Albrecht, H.J. Rohwedder, H.R. Wiedemann, Dysosteosclerosis–a special form of generalized osteosclerosis, Fortschr Geb Rontgenstr Nuklearmed 109 (1968) 504–512.

[35] K. Wang, M. Li, H. Hakonarson, ANNOVAR: functional annotation of genetic variants from high-throughput sequencing data, Nucleic Acids Res. 38 (2010) e164.

[36] M.P. Whyte, D. Wenkert, W.H. McAlister, D.V. Novack, A.R. Nenninger, X. Zhang, M. Huskey, S. Mumm, Dysosteosclerosis presents as an "osteoclast-poor" form of osteopetrosis: comprehensive investigation of a 3-year-old girl and literature review, J. Bone Miner. Res. 25 (2010) 2527–2539.

[37] X.Y. Zhang, J.W. He, W.Z. Fu, C. Wang, Z.L. Zhang, Novel mutations of TCIRG1 cause a malignant and mild phenotype of autosomal recessive osteopetrosis (ARO) in four Chinese families, Acta Pharmacol. Sin. 38 (2017) 1456–1465.

## Supplementary Data

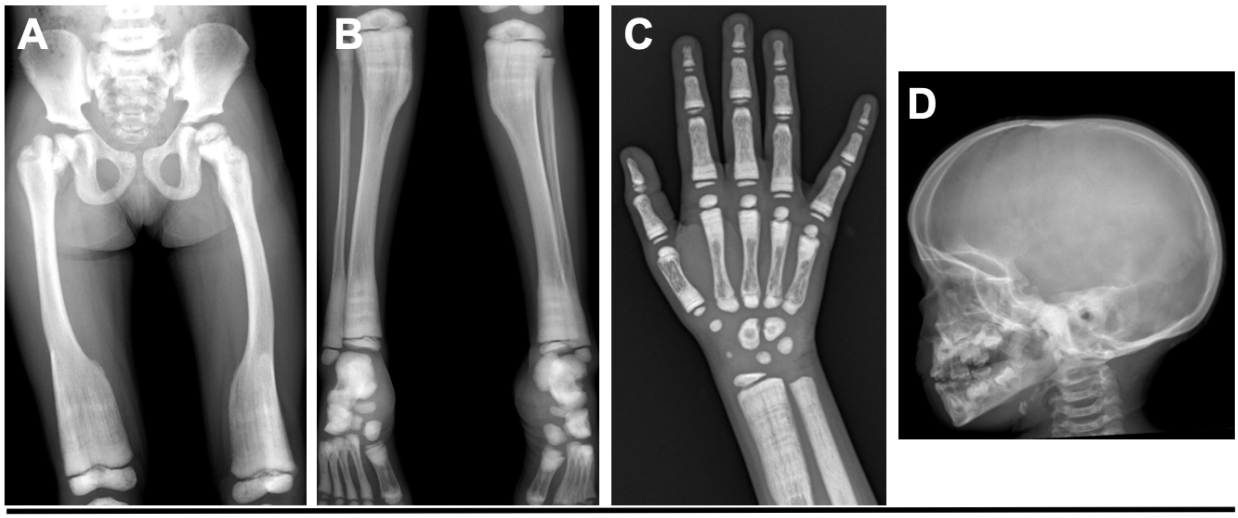


**Patient 4, 4y 9m** *TCIRG1* [c117+4 A>C;p.Ala796fs*34]

Supplementary Fig.1

**Supplementary Table 1. Genes contained in gene panel**

| | | | |
|---|---|---|---|
| ACP5 | ESR1 | MAFB | SOST |
| ADAMTS2 | FAM123B | MMP2 | SP7 |
| ALPL | FAM20C | OSTM1 | SPP1 |
| ANKH | FBLN5 | PHEX | TBXAS1 |
| ARP6V0A2 | FERMT3 | PLEKHM1 | TCIRG1 |
| BMP1 | FGF23 | PLOD1 | TGFB1 |
| BMP2 | FKBP10 | PLOD2 | TMEM38B |
| CAS2 | GJA1 | PPIB | TNFRSF11A |
| CASR | GORAB | PTH1R | TNFRSF11B |
| CLCN7 | HPGD | PYCR1 | TNFRSF11 |
| COL1A1 | IFITM5 | RASGRP2 | TREM2 |
| COL1A2 | IKBKG | RUNX2 | TYROBP |
| CRTAP | LMED3 | SERPINF1 | VDR |
| CTSK | LEPRE1 | SERPINH1 | WNT1 |
| DLX3 | LMNA | SLC29A3 | WNT16 |
| DMP1 | LRP4 | SLC34A3 | ZMPSTE24 |
| EFEMP2 | LRP5 | SLC39A13 | |
| ENPP1 | LRP6 | SNX10 | |

**Supplementary Table 2. Pathogenicity predictions for all variants**

| Patient | Clinical findings | Mutation | State | ExAC | 1000 Genomes | HumanSplicing Finder | Mutation Taster | Poly Phen | SIFT |
|---|---|---|---|---|---|---|---|---|---|
| 1 | Diffuse osteosclerosis, translucency of the long bones, flattened vertebrae, pathologic fractures | SLC29A3 c.302_303insCTACTTTGAGAGCTACCT (p.Asn101delinsAsnTyrPheGluSerTyrLeu) | homozygous | not annotated | not annotated | Alteration of splicing | D.C. | n.a. | n.a. |
| 2 | Osteosclerosis of the proximal femur, the pelvis and vertebrae | SLC29A3 c.1172C>A (p.Pro391His) | homozygous | 2/121392 (heterozygous); not annotated in homozygous state | not annotated | No changes | D.C. | D.C. | D.C. |
| 3 | Sclerosis of the proximal humerus, modeling defect, metaphysel flaring of tibia and femur, sandwich vertebrae | TCIRG1 c.117+4A>C (paternal) | compound heterozygous | 9/118758 (heterozygous) | not annotated | Alteration of splicing | D.C. | ? | ? |
| | | TCIRG1 c.2380_2381delCT (maternal) (p.Ala796fs*34) | compound heterozygous | not annotated | not annotated | Alteration of splicing | D.C. | D.C. | D.C. |

D.C. = disease causing
n.a. = not applicable

**Howaldt, A.,** S. Nampoothiri, D. Yesodharan, S. Udayakumaran, P. Subash, and U. Kornak,

**Four novel mutations in EFNB1 in Indian patients with craniofrontonasal syndrome.**

J Hum Genet, 2019. 64(9): p. 867-873. [61]

https://doi.org/10.1038/s10038-019-0638-9

Journal of Human Genetics (2019) 64:867–873
https://doi.org/10.1038/s10038-019-0638-9

ARTICLE

# Four novel mutations in *EFNB1* in Indian patients with craniofrontonasal syndrome

Antonia Howaldt[1] · Sheela Nampoothiri[2] · Dhanya Yesodharan[2] · Suhas Udayakumaran[3] · Pramod Subash[4] · Uwe Kornak[1,5,6]

Received: 18 February 2019 / Accepted: 21 June 2019 / Published online: 8 July 2019


## Abstract

Craniofrontonasal syndrome (CFNS) (OMIM #304110) is a very rare, X-linked developmental disorder characterized by facial stigmata, including hypertelorism, frontonasal dysplasia, craniosynostosis, bifid nasal tip, and digital abnormalities. CFNS is caused by mutations in the Ephrin 1 gene (*EFNB1*) located at Xq13.1, which encodes the transmembrane protein Ephrin B1. Interestingly, heterozygous females are more severely affected than hemizygous males. We report on four individuals from four unrelated Indian families with mild-to-severe CFNS. All patients had variable degrees of hypertelorism and nasal bridge depression, which did not correlate with changes in other tissues. Although patients 3 and 4 showed the most severe facial dysmorphism and syndactyly, there were no structural CNS changes or developmental delay. In contrast, patient 1 displayed agenesis of corpus callosum and developmental delay, although facial and finger abnormalities were milder. Patients 1, 2, and 4 showed different degrees of clefting. DNA sequencing revealed four previously undescribed heterozygous mutations in exons 1 and 2 of *EFNB1*. Patient 1 carried the second single amino acid deletion reported up to date. The other three affected individuals harbored frameshift mutations, leading to premature termination codons. Our findings broaden the spectrum of *EFNB1* mutations and illustrate the absence of an obvious correlation between mutation type, severity, and expression of symptoms.

## Introduction

Craniofrontonasal syndrome (CFNS) (OMIM #304110) has first been described in 1979 by Cohen [1]. It is an X-linked disorder caused by mutations in the Ephrin B1 gene *(EFNB1)*, which is located on the short arm of the X chromosome (Xp13.1) [2]. The paucity of male CFNS patients has been described in the literature [3]. It is known that heterozygous females are more severely affected than hemizygous males [4–6]. In females, characteristic abnormalities include severe hypertelorism, depressed nasal bridge, and coronal synostosis. Occasionally, cleft lip and palate, diaphragmatic hernias, and corpus callosum agenesis or dysgenesis are present. Hemizygous males show no or mild signs, such as hypertelorism. Longitudinal ridging of the nails, syn- or poly-dactyly, and wiry hair commonly occur in CFNS [2, 5–7].

**Supplementary information** The online version of this article (https://doi.org/10.1038/s10038-019-0638-9) contains supplementary material, which is available to authorized users.

✉ Uwe Kornak
uwe.kornak@charite.de

[1] Institute for Medical Genetics and Human Genetics, Charité—Universitätsmedizin Berlin, corporate member of Freie Universität Berlin, Humboldt-Universität zu Berlin, and Berlin Institute of Health, Berlin, Germany

[2] Division of Paediatric Genetics, Amrita Institute of Medical Sciences and Research Centre, Cochin, Kerala, India

[3] Division of Paediatric Neurosurgery, Amrita Institute of Medical Sciences and Research Centre, Cochin, Kerala, India

[4] Division of Craniomaxillofacial surgery, Amrita Institute of Medical Sciences and Research Centre, Cochin, Kerala, India

[5] Max Planck Institute for Molecular Genetics, Berlin, Germany

[6] BIH Center for Regenerative Therapies, Charité—Universitätsmedizin Berlin, corporate member of Freie Universität Berlin, Humboldt-Universität zu Berlin, and Berlin Institute of Health, Berlin, Germany

*EFNB1* codes for Ephrin B1, which is a transmembrane protein of 346 amino acids (ENST00000204961.4). Ephrin B1 binds to Eph receptor kinases [8]. Eph/ephrin complexes play crucial roles in neural development and plasticity, as well as morphogenesis through formation of boundaries [9, 10]. Twigg et al. [11] proved that the *Efnb1* expression is particularly high in murine neural crest cells. While the complete loss of *Efnb1* in mice is perinatally lethal, female *Efnb1*$^{+/-}$ mutants exhibit dysmorphic features characteristic of CNFS, which are absent in hemizygous males [12]. This phenomenon might be explained by difficulties establishing boundaries in the mosaic state arising from X inactivation intermingling *EFNB1*-negative and *EFNB1*-positive cells [13]. In hemizygous males, the function of EFNB1 might be taken over by a related ephrin.

To date, a total of 116 mutations in *EFNB1* have been described, the majority of which are missense mutations, followed by the occurrence of small deletions and splice-site mutations. Here, we report on four additional patients from four different families who carry four novel *EFNB1* mutations and demonstrate clinical variability in CFNS.

## Materials and methods

### Sanger sequencing

Written informed consent of the patients was acquired prior to genetic testing. DNA was obtained from the whole-blood samples. The five exons and exon–intron boundaries of *EFNB1* (NM_004429) were amplified using oligonucleotide primers. Primer pairs were 5′-AGAAGAGCGACAC CGAAGC-3′ and 5′- AGACCTCCCCACATGCACT-3′ yielding a 379-bp product for exon 1, 5′- CCTGAGGCTG ACCATCTTCT-3′ and 5′- GTTAAGCCCAGGGAGAG AGC-3′ resulting in a 357-bp product for exon 2, 5′-TGGG AGTTTCTGGGTAATGC-3′ and 5′-CTGTTCCAAAGGT CAAACAGG-3′ yielding a 223-bp product for exon 3, 5′-A TGACTGAGGGCACCTATGC-3′ and 5′-GGGCCTAAC AAGGTGACAGA-3′ yielding a 250-bp product for exon 4, and 5′-GCCTGAAATCTGCTGTGTGT-3′ and 5′-AA ATACAAAGGTGGGCACAG-3′ yielding a 585-bp product for exon 5. The PCR products were sequenced on an ABI3730xl DNA Analyzer (Applied Biosystems).

### Mutation analysis

The sequencing data were compared with the *EFNB1* cDNA reference sequence GenBank accession number NM_004429 and analyzed using the software Geneious [14]. Further in silico analysis of the mutations was performed by the prediction tools MutationTaster [15] and Human Splicing Finder [16].

### Ephrin ectodomain 3D model

The ectodomain structure of the closely related Ephrin B2 (1iko) was uploaded to the CCP4 software [17, 18]. The residues Ile63, Cys64, and Cys101 were projected as ball-and-stick structures onto the ribbon-type protein model.

## Results

### Clinical presentation

The clinical findings of the four unrelated female patients are summarized in Table 1 and the corresponding images are shown in Figs. 1 and 2. All patients described in this paper are the first children of Indian origin born to non-consanguineous parents, who did not show any signs of CFNS.

**Patient 1** was referred for dysmorphic evaluation and developmental delay. Hypothyroidism was diagnosed in the newborn period and treated with 25 µg thyroxine. On examination at the age of 6 months, she presented with a weight of 5.5 kg (<3rd centile), length of 64 cm (3rd centile), and head circumference of 39.5 cm (<3rd centile). Head control was attained. She had a coarse face, a hoarse voice, a small anterior fontanel, significant hypertelorism, bilateral epicanthic folds, bilateral low-set ears, macrostomia, a tongue tie, a thick upper midline frenulum, a microform cleft upper lip, and a short neck. She had an extremely flat nasal bridge, anteverted nares, and a midline crease of the tip of the nose (Fig. 1a). Brachydactyly and hyperelasticity of finger joints were evident (Fig. 2a). The inspection of the feet revealed a bilateral splintering of the big toes (Fig. 2b, c) and a medially deviated third toe with bilateral undertoeing (Fig. 2c). Magnetic resonance imaging (MRI) showed agenesis of corpus callosum.

**Patient 2** was born at term by normal delivery (birth weight 3.85 kg (75−90th centile)) and started to crawl at 5 months of age. Clinical examination demonstrated a head circumference of 39 cm (3rd centile), a small anterior fontanel, a coarse face, hypertelorism, downslanting palpebral fissures, brachycephaly, a small cleft of the upper lip, low-set overfolded pinna, a high-arched palate, and a short neck (Fig. 1b). No interdigital webbing or abnormalities of fingers and toes were present. A brain MRI at the age of 5 months revealed a corpus callosum (callosal) dysgenesis. She had a unicoronal synostosis (anterior plagiocephaly) and underwent fronto-orbital advancement and hypertelorism correction. At 2 ½ years of age, she had a weight of 10 kg (<3rd centile), height 85 cm (3rd centile), and head circumference of 44 cm (<3rd centile). She could walk without support but had unclear speech.

**Table 1** Clinical features and genotype of four individuals with craniofrontonasal syndrome

| | Patient 1, female | Patient 2, female | Patient 3, female | Patient 4, female |
|---|---|---|---|---|
| Age at examination | 5 months | 2 years 6 months | 4 years 6 months | 16 years |
| Consanguinity | No | No | No | No |
| *EFNB1* mutation screening | | | | |
| DNA level | c.186_188delCAT | c.404_405insTACATTAC | c.196_197insC | c.43_43delG |
| Protein level | p.Ile63del | p.Ser136Thrfs*26 | p.Arg66Profs*9 | p.Ala15Argfs*31 |
| Exon (E); zygosity | E 2; heterozygous | E 2; heterozygous | E 2; heterozygous | E 1; heterozygous |
| Clinical manifestations (HPO terms) | | | | |
| Hypertelorism (HP:0000316) | ++ | ++ | +++ | +++ |
| Epicanthus (HP:0000286) | Yes | No | No | No |
| Downslanting palpebral fissures (HP:0000494) | + | + | ++ | ++ |
| Anteverted nares (HP:0000463) | Yes | Yes | No | No |
| Depressed nasal bridge (HP:0005280) | Yes | Yes | Yes | Yes |
| Midline nasal groove (HP:0004112) | Yes | Yes | Yes | Yes |
| Abnormality of the pinna (HP:0000377) | No | Yes | No | No |
| Low-set ears (HP:0000369) | Yes | Yes | Yes | Yes |
| Coarse facial features (HP:0000280) | Yes | Yes | No | No |
| Midface retrusion (HP:0011800) | No | No | Yes | No |
| Micrognathia (HP:0000347) | Yes | Yes | Yes | Yes |
| High palate (HP:0000218) | No | Yes | Yes | Yes |
| Anterior open bite (HP:0200095) | No | No | Yes | Yes |
| Cleft upper lip (HP:0000204) | Yes | Yes | No | Yes |
| Bilateral cleft lip and palate (HP:0002744) | No | No | No | No |
| Ankyloglossia (HP:0010296) | No | No | No | No |
| Hoarse voice (HP:0001609) | Yes | No | No | No |
| Short neck (HP:0000470) | Yes | Yes | Yes | Yes |
| Small anterior fontanel (HP:0000237) | Yes | Yes | No | No |
| Dysgenesis of corpus callosum (HP:0006996) | No | Yes | No | No |
| Agenesis of corpus callosum (HP:0001274) | Yes | No | No | No |
| Plagiocephaly (HP:0001357) | Yes | Yes | Yes | No |
| Craniostenosis (HP:0001363) | Yes | Yes | Yes | Yes |
| Global developmental delay (HP:0001263) | Yes | No | No | No |
| Brachydactyly (HP:0001156) | Yes | No | Yes | No |
| Broad thumb (HP:0011304) | No | No | Yes | No |
| 3,4 syndactyly (HP:0006097) | No | No | Yes | Yes |
| Partial duplication of the distal phalanx of the fourth finger (HP:0009981) | No | No | No | Yes |
| Longitudinal ridging of toe nails (HP:001807) | Yes | Yes | Yes | Yes |
| Longitudinal ridging of finger nails (HP:001807) | No | No | Yes | Yes |
| Shoulder girdle muscle atrophy (HP:0003724) | No | No | Yes | Yes |
| Limited Shoulder movement (HP:0006467) | No | No | Yes | Yes |
| Low-set nipples (HP:0002562) | No | No | Yes | Yes |

**Patient 3** had an unremarkable family history. She showed normal development and intelligence. On examination at the age of 4 ½ years, her height was measured at 98 cm (3rd centile) and the head circumference at 48 cm (<3rd centile). Examination of the face revealed plagiocephaly and severe hypertelorism, a broad nasal root and tip, antimongoloid slant of the eyes, prognathism, and an anterior open bite (Fig. 1c). Cranial imaging showed unilateral left-sided coronal craniostenosis. She underwent fronto-orbital advancement for correction of unilateral coronal synostosis and facial bipartition for correction of hypertelorism. The neck was short and showed webbing,

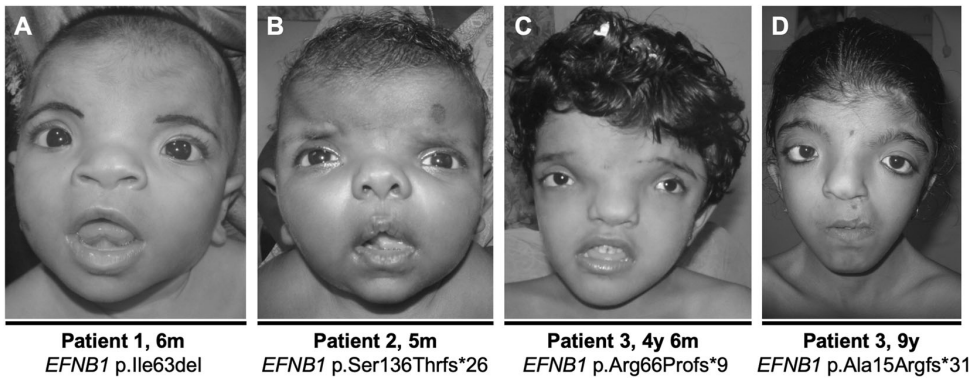


**Fig. 1** Variable craniofacial features of four female CFNS patients. All patients present with hypertelorism, depressed nasal bridge, and low-set ears. Patient 1 (**a**) and patient 2 (**b**) present with anteverted nares, patient 2 additionally with a high palate and a cleft upper lip. Patient 3 (**c**) and patient 4 (**d**) show downslanting palpebral fissures. Patient 3 additionally presents with midface retrusion, anterior open bite, and short neck, patient 4 with cleft upper lip and orbital dystopia

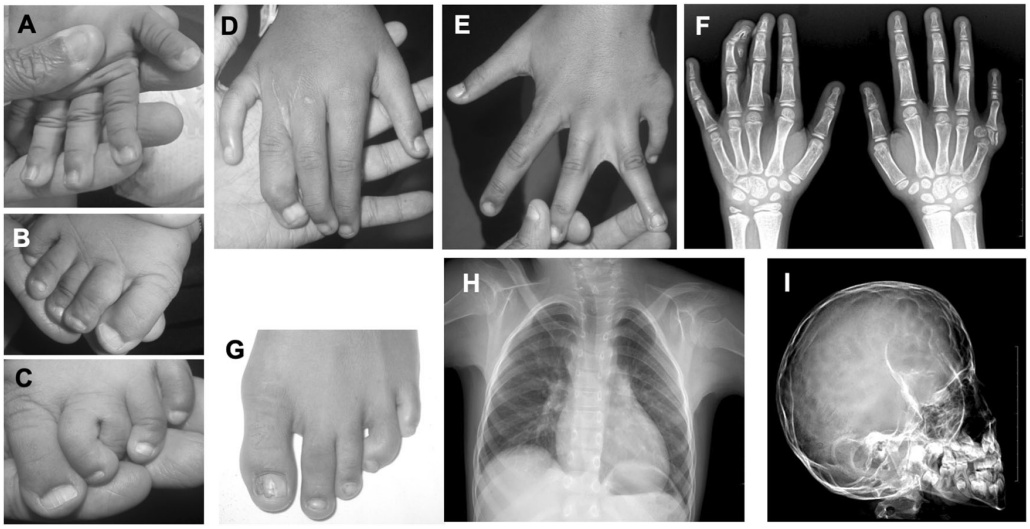


**Fig. 2** Additional skeletal findings. Upper and lower extremities of patient 1 (**a–c**) and patient 4 (**d–h**). Patient 1 presents with **a** brachydactyly and a broad thumb, **b** bilateral undertoeing, and **c** a medially deviated third toe of the left foot. Patient 2 presents with **d** complete III–IV syndactyly of the right hand (operated) with fused nails at the fourth finger and **e** partial cutaneous III/IV syndactyly of the left hand. **g** Longitudinal ridging of the left big toe. **f** Radiographs revealed an osseous duplication of the middle and distal phalanges of the fourth finger of the left hand, **h** high ridging scapula with elongated clavicles, and **i** lateral view of skull shows severe craniostenosis with copper beaten appearance

the chest was flattened, and the nipples were low placed. The patient was unable to elevate the shoulders completely, with prominent wasting of infraclavicular muscles. Dysmorphic features of the hands included a complete III/IV syndactyly of the left hand and a partial cutaneous syndactyly of the fingers 2–5 on the right hand. Longitudinal ridging of big toes and other toes was detected and significantly more distinct on the left side.

**Patient 4** presented with a broad nasal root and tip, downslanting palpebral fissures, severe hypertelorism, and anterior open bite with normal intelligence (Fig. 1d). She had a webbed neck, dropping of shoulders, pectus excavatum, and low-lying and asymmetrical nipples. The inspection of the extremities revealed complete cutaneous III–IV syndactyly of the right hand, which was surgically treated (Fig. 2d), partial cutaneous III/IV syndactyly of the left hand (Fig. 2e), and longitudinal ridging of third fingers of both hands. Longitudinal ridging of the big toes and other toes was also evident and more distinct on the left side (Fig. 2g). Radiographs revealed an osseous duplication of middle and distal phalanges of the fourth finger of the right hand (Fig. 2f). She had left postal axial polydactyly, which

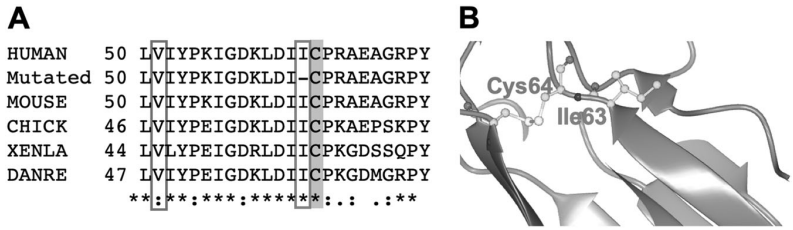


**Fig. 3** Consequences of the p.Ile63del mutation. **a** Alignment of the p.Ile63del mutation (red box) identified in patient 1 and the previously found single amino acid deletion p.Val51del (blue box). The adjacent Cys64 cysteine residue is marked in orange. Note the high evolutionary conservation of the sequence harboring both mutations. **b** A 3D model of the EFNB1 ectodomain showing the secondary structure as ribbon and side chains of the amino acids Ile63 and Cys64 as ball and stick (green = carbon, red = oxygen, and blue = nitrogen). The deleted Ile63 lies at the end of a β-sheet (gray arrow) and the adjacent cysteine forms an essential disulfide bridge (yellow), which—by prediciton—will get lost as a consequence of the deletion

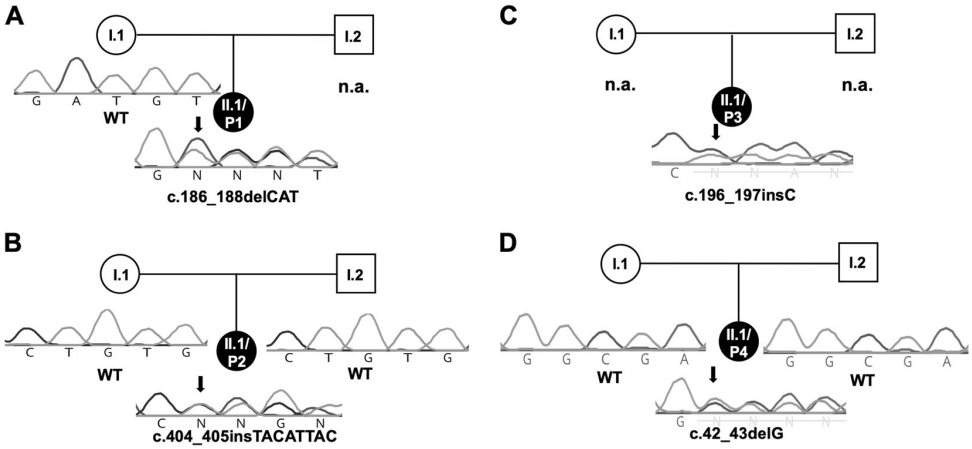


**Fig. 4** Pedigrees and segregation of mutations found in CFNS patients. Sanger validation and segregation of the *EFNB1* mutations c.186_188delCAT in patient 1 (**a**), c.404_405insTACATTAC (p.S136Tfs*26) patient 2 (**b**), c.196_197insC (p.Arg66Profs*9) in patient 3 (**c**), and c.42_43delG (p.Ala15Argfs*31) in patient 4 (**d**)

was excised, and left-sided cleft lip and palate, which was surgically repaired during infancy. She had a large fossa ovalis, an atrial septal defect which was corrected by device closure at 9 ½ years of age. The patient also had a high-ridging scapula with elongated clavicles (Fig. 2h) and severe craniostenosis with copper-beaten appearance (Fig. 2i). Bicoronal synostoses with brachycephaly were evident and she underwent hypertelorism correction by facial bipartition technique and maxillary distraction.

In all four cases, CFNS was the suspected diagnosis, but for patient 2, the differential diagnosis of Teebi-type hypertelorism (OMIM #145420) was also considered.

## Mutation analysis

Since the clinical findings were suggestive of CFNS, we amplified *EFNB1* by PCR and analyzed the gene by Sanger sequencing. This revealed four heterozygous mutations in exons 1 and 2 of *EFNB1* in the index patients, which were not listed in ExAC, gnomAD, or the 1000 genomes project. Investigation of the available parent DNAs revealed wild-type sequences. An overview of the Sanger sequencing and segregation testing is shown in Fig. 4, and bioinformatic pathogenicity predictions are summarized in Supplementary Table 1.

The heterozygous mutation c.186_188delCAT (p.Ile63del) in exon 2 detected in **patient 1** affects a highly conserved amino acid in the extracellular ephrin domain next to a cysteine residue forming a disulfide bridge (Fig. 3a, b). The mutation was confirmed by Sanger sequencing, but could not be detected in the index' mother (Fig. 4a). DNA of the father was not available. The variant is ranked pathogenic due to high amino acid conservation, but no splice alterations are predicted (ACMG class: likely pathogenic).

**Patient 2** carries the mutation *EFNB1* c.404_405insTACATTAC (p.Ser136Thrfs*26) (Fig. 4b). In silico analysis by the Human Splicing Finder indicates a possible alteration of splicing (ACMG class: pathogenic). In **patient 3**, the mutation *EFNB1* c.196_197insC

(p.Arg66Profs*9) was detected (Fig. 4c). No DNA from other family members was available. According to in silico analysis with the Human Splicing Finder, the original exonic splicing enhancer site is altered or broken in the setting of the mutation, most likely causing an alteration of splicing (ACMG class: likely pathogenic). The mutation c.42_43delG (p.Ala15Argfs*31) was found in **patient 4** (Fig. 4d). Sequencing of the parents revealed a wild-type sequence. The activation of an exonic cryptic donor splice site is predicted by the Human Splicing Finder (ACMG class: pathogenic).

## Discussion

In this study, we describe four female individuals from four different Indian families with characteristic stigmata of CFNS. By a targeted screening approach through Sanger sequencing, we found four novel disease-causing mutations in the *EFNB1* gene, three of them are frameshift mutations and one is a small deletion.

All mutations described were neither annotated in ExAC nor in the 1000 genomes project. The heterozygous mutation *EFNB1* c.186_188delCAT (p.Ile63del) in patient 1 is located in the highly conserved extracellular ephrin domain, which is crucial for receptor ligand recognition and complex formation [19]. This mutation is the only one of our series, for which no significant effect on splicing is predicted. The only single amino acid deletion reported so far is c.151_153delGTG (p.Val51del) described by Twigg et al. [3], which is in the vicinity of p.Ile63del. The two female carriers of this mutation exclusively revealed typical facial features and coronal craniosynostosis. The phenotype of patient 1 is considerably more severe, especially due to corpus callosum agenesis and developmental delay. In how far the latter might also be attributable to hypothyroidism is currently unknown. The strong effect of the p.Ile63del mutation is surprising, since it deletes one of the two consecutive isoleucine residues. We hypothesize that due to this deletion, the cysteine at position 64 loses its ability to form a disulfide bridge with cysteine 101, which is a strong stabilizer of the tertiary protein structure. The variant most similar to c.404_405insTACATTAC (p.Ser136Thrfs*26) found in patient 2 is c.296_297delTCinsGGTGCTCG (p.Thr100Valfs*62) reported by Inoue et al. [20]. The affected patient had hypertelorism, depressed nasal bridge, bifid nasal tip, bicoronal synostosis, and bilateral cleft lip and palate. No mutations similar to c.196_197insC (p.Arg66-Profs*9) and c.42_43delG (p.Ala15Argfs*31) detected in patients 3 and 4, respectively, have been reported to date.

Mutations with premature termination codons (PTCs) are known to cause nonsense-mediated mRNA decay (NMD) or lead to severely truncated, instable proteins. In some cases, an escape of NMD is possible. We predict that the frameshift mutations described in patients 2, 3, and 4 lead to alternative splicing and result in NMD, with an overall loss-of-function effect. The mutations p.Val51del and p.Ile63del demonstrate how sensitive the Ephrin B1 protein is toward alterations of such kind and support the prediction that even if alternative splicing leads to in-frame products, the resulting larger deletions will also have a loss-of-function effect. Chacon-Camacho et al. [21] analyzed the truncating mutation EFNB1 c.445_449delGAGGG in exon 3 at the expression level and detected a severe decrease in the expression level of EFNB1 mRNA, which confirmed the degradation by NMD. Since no patient RNA was available for our studies, we could not perform investigations on the RNA level.

The facial changes in patients 3 and 4 are more pronounced than in patients 1 and 2. On the other hand, patients 1 and 2 had corpus callosum anomalies. An explanation for the phenotype variability could be the random X inactivation in females, which has been described in CFNS patients [22]. In heterozygous females, the X inactivation causes a somatic mosaicism, in which cells with defective *EFNB1* on their active X chromosome are functionally *EFNB1* null mutants. In this mosaic pattern, a higher share of mutated cells brings about a more severe phenotype and can thus explain the range in CFNS severity. Carrel and Willard [23] showed that the escape of X inactivation could contribute to the interindividual phenotypic differences of heterozygous females.

Some syndromes caused by mutations in different genes have overlapping features with CFNS. Three types of frontonasal dysplasia (FND) are caused by mutations in different genes. Type 1 (FND1, OMIM #136760) is caused by mutations in *ALX3*, Type 2 by mutations in *ALX4* (FND2, OMIM #613451), and Type 3 by mutations in *ALX1* (FND3, OMIM #613456) [24]. Acrofacial dysostosis (AFD1, OMIM #154400), also known as Nager syndrome, is caused by mutations in *SF3B4*. In addition to craniofacial features similar to CFNS, they have characteristic upper-extremity deformities, but no lower-extremity involvement [25]. Acromelic frontonasal dysostosis (OMIM #603671) is another rare syndrome similar to CFNS caused by heterozygous mutations in *ZSWIM6*. It comprises craniofacial malformations similar to CFNS (e.g., FND and corpus callosum agenesis), as well as nonfacial traits, e.g., brain and limb malformations (tibial hemimelia and preaxial polydactyly) [26].

In conclusion, CFNS can be accounted as part of a spectrum disorder of craniofacial and limb anomalies. Our findings broaden the spectrum of *EFNB1* mutations and demonstrate that there is no obvious genotype–phenotype correlation, since the deletion of a single N-terminal amino acid has the same effect as mutations leading to PTCs.

**Acknowledgements** We would like to acknowledge Prof. Raoul C. Hennekam, Department of Pediatrics, AMC, The Netherlands) for providing the expert opinion on the phenotypic evaluation of the index cases. We are grateful to the patients and family members, whose cooperation made this study possible. This study was supported by the Berlin Institute of Health.

## Compliance with ethical standards

**Conflict of interest** The authors declare that they have no conflict of interest.

**Web resources:** The URLs for data presented herein are as follows: Ensembl Genome Browser, http://www.emsembl.org. Mutation Taster, http://www.mutationtaster.org/. Online Mendelian Inheritance in Man (OMIM), http://www.ncbi.nlm.nih.gov/omim. Human Splicing Finder, http://www.umd.be/HSF3/HSF.shtml. Geneious, https://www.geneious.com/. Protein Data Bank in Europe, https://www.ebi.ac.uk/pdbe/entry/pdb/1iko



## References

1. Cohen MM, Jr. Craniofrontonasal dysplasia. Birth Defects Orig Artic Ser. 1979;15:85–9.
2. Wieland I, Jakubiczka S, Muschke P, Cohen M, Thiele H, Gerlach KL, et al. Mutations of the ephrin-B1 gene cause craniofrontonasal syndrome. Am J Hum Genet. 2004;74:1209–15.
3. Twigg SR, Matsumoto K, Kidd AM, Goriely A, Taylor IB, Fisher RB, et al. The origin of EFNB1 mutations in craniofrontonasal syndrome: frequent somatic mosaicism and explanation of the paucity of carrier males. Am J Hum Genet. 2006;78:999–1010.
4. Devriendt K, Van Mol C, Fryns JP. Craniofrontonasal dysplasia: more severe expression in the mother than in her son. Genet Couns. 1995;6:361–4.
5. Grutzner E, Gorlin RJ. Craniofrontonasal dysplasia: phenotypic expression in females and males and genetic considerations. Oral Surg Oral Med Oral Pathol. 1988;65:436–44.
6. Morris CA, Palumbos JC, Carey JC. Delineation of the male phenotype in carniofrontonasal syndrome. Am J Med Genet. 1987;27:623–31.
7. Wieacker P, Wieland I. Clinical and genetic aspects of craniofrontonasal syndrome: towards resolving a genetic paradox. Mol Genet Metab. 2005;86:110–6.
8. Davis S, Gale NW, Aldrich TH, Maisonpierre PC, Lhotak V, Pawson T, et al. Ligands for EPH-related receptor tyrosine kinases that require membrane attachment or clustering for activity. Science. 1994;266:816–9.
9. Pasquale EB. Eph receptor signalling casts a wide net on cell behaviour. Nat Rev Mol Cell Biol. 2005;6:462–75.
10. Klein R. Eph/ephrin signaling in morphogenesis, neural development and plasticity. Curr Opin Cell Biol. 2004;16:580–9.
11. Twigg SR, Kan R, Babbs C, Bochukova EG, Robertson SP, Wall SA, et al. Mutations of ephrin-B1 (EFNB1), a marker of tissue boundary formation, cause craniofrontonasal syndrome. Proc Natl Acad Sci USA. 2004;101:8652–7.
12. Davy A, Aubin J, Soriano P. Ephrin-B1 forward and reverse signaling are required during mouse development. Genes Dev. 2004;18:572–83.
13. Davy A, Bush JO, Soriano P. Inhibition of gap junction communication at ectopic Eph/ephrin boundaries underlies craniofrontonasal syndrome. PLoS Biol. 2006;4:e315.
14. Kearse M, Moir R, Wilson A, Stones-Havas S, Cheung M, Sturrock S, et al. Geneious basic: an integrated and extendable desktop software platform for the organization and analysis of sequence data. Bioinformatics. 2012;28:1647–9.
15. Schwarz JM, Rodelsperger C, Schuelke M, Seelow D. MutationTaster evaluates disease-causing potential of sequence alterations. Nat Methods. 2010;7:575–6.
16. Desmet FO, Hamroun D, Lalande M, Collod-Beroud G, Claustres M, Beroud C. Human Splicing Finder: an online bioinformatics tool to predict splicing signals. Nucleic Acids Res. 2009;37:e67.
17. McNicholas S, Potterton E, Wilson KS, Noble ME. Presenting your structures: the CCP4mg molecular-graphics software. Acta Crystallogr D Biol Crystallogr. 2011;67:386–94.
18. Toth J, Cutforth T, Gelinas AD, Bethoney KA, Bard J, Harrison CJ. Crystal structure of an ephrin ectodomain. Dev Cell. 2001;1:83–92.
19. Makarov R, Steiner B, Gucev Z, Tasic V, Wieacker P, Wieland I. The impact of CFNS-causing EFNB1 mutations on ephrin-B1 function. BMC Med Genet. 2010;11:98.
20. Inoue Y, Sakamoto Y, Sugimoto M, Inagaki H, Boda H, Miyata M, et al. A family with craniofrontonasal syndrome: the first report of familial cases of craniofrontonasal syndrome with bilateral cleft lip and palate. Cleft Palate Craniofacial J. 2018;55:1026–9.
21. Chacon-Camacho OF, Arce-Gonzalez R, Villegas-Ruiz V, Pelcastre-Luna E, Uria-Gomez CE, Granillo-Alvarez M, et al. Identification and expression analysis of a novel intragenic EFNB1 mutation causing craniofrontonasal syndrome. Meta Gene. 2014;2:25–31.
22. Wieland I, Makarov R, Reardon W, Tinschert S, Goldenberg A, Thierry P, et al. Dissecting the molecular mechanisms in craniofrontonasal syndrome: differential mRNA expression of mutant EFNB1 and the cellular mosaic. Eur J Hum Genet. 2008;16:184–91.
23. Carrel L, Willard HF. X-inactivationprofile reveals extensive variability in X-linked gene expression in females. Nature. 2005;434:400–4.
24. Sedano HO, Cohen MM Jr, Jirasek J, Gorlin RJ. Frontonasal dysplasia. J Pediatr. 1970;76:906–13.
25. Bernier FP, Caluseriu O, Ng S, Schwartzentruber J, Buckingham KJ, Innes AM, et al. Haploinsufficiency of SF3B4, a component of the pre-mRNA spliceosomal complex, causes Nager syndrome. Am J Hum Genet. 2012;90:925–33.
26. Smith JD, Hing AV, Clarke CM, Johnson NM, Perez FA, Park SS, et al. Exome sequencing identifies a recurrent de novo ZSWIM6 mutation associated with acromelic frontonasal dysostosis. Am J Hum Genet. 2014;95:235–40.

# Supplementary Data

**Supplementary Table 1. Characterization of EFNB1 variants**

| ID | Mutation | State | ExAC | 1000 Genomes | Human Splicing Finder | Mutation Taster | ACMG Class |
|---|---|---|---|---|---|---|---|
| **Patient 1** | c.186_188delCAT; p.(Ile63del) | heterozygous | not annotated | not annotated | no changes | disease causing | likely pathogenic |
| **Patient 2** | c.404_405insTACATTAC; p.(Ser136Thrfs*26) | heterozygous | not annotated | not annotated | alteration of splicing | disease causing | pathogenic |
| **Patient 3** | c.196_197insC; p.(Arg66Profs*9) | heterozygous | not annotated | not annotated | alteration of splicing | disease causing | likely pathogenic |
| **Patient 4** | c.43_43delG; p.(Ala15Argfs*31) | heterozygous | not annotated | not annotated | alteration of splicing | disease causing | pathogenic |

**Howaldt, A.,** A.F. Hennig, T. Rolvien, U. Rössler, N. Stelzer, A. Knaus, S. Böttger, J. Zustin, S. Geißler, R. Oheim, M. Amling, H.P. Howaldt, and U. Kornak, **Adult Osteosclerotic Metaphyseal Dysplasia With Progressive Osteonecrosis of the Jaws and Abnormal Bone Resorption Pattern Due to a LRRK1 Splice Site Mutation.** J Bone Miner Res, 2020. **35**(7): p. 1322-1332. [62]

https://doi.org/10.1002/jbmr.3995

ORIGINAL ARTICLE

JBMR®

# Adult Osteosclerotic Metaphyseal Dysplasia With Progressive Osteonecrosis of the Jaws and Abnormal Bone Resorption Pattern Due to a *LRRK1* Splice Site Mutation

Antonia Howaldt,[1,2] Anna Floriane Hennig,[1,2,3] Tim Rolvien,[4,5] Uta Rössler,[1,2] Nina Stelzer,[1,2] Alexej Knaus,[6] Sebastian Böttger,[7] Jozef Zustin,[4] Sven Geißler,[2] Ralf Oheim,[4] Michael Amling,[4] Hans-Peter Howaldt,[7] and Uwe Kornak[1,2,8,9]

[1]Institut für Medizinische Genetik und Humangenetik, Charité – Universitätsmedizin Berlin, Corporate Member of Freie Universität Berlin, Humboldt-Universität zu Berlin, and Berlin Institute of Health, Berlin, Germany
[2]BIH Center for Regenerative Therapies, Charité – Universitätsmedizin Berlin, Corporate Member of Freie Universität Berlin, Humboldt-Universität zu Berlin, and Berlin Institute of Health, Berlin, Germany
[3]Freie Universität Berlin, Berlin, Germany
[4]Department of Osteology and Biomechanics, University Medical Center Hamburg-Eppendorf, Hamburg, Germany
[5]Department of Orthopedics, University Medical Center Hamburg-Eppendorf, Hamburg, Germany
[6]Institute for Genomic Statistics and Bioinformatics, University Hospital Bonn, Rheinische Friedrich-Wilhelms-Universität Bonn, Bonn, Germany
[7]Department for Maxillo Facial Surgery, Justus Liebig University Gießen, Gießen, Germany
[8]Max Planck Institute for Molecular Genetics, Berlin, Germany
[9]Institute of Human Genetics, University Medical Center Göttingen, Göttingen, Germany

**ABSTRACT**

Osteosclerotic metaphyseal dysplasia (OSMD) is a rare autosomal recessive sclerosing skeletal dysplasia. We report on a 34-year-old patient with sandwich vertebrae, platyspondyly, osteosclerosis of the tubular bones, pathologic fractures, and anemia. In the third decade, he developed osteonecrosis of the jaws, which was progressive in spite of repeated surgical treatment over a period of 11 years. An iliac crest bone biopsy revealed the presence of hypermineralized cartilage remnants, large multinucleated osteoclasts with abnormal morphology, and inadequate bone resorption typical for osteoclast-rich osteopetrosis. After exclusion of mutations in *TCIRG1* and *CLCN7* we performed trio-based exome sequencing. The novel homozygous splice-site mutation c.261G>A in the gene *LRRK1* was found and co-segregated with the phenotype in the family. cDNA sequencing showed nearly complete skipping of exon 3 leading to a frameshift (p.Ala34Profs*33). Osteoclasts differentiated from the patient's peripheral blood monocytes were extremely large. Instead of resorption pits these cells were only capable of superficial erosion. Phosphorylation of L-plastin at position Ser5 was strongly reduced in patient-derived osteoclasts showing a loss of function of the mutated LRRK1 kinase protein. Our analysis indicates a strong overlap of *LRRK1*-related OSMD with other forms of intermediate osteopetrosis, but an exceptional abnormality of osteoclast resorption. Like in other osteoclast pathologies an increased risk for progressive osteonecrosis of the jaws should be considered in OSMD, an intermediate form of osteopetrosis. © 2020 The Authors. *Journal of Bone and Mineral Research* published by American Society for Bone and Mineral Research.

**KEY WORDS:** LRRK1; NEXT GENERATION SEQUENCING; OSTEOPETROSIS; OSTEOSCLEROTIC METAPHYSEAL DYSPLASIA; TRIO-BASED EXOME SEQUENCING


Received in original form October 16, 2019; revised form February 14, 2020; accepted February 27, 2020. Accepted manuscript online March 2, 2020.
Address correspondence to: Prof. Uwe Kornak, MD, PhD, Charité – Universitätsmedizin Berlin, Institute of Medical Genetics and Human Genetics, Augustenburger Platz 1, 13353 Berlin, Germany. E-mail: uwe.kornak@charite.de
Additional Supporting Information may be found in the online version of this article.
The peer review history for this article is available at https://publons.com/publon/10.1002/jbmr.3995.

Journal of Bone and Mineral Research, Vol. 35, No. 7, July 2020, pp 1322–1332.
DOI: 10.1002/jbmr.3995

## Introduction

Osteosclerotic metaphyseal dysplasia (OSMD; OMIM #615198) is a rare sclerosing skeletal dysplasia first described by Nishimura and Kozlowski in 1993.[1] It is characterized by osteosclerosis of the long bones (predominantly at the metaphyses) and vertebrae, ribs, clavicles, and iliac crest. Developmental delay, hypodontia, and seizures were also reported to be part of the clinical picture.[1] It is a very rare autosomal-recessive disease with a prevalence of <1:1,000,000, caused by mutations in the leucine-rich repeat kinase 1 (*LRRK1*) gene. To date, four families with five affected individuals carrying biallelic *LRRK1* mutations have been reported.[2–4] LRRK1 is a protein of the ROCO family composed of four ankyrin repeat (ANK) domains, seven leucine-rich (LRR) domains, a Ras of complex proteins (Roc) guanosine triphosphatase (GTPase) domain, a C-terminal of Roc (COR) domain, a serine/threonine kinase-domain, and WD40 domain.[5,6] In murine osteoclasts it was shown to play a role in bone resorption by regulating the formation of the sealing zone.[7] Lrrk1 associates with C-terminal Src-kinase (Csk) and phosphorylates the cellular Rous sarcoma oncogene c-Src as well as the actin regulating proteins L-plastin and Cdc42.[8,9]

Osteonecrosis of the jaw (ONJ) was described by Edwards and colleagues in 2002 as a side effect of treatment with antiresorptive drugs such as intravenous bisphosphonates.[10] Risk factors for medication-related osteonecrosis of the jaws (MRONJ) include diabetes, malignancies, oral surgical procedures, and poor oral hygiene,[11,12] ONJ has also be observed in patients with osteopetrosis.[13,14]

Here, we report on a patient with severe ONJ and clinical, radiological, and histological signs of osteoclast-rich osteopetrosis caused by a *LRRK1* splice site mutation. We compare this case with other patients of *LRRK1*-related OSMD and describe the effect of the loss of the LRRK1 kinase on the function of human osteoclasts.

## Patients and Methods

### Biopsy studies

An iliac crest bone biopsy was obtained to further characterize the detailed skeletal characteristics. The specimen was fixed in 3.7% formaldehyde, dehydrated, embedded in methyl methacrylate, and cut on a microTec rotation microtome (CVT 4060E; microTec, Walldorf, Germany). Five-micrometer (5-µm) sections were stained by toluidine blue, trichrome Masson-Goldner, and von Kossa. Histomorphometric analysis was performed according to the ASBMR standards[15] and compared to reference values.[16]

Additionally, the bone mineralization density distribution (BMDD) in the trabecular bone was analyzed by quantitative backscattered electron imaging (qBEI; LEO 435 VP; LEO Electron Microscopy Ltd., Cambridge, UK) as described.[17] Six images per specimen were taken (magnification ×100) and evaluated using a custom MATLAB-based program (TheMathWorks, Inc., Natick, MA, USA). Histomorphometry and BMDD values were furthermore compared to previously published patients with CLCN7-related autosomal dominant osteopetrosis type II[16] as well as to reference values from the literature.[18]

### Next generation sequencing

Before next generation sequencing was initiated, mutations in *TCIRG1* and *CLCN7* were excluded by Sanger sequencing. For the patient, the two siblings and his parents, libraries for trio-based exome sequencing (WES) were prepared using NEBNext DNA Library Prep Master Mix Set for Illumina (New England BioLabs, Ipswich, MA, USA). Enrichment of the target regions was done using the SureSelect Human Exome Kit V6 (Agilent Technologies, Santa Clara, CA, USA) and run on a HiSeq 2500 Sequencer (Illumina, San Diego, CA, USA) with a 150-bp paired-end sequence length. The sequences were aligned to the human genome (GRCh37) with Burrows-Wheeler Alignment tool (BWA)[19] and the variants were detected with the Genome Analysis Toolkit (GATK), version 2.6 (https://gatk.broadinstitute.org/hc/en-us).[20] The exome genotyping accuracy was estimated to be above 0.9999 based on the variant calls.[21] Variants were detected with SAMtools (http://www.htslib.org/), annotated with ANNOVAR (http://annovar.openbioinformatics.org/en/latest/).[22] All exons with pathogenic variants in ClinVar (NIH, NCBI, Bethesda, MD, USA; https://www.ncbi.nlm.nih.gov/clinvar/) were covered at a minimum of 20 reads. Ninety-five percent (95%) of the remnant exome target region was also covered by more than 20 reads.

### Bioinformatic filtering of variants

The variants were analyzed by the Gene-Talk platform[23] and the pathogenic potential of individual candidate variants was evaluated by MutationTaster (http://www.mutationtaster.org/).[24] For further analysis, we only analyzed homozygous variants that were not represented by more than three individuals in the 1000 Genomes Project (https://www.internationalgenome.org/) cohort, Genome Aggregation Database (gnomAd; https://gnomad.broadinstitute.org/) or Exome Aggregation Consortium (ExAC[25]) and which were not annotated as benign polymorphisms by MutationTaster.

### PCR and Sanger sequencing

The respective exons and exon–intron boundaries of *LRRK1* (NM_024652) were amplified using oligonucleotide primers (sequences available upon request) and sequenced on an ABI3730xl DNA Analyzer (Applied Biosystems, Foster City, CA, USA).

### Culturing of patient mesenchymal stem cells and osteoblasts

Primary human osteoblasts and mesenchymal stem cells (MSCs) were received from the Core-Facility "Tissue Harvesting" of the Berlin Institute of Health (BIH) Center for Regenerative Therapies (BCRT). Written informed consent was given, and ethics approval was obtained from the local ethics committee/institutional review board (IRB) of the Charité University Hospital. Cells were isolated from metaphyseal bone marrow (BM) or cancellous bone biopsies, respectively, from patients undergoing hip replacement at Charité University Hospital as described.[26,27] Briefly, MSCs were isolated by density gradient centrifugation using Histopaque-1077 (Sigma-Aldrich, St. Louis, MO, USA) and subsequent plastic adherence. Cells were cultured and expanded in Dulbecco's modified Eagle's medium (DMEM Low Glucose; Gibco, Grand Island, NY, USA) with 10% fetal calf serum (Biochrom, Berlin, Germany), 5mM L-alanyl-l-glutamine (Gibco, Grand Island, NY, USA), 100 U/mL penicillin plus 100 µg/mL streptomycin (Biochrom, Berlin, Germany). MSC phenotype and

in vitro differentiation potential was confirmed according the minimal criteria for defining multipotent mesenchymal stem cells of the International Society for Cellular Therapy.[28] To isolate human osteoblasts, cancellous bone specimens from the same patients were extensively washed in PBS and subsequently cut into small pieces with a scalpel. The pieces were transferred into a culture flask and expanded in the same medium used for MSCs for 3 to 4 weeks until reaching approximately 80% confluency. Osteogenic potential of the isolated cells were validated using Alizarin staining and alkaline phosphatase (ALP) activity.[29]

### In vitro osteoclastogenesis

To generate human osteoclasts, peripheral blood was collected and peripheral blood mononuclear cells (PBMCs) were isolated by density gradient centrifugation and later differentiated into active osteoclasts by growth factors. The experiment was done with two independent 30-mL heparinized blood samples from the patient and a healthy donor. The blood sample was split into two parts and each half was diluted by PBS in a 1:2 solution (15 mL peripheral blood + 15 mL PBS). In each 50-mL Falcon tube, 15 mL Biocoll Separating Solution (1077 g/mL; Biochrom, Berlin, Germany) were transferred as the bottom layer and carefully topped with 30 mL blood solution (1:2 dilution with PBS) without mixing the layers. The tubes were centrifuged for 30 min at 400*g* without break at room temperature (RT). The supernatant was removed and the interphase (PBMCs) was harvested and collected in a new Falcon tube. A maximum of 10 mL PBMCs were topped with 40 mL PBS and centrifuged for another 10 min at 300*g*. The supernatant was removed and the PBMC pellet resuspended in 5 mL PBS. The PBMC suspension of each Falcon tube was pooled and filled up to 50 mL. The cell number was determined and the PBMCs were seeded out at density of $3 \times 10^5$ cells per 24-well plate. The cells were resuspended in medium composed of Alpha-MEM (Gibco, Grand Island, NY, USA) + 10% FCS (Lonza, Basel, Switzerland) + 1% Ultraglutamine (Gibco, Grand Island, NY, USA), 1% Penicillin/Streptomycin (Gibco, Grand Island, NY, USA) + 15 ng/mL recombinant human macrophage colony-stimulating factor (rhM-CSF) (R&D Systems, Minneapolis, MN, USA; #216-MCC). The medium was changed every 2 to 3 days. In a 24-well plate, 700 µL was removed and replaced with fresh medium. At day 3, recombinant human RANKL (rhRANKL) (PeproTech, Rocky Hill, NJ, USA; #310-01) was first added to the medium at a concentration of 50 ng/mL. At day 5, the first osteoclasts were detected. At day 14, osteoclast staining was performed.

### Osteoclast staining

In vitro differentiated osteoclasts were fixed at day 14 with 4% paraformaldehyde (PFA) and permeabilized with 0.1% saponin. Osteoclasts were stained for 15 min at RT for tartrate resistant acid phosphatase (TRAP) activity using 0.1 mg/mL Napthol AS-MX phosphate disodium salt (Sigma-Aldrich, Taufkirchen, Germany) and 0.6 mg/mL Fast Red Violet LB Salt (Sigma-Aldrich, Taufkirchen, Germany) in 40mM sodium acetate and 10mM sodium tartrate. Actin in osteoclasts was stained overnight at 4°C with fluorescently-labeled phalloidin (Alexa Fluor 488; Life Technologies, Inc., Grand Island, NY, USA; 1:400) and 4′,6-diamidino-2-phenylindole (DAPI) (Life Technologies, Darmstadt, Germany) was used to stain nuclei (15 min RT, 1 µg/mL). Fluorescence microscopy of stained osteoclasts was performed with an Olympus BX60 microscope (Olympus, Waltham, MA, USA). Two independent experiments were performed, each with three coverslips.

### Resorption assay

At day 6 of osteoclast differentiation, osteoclasts were lifted by incubating the culture with StemPro Accutase (Thermo Fisher Scientific, Waltham, MA, USA) for 10 min at 37°C and then detached with a cell scraper. Osteoclasts were seeded in Alpha-MEM with 10% FBS Superior, 1% Penicillin/Streptomycin, 1% Ultraglutamine, 50 ng/mL rhM-CSF and rhRANKL at a density of $6.7 \times 10^4$/dentine slice in 96-well plates and osteoclast culture on dentine was continued for 5 days. Half of the culture medium was replaced by fresh medium 2 days after osteoclast transfer. At culture termination, the cells were removed from the dentine slices and resorption events were visualized with 0.25% toluidine blue (Sigma-Aldrich). Three independent experiments were performed, each including three dentine slices. For 3D visualization of resorption traces cleaned dentine discs were labeled by incubation with 1% WGA-Texas Red (Life Technologies) in 1% BSA/PBS and imaged using a LSM 700 confocal microscope (Zeiss, Inc., Thornwood, NY, USA) as described.[30]

### RNA isolation

Trizol-based (Life Technologies) RNA isolation of human MSCs (hMSCs), human osteoblasts (hOBs), and human osteoclasts (hOCs) was performed with the Direct-zol RNA kit (Zymo Research, Irvine, CA, USA). Two 25-$cm^2$ wells were lysed for each cell identity. RNA concentration and quality was measured by the NanoDrop system (Thermo Fisher Scientific).

### cDNA sequencing

RNA was reverse transcribed into cDNA with the RevertAid First Strand cDNA Synthesis Kit (Thermo Fisher Scientific, Hennigsdorf, Germany) and *LRRK1* was sequenced with oligonucleotide primers (sequences available upon request) and sequenced on an ABI3730xl DNA Analyzer (Applied Biosystems, Dreieich, Germany).

### Immunoblot analyses

Cultured osteoblasts and MSCs were lysed. Cell lysates (20 µg) were transferred to a NuPAGE 3-8% Tris-Acetate protein gel (Invitrogen, Carlsbad, CA, USA). The Phospho-Ser5-L-plastin antibody (Signalway Antibody, College Park, MD, USA; #12455), the L-plastin Antibody (Abcam, Cambridge, MA, USA; #ab206322), the β-Actin Antibody (13E5) (Cell Signaling Technology, Beverly, MA, USA; #4970) and Cathepsin K antibodies (Abcam, Cambridge, MA, USA ;#ab49893) were used for protein detection. Lysates from two independent osteoclast cultures were analyzed. Although differences in L-plastin phosphorylation are evident, no significance levels were calculated because no blood sample for a third independent experiment was obtained.

### Ethics

This study has been approved by the local ethics committee (EA2/010/19).

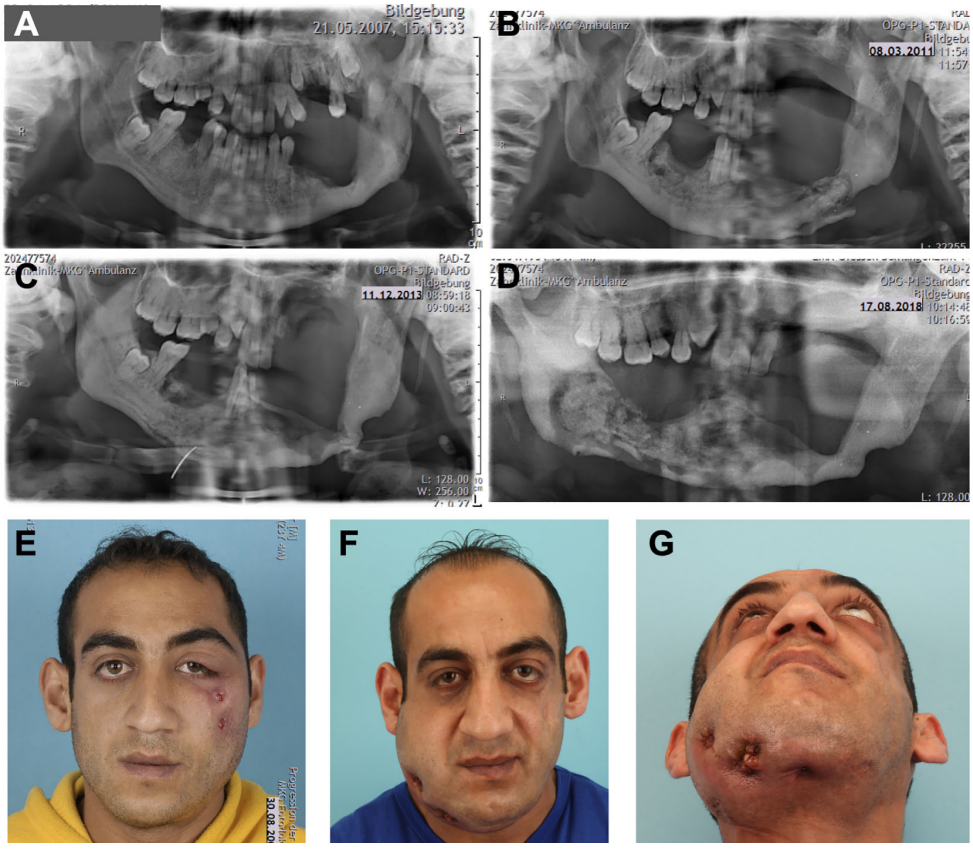


**Fig. 1.** Craniofacial phenotype. (*A–D*) Panoramic X-ray of the jaws. (*A*) Status post teeth removal in left mandible and sclerosing bone transformation. (*B*) After 4 years, loss of teeth in left upper jaw and mandible, pathologic fracture of the left mandible. (*C*) Spontaneous bone healing within two years, after intermittent sequester removal. (*D*). Five years later, progressive bone necrosis and sequester formation of right mandible resulting in loss of all teeth in lower mandible. (*E*) Initial presentation at 23 years of age with infraorbital fistulas due to necrotic maxillary bone. (*F,G*) Presentation at 34 years of age with perimandibular and submandibular fistulas caused by multiple sequestra of the right mandible.

## Results

### Case report

The male patient from a Bulgarian family without known consanguinity first presented in hospital at the age of 23 years with circumscribed necrosis in the premolar region of the right mandible and molar region of the left maxilla (Fig. 1*A–D*; Supporting Information Fig. S1), causing infraorbital fistulas (Fig. 1*E*). Two years prior to presentation, the molars in the left mandible had been removed due to chronic inflammation and pain. Otherwise, his childhood and adolescence were uneventful. Also, the parents and his two siblings have no history of any bone disease or fractures.

The patient's clinical management was performed as follows: the necrotic jaw bone was conservatively removed without jeopardizing the integrity and stability of the mandible, as it is frequently practiced in MRONJ. Despite this conservative treatment regimen, an atraumatic fracture of the left mandible occurred (Fig. 1*B*), which healed up within 2 years after intermittent sequester removal (Fig. 1*C*). Osteosynthesis of the mandibular fracture was deferred due to poor bone quality at the fracture site and limited soft tissue coverage. Between ages 32 and 34 years, the patient developed disintegration and sequester formation on the right side of his mandible. In the context of conservative sequestrectomy, also the remnant teeth of his mandible were removed (Fig. 1*D*). ONJ led to soft tissue infection and fistula formation, initially in the zygomatic prominence (Fig. 1*E*) and years later in the submandibular region (Fig. 1*F,G*). Surgical drainage and antibiotics enabled the local control of the necrotic and infected bone.

Although the course of the osteonecrosis was not unusual for MRONJ there was no history of any medication explaining the pathology. Instead, the patient presented with additional skeletal findings. Kyphoscoliosis (Fig. 2*A,I*) and short stature were noted and radiographs of the spine revealed osteosclerotic sandwich vertebrae with endplate deformities and mild flattening (Fig. 2*A–D*). The diaphyseal cortical bone of the right femur appeared thinned, whereas (Fig. 2*E*) the cortical bone of the left femur was thickened (Fig. 2*F*). The differences in cortical thickness could be due to unloading because there was a history of

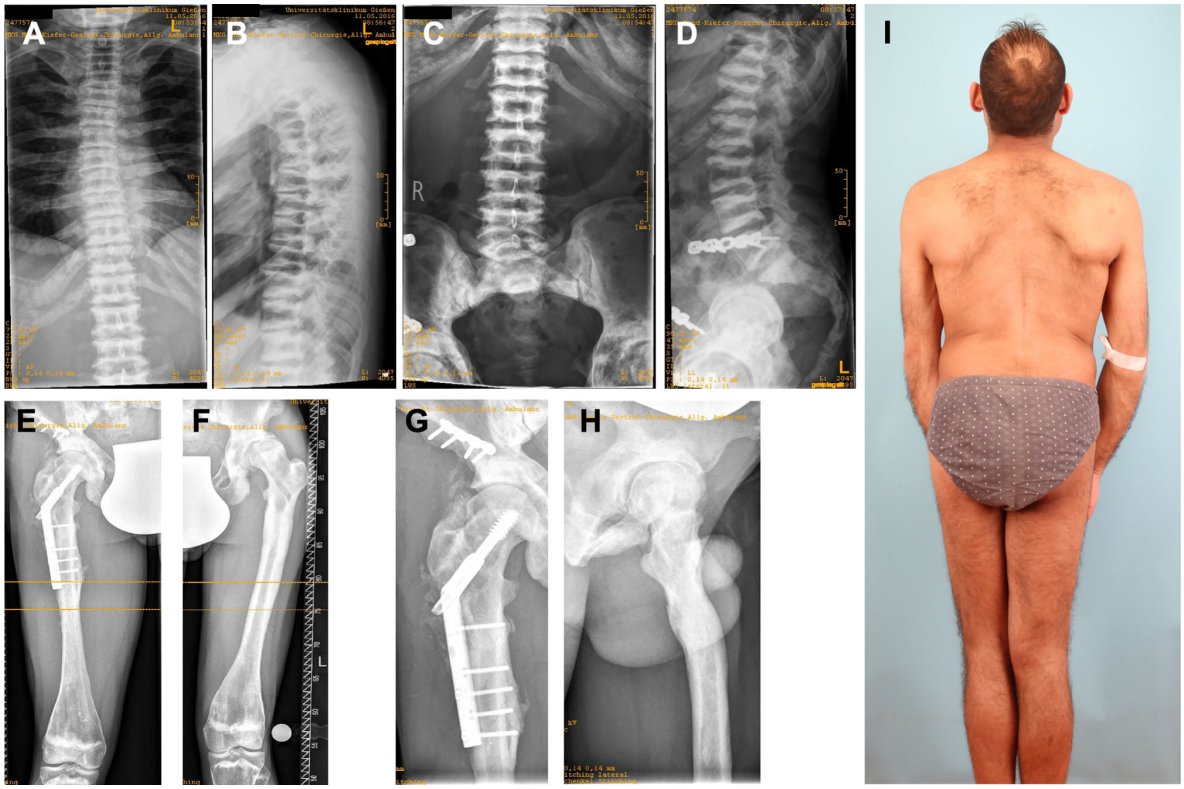


**Fig. 2.** Osteopetrotic changes in the axial and appendicular skeleton. (*A*) Scoliosis of cervical spine with irregular corticospongious appearance of the ribs. (*B*) Kyphosis, sandwich appearance of vertebrae and platyspondyly. (*C*,*D*) Lumbar spine and sacroiliac joint revealing sclerotic sandwich vertebrae. (*E*) Osteosynthetic material after right-sided pathologic femur shaft fracture. (*F*) Diaphyseal thickening and metaphyseal modeling defect of femur. (*G*) Osteosynthesis after pathologic pelvis fracture and (*H*) a modeling defect of proximal femur. (*I*) Full-body picture of patient's back shows kyphoscoliosis and leg asymmetry.

several pathologic fractures (Fig. 2*E*,*F*). At the age of 25 years, he suffered from a right-sided proximal femur shaft fracture and a pelvic fracture without adequate trauma (Fig. 2*E*), and sustained another right-sided femur shaft fracture at the age of 31 years. These fractures were surgically treated (Fig. 2*E*,*G*) and healing was uneventful. The femurs showed modeling defects with metaphyseal widening (Fig. 2*H*). The radiological picture was compatible with the diagnoses of autosomal dominant osteopetrosis type 2 (ADOII) or dysosteosclerosis. His intellectual development is in the normal range. The phenotype is summarized in Table 1 and compared to published patients with *LRRK1* mutations for which sufficient clinical details were available.

## Bone biopsy findings

The histological and histomorphometric analysis of the patient's transiliac bone biopsy was consistent with osteoclast-rich osteopetrosis (Fig. 3). The trabecular bone displayed an osteopetrosis-like increase in trabecular bone mass (Fig. 3*A*). Furthermore, mineralized cartilage remnants were detected throughout the biopsy (Fig. 3*B*). Although few eroded surfaces were seen, there were several multinucleated osteoclasts with a flat shape as well as no visible resorption lacunae both indicating impaired resorption activity (Fig. 3*C*). Bone histomorphometry indicated higher microstructural indices (primarily higher trabecular thickness), normal osteoid levels, and a higher osteoclast surface compared to previously published age-matched reference values (Fig. 3*D*).

Backscattered electron microscopy revealed high matrix mineralization including the presence of hypermineralized cartilage remnants (Fig. 4*A*,*B*), which are similarly found in ADOII. BMDD histograms showed an overall shift toward higher calcium content with a second peak attributable to hypermineralized cartilage remnants (Fig. 4*C*), while overall calcium distribution values such as the mean calcium content (CaMean) and the heterogeneity of the calcium distribution (CaWidth) were comparable to those found in ADOII (Fig. 4*D*,*E*).

## Identification of a *LRRK1* splice site mutation leading to skipping of exon 3

Sanger sequencing of the main osteopetrosis genes *CLCN7* and *TCIRG1* revealed no mutations. In the following, we performed trio exome sequencing, which identified the homozygous variant c.261G>A in the gene *LRRK1* in the patient. Segregation analysis proved the parental transmission; the parents and one sibling carry the mutation in a heterozygous state (Fig. 5*A*). The mutation is not listed in ExAC, gnomAD, or the 1000 Genomes project. The sequence change does not introduce a novel amino

**Table 1.** Clinical Presentation and *LRRK1* Mutations Found in OSMD

| Characteristic | This report | Iida and colleagues[3] | Guo and colleagues[2] | |
|---|---|---|---|---|
| Gender | Male | Male | Male | Female |
| Age today | 34 years | 2 years | 12–14 years | 25 years |
| Ethnicity | Bulgarian | Moroccan | Indian | Indian |
| Consanguinity | No | Yes | No | No |
| Affected siblings | No | ? | Yes | Yes |
| Gene | LRRK1 | LRRK1 | LRRK1 | |
| Mutation | c.261G>A; p.(Ala34Profs*33) | c.5938_5944delGAGTGGT (prolonged protein +29 AA) | c.5917_5972insG; p.(Glu1980Alafs*66) | |
| Zygosity | Homozygous | Homozygous | Homozygous | |
| Clinical manifestations (HPO terms) | | | | |
| Pathologic fractures (HP:0002756) | + | + | + | + |
| Coxa vara (HP:0002812) | + | n.d. | + | n.d. |
| Short stature (HP:0004322) | + | + | – | – |
| Failure to thrive (HP:0001508) | – | + | – | – |
| Mild global developmental delay (HP:0011342) | – | + | – | – |
| Anemia (HP:0001903) | + | n.d. | – | n.d. |
| Hepatomegaly (HP:0002240) | n.d. | – | + | n.d. |
| Facial dysmorphism | + | n.d. | + | – |
| Abnormality of the teeth (HP:0000164) | + | +, hypodontia | +, crowding of teeth | – |
| Recurrent infections (HP:0002719) | + | n.d. | – | – |
| Radiographic findings | | | | |
| Sandwich appearance of vertebral bodies (HP:0004618) | + | + | + | + |
| Flattened vertebrae (HP:0000926) | + | – | – | – |
| Erlenmeyer flask deformity of the femurs (HP:0004975) | + | n.d. | + | n.d. |
| Dense metaphyseal bands (HP:0100959) | + | + | + | + |
| Thickened ribs (HP:0000900) | + | n.d. | + | n.d. |
| Osteosclerosis of the calvaria and base of the skull (HP:0005746) | n.d. | – | + | n.d. |

HPO = Human Phenotype Ontology; n.d. = not determined.

acid, but it affects the last nucleotide of exon 3. Accordingly, Human Splicing Finder (http://www.umd.be/HSF/) predicted an alteration of splicing due to an alteration of an exonic ESE site.[31]

We therefore performed RT-PCR using mRNAs isolated from MSCs, osteoblasts, and osteoclasts from the patient an from healthy controls. Amplification of exons 2 to 6 resulted in a band of 900 bp in controls, but a shortened band of approximately 800 bp in all cells from the patient (Fig. 5*B*). Sanger sequencing of the shortened band revealed a skipping of exon 3 leading to deletion of 164 bases and a frameshift c.98_261del; p.(Ala34Profs*33)(Fig. 5*C*).

### Increased size of *LRRK1*-deficient osteoclasts and superficial bone erosion

In order to better understand the consequences of the identified *LRRK1* mutation, we investigated osteoclasts differentiated from circulating monocytes from the patient and a healthy control individual. Osteoclasts carrying the mutation showed a faster differentiation compared to wild-type osteoclasts resulting in giant osteoclasts, which is in line with the findings in the bone biopsy (Fig. 6*A*; Supporting Fig. 2). When the osteoclasts were seeded on dentine discs, control cells were able to form high numbers of resorption pits (Fig. 6*A*). In contrast, mutated osteoclasts formed broad areas with only superficial bone erosion that can best be visualized by confocal microscopy (Fig. 6*A*). This effect, sometimes called "pseudo-resorption," occurs much more rarely in healthy osteoclasts. This abnormal resorption behavior also becomes obvious when comparing the much lower number and area of resorption pits excavated by *LRRK1*-deficient cells (Fig. 6*B*,*C*) with the total toluidine-stained area indicating any surface roughness (Fig. 6*D*), which is comparable to control osteoclasts.

Because it was reported that LRRK1 phosphorylates L-plastin, we compared levels of total L-plastin levels to L-plastin with Ser5 phosphorylation (Fig. 6*E*). We used this as a readout for LRRK1 function, because the determination of LRRK1 protein levels was impossible due to the lack of antibodies suitable for immunoblotting. *LRRK1* mutated osteoclasts showed normal levels of unphosphorylated L-plastin, but a strong reduction of the phosphorylated form to around 20% (Fig. 6*F*). High cathepsin K levels confirmed otherwise normal osteoclast differentiation.

## Discussion

We describe the fourth known human *LRRK1* mutation in an adult individual with OSMD. Besides pathologic long bone fractures the patient suffered from a severe progressive ONJ starting in the third decade and finally leading to loss of most teeth. We

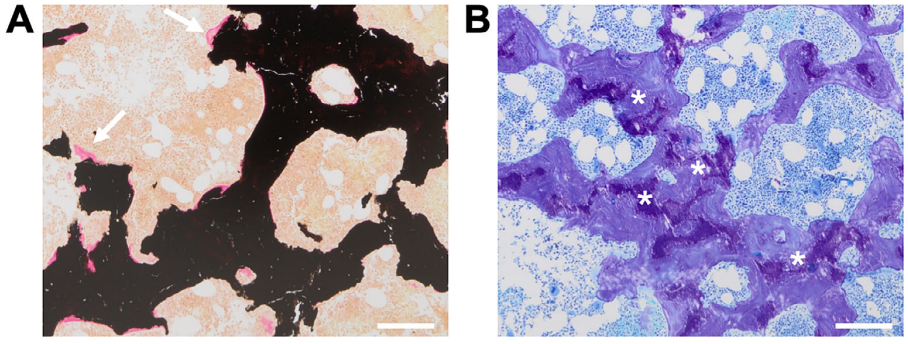


| Parameter | LRRK1 | Ref. |
|---|---|---|
| BV/TV (%) | 32.2 | 21.5±14.8 |
| Tb.Th (µm) | 165.9 | 118.7±81.0 |
| Tb.N (1/mm) | 1.94 | 1.9±0.3 |
| Tb.Sp (µm) | 349.3 | 428.9±101.9 |
| OV/BV (%) | 3.6 | 2.0±1.0 |
| O.Th (µm) | 14.8 | 6.5±2.9 |
| OS/BS (%) | 19.4 | 16.2±6.7 |
| N.Ob/B.Pm (1/mm) | 1.98 | 1.1±1.0 |
| Ob.S/BS (%) | 2.8 | 1.3±1.0 |
| N.Oc/B.Pm (1/mm) | **0.57** | 0.1±0.2 |
| Oc.S/BS (%) | **4.7** | 0.1±0.3 |

**Fig. 3.** Histological characterization of an iliac crest biopsy. (*A*) Von Kossa/van Gieson staining showing a general increase in trabecular bone mass (primarily trabecular thickening) and no increased osteoid indices (white arrows). (*B*) Toluidine staining (overview) with cartilage remnants (asterisks). (*C*) Flat, multinucleated osteoclast (white arrow) and no visible resorption lacuna (ie, eroded surface) indicative of defective bone resorption. (*D*) Bone histomorphometry pointing to increased bone mass, slightly elevated osteoid levels, and a markedly higher osteoclast surface per bone surface compared to previously published age-matched reference values.[16]

confirmed a LRRK1 loss of function and found striking morphological changes in cultured osteoclasts as well as an altered resorption behavior.

To date, four individuals from four different families have been described to carry biallelic mutations in *LRRK1* leading to osteosclerosis. As shown in Table 1, the OSMD patients described so far closely resemble our patient.[2–4] All presented with pathologic and recurrent fractures and osteosclerosis at multiple skeletal sites, predominantly at the metaphyses and vertebral bodies. Different degrees of osteosclerosis of ribs and skull and of Erlenmeyer flask deformity of the femurs were present. The clinical presentation of OSMD is thus highly overlapping with intermediate osteopetrosis due to *CLCN7* mutations or *TCIRG1* splice mutations, ADOII due to *CLCN7* mutations, and dysosteosclerosis due to *CSF1R*, *SLC29A3*, and *TNFRSF11A* mutations.[32–36] It thus seems justified to subsume all these disorders under the term osteopetrosis because they all share impaired osteoclast function as the mechanistic basis.

Our patient is the only one who presented with progressive ONJ with sequester formation causing local infections as frequently seen in MRONJ. The resection of the right-sided mandible was considered but deferred on. In the setting of a slowly progressing destruction of the mandible, no clear resection border could be determined. Commonly practiced microvascular fibula graft reconstruction was deferred on due to the high perceived risk and increased donor site morbidity in a patient suffering from repeated pathologic fractures. Of the different factors triggering ONJ the patient had poor oral hygiene and a history of tooth extraction due to impacted teeth. Dental crowding and persistent primary teeth have been described in OSMD.[2] Another risk factor for ONJ is impaired osteoclast function, which is often secondary to antiresorptive treatment in MRONJ or to hereditary osteopetrosis in ONJ.[13,14] Given its rarity it is difficult to judge whether ONJ is more frequent in OSMD than in other forms of osteopetrosis.

We report the first *LRRK1* mutation affecting splicing. The mutation is placed at the last base pair of exon 3 and causes skipping of the entire exon 3. Although the resulting frameshift is predicted to lead to a premature stop codon we found no evidence for a significant nonsense-mediated mRNA decay (NMD). The other described mutations described are more C-terminal: the homozygous frameshift deletion *LRRK1* c.5938_5944delGAGTGGT leading to a stop-loss and a protein prolonged by 29 amino acids in a 2-year-old Moroccan male, the homozygous insertion *LRRK1* c.5917_5972insG; p.(Glu1980Alafs*66) in Indian siblings, and the p.Glu929* nonsense mutation found in an Iranian patient.[2–4] The phenotypic similarities do not point toward a milder effect of these C-terminal mutations that could lead to a stable truncated protein. Because the large LRRK1 protein is difficult to detect by immunoblot no information is available on the exact consequences of these mutations. Therefore, we opted for a functional readout to test for the function of the protein. As shown by Si and colleagues[8] in murine osteoclasts, our patient shows a reduction of L-plastin Ser5 phosphorylation

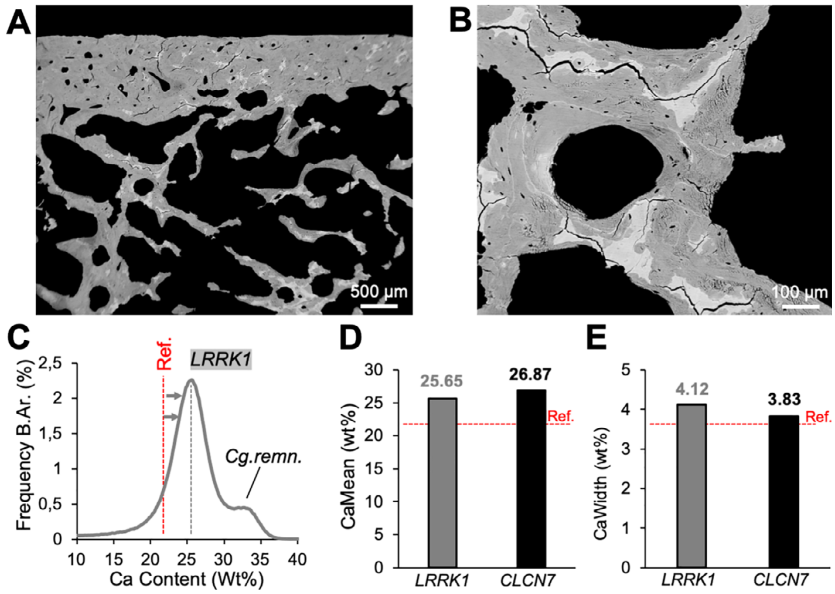


**Fig. 4.** Backscattered electron imaging. (*A*) Biopsy overview indicating hypermineralized areas corresponding to cartilage remnants. (*B*) Confirmation of highly mineralized bone areas at higher magnification. (*C*) BMDD histogram demonstrates overall high matrix mineralization, partly due to cartilage remnants (second peak). (*D*,*E*) CaMean and CaWidth are overall higher compared to reference values[18] and similar to *CLCN7*-related autosomal dominant osteopetrosis type II.[16]

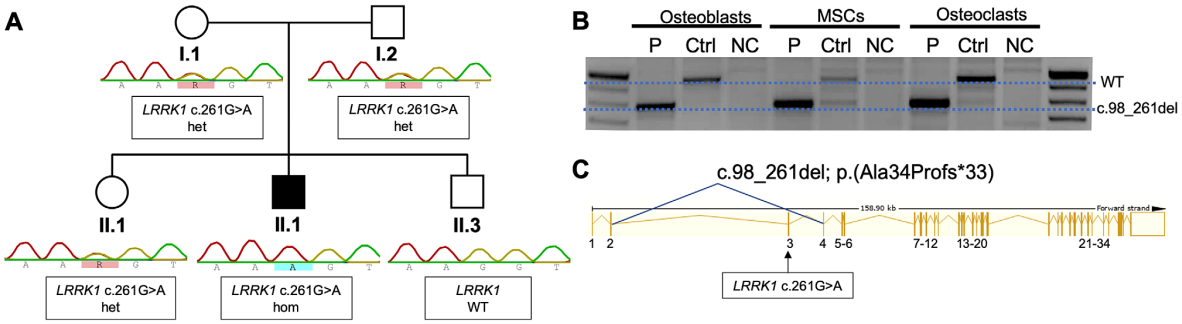


**Fig. 5.** Genetic analysis. (*A*) Segregation of the mutation *LRRK1* c.261G>A by Sanger sequencing. The index (II.1/P2) is affected and carries the mutation in a homozygous state. The clinically unaffected parents carry the mutation in a heterozygous state. (*B*) RT-PCR of exons 2–6 of *LRRK1* in patient-derived osteoblasts, MSCs, and osteoclasts (P) compared to a healthy control (Ctrl) and a negative control (NC). The PCR product of the primer pairs (exon 2–6) yielded a 957-bp product (WT). A smaller band of approximately 800 bp was detected in all cell lines carrying the *LRRK1* splice site mutation indicating abnormal splicing. Sequencing of the lower band showed skipping of exon 3. (*C*) Schematic representation of the *LRRK1* gene showing skipping of exon 3 leading to a frameshift mutation c.98_261del; p.Ala34Profs*33. MSC = mesenchymal stem cell.

in *LRRK1* mutated osteoclasts by around 80% compared to a healthy control.

Iliac crest histology revealed a dense trabecular bone microstructure associated with multinucleated osteoclasts with signs of inadequate bone resorption (ie. flat shape, few eroded surfaces). qBEI pointed to high matrix mineralization, which was partly due to hypermineralized cartilage remnants. Taken together, the micro-morphological pattern is compatible with osteoclast-rich osteopetrosis such as found in ADOII.[16] Interestingly, hypermineralized cartilage remnants indicative of resorption defects were previously also found in gnathodiaphyseal dysplasia.[18] The high abundance of large osteoclasts clearly distinguishes *LRRK1*-related osteopetrosis from the differential diagnosis dysosteosclerosis, which rather is osteoclast-poor.[32,33,37]

Murine osteoclasts lacking *Lrrk1* revealed a reduced resorption pit area, and pits were smaller and shallower compared to knockout (KO) cultures, and only few osteoclasts formed a typical

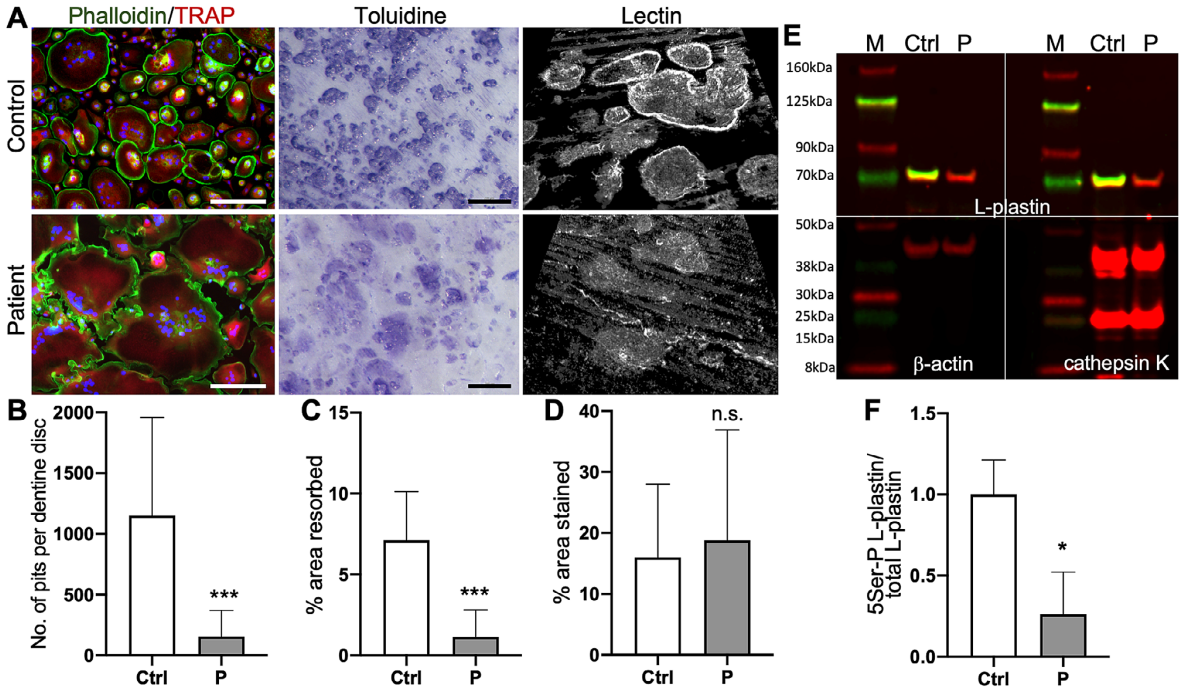


**Fig. 6.** Osteoclast differentiation and functional characterization. (*A*) Fluorescence imaging of osteoclasts, resorption pits stained by toluidine and WGA lectin. Fluorescence images reveal increased size of patient-derived osteoclasts compared to cells from healthy control. Staining: DAPI (blue) for nuclei detection, phalloidin (green), TRAP (red). Scale bar = 200 μm. Toluidine-stained dentine disc from resorption assay reveals almost complete absence of resorption pits, but abundant superficial pseudo-resorption by mutant osteoclasts. Scale bar = 200 μm. WGA lectin–stained resorption pits imaged by confocal microscopy Z-stack. Control cells form deep resorption pits and some superficial erosions, while *LRRK1*-deficient cells mostly produce superficial erosions. (*B–D*) Quantification of resorption assay. (*B*) Number of pits per dentine disc, (*C*) total pit area/dentine area, (*D*) total toluidine-stained area/dentine area. (*E*) Immunoblot of osteoclast lysates from control (Ctrl) and patient (P). Reduced L-plastin Ser5 phosphorylation (green) in patient-derived osteoclasts, but comparable levels of unphosphorylated L-plastin (red). β-Actin was used as an endogenous control. Cathepsin K detection confirmed solid upregulation in patient and control typical for otherwise normally differentiated osteoclasts. (*F*) Quantification of 5Ser-P L-plastin/L-plastin fold-change. All osteoclast experiments were performed three times, representative images are shown. WGA = wheat germ agglutinin.

sealing zone.[3,7] Although osteoclasts from our patient formed broad toluidine-stained eroded areas instead of pits or trenches, we think that this defect is also due to an abnormal sealing zone, which may lead to a leaking of protons and proteases out of the resorption lacuna. However, the increased size of *LRRK1*-mutated osteoclasts cannot readily be explained by a cytoskeletal problem. This could be due to an enhanced migration facilitating fusion of a polykaryon with mononuclear precursors.[38] Interestingly, also osteoclasts from *Clcn7*-deficient mice and a patient with *CLCN7*-related autosomal recessive osteopetrosis have a larger diameter for an unknown reason.[30,39,40]

*Lrrk1*$^{-/-}$ mice were resistant to ovariectomy (OVX)-induced bone loss at the spine, femur, and tibia and showed elevated total bone mass density (BMD) at all three skeletal sites at time of OVX.[7] *LRRK1* has hence been contemplated as a potential target for osteoanabolic therapy.[41] However, only few cases of *LRRK1* mutations in patients are described to date and only little is known about osteoclast pathology in the *LRRK1*-mutated setting. A deeper understanding of the effect *LRRK1* mutations in humans have on osteoclasts is inevitable in the process of considering LRRK1 as a feasible drug target.

## Conclusion

In conclusion, we describe the first patient with OSMD and ONJ caused by a *LRRK1* splice-site mutation. Although the micromorphological analyses conducted pointed to the presence of osteoclast-rich osteopetrosis, our findings may lead to a better understanding of OSMD, the advancement of osteopetrosis, and potentially also osteoporosis treatment. When discussing LRRK1 as a potential drug target for treating low BMD/osteoporosis the possibility of MRONJ as a side effect should be kept in mind.

## Disclosures

The authors report no conflict of interest.

## Acknowledgments

This study was supported by a stipend from the Berlin Institute of Health (BIH) to AH. This project has received funding from the European Community's Seventh Framework Programme under

grant agreement no. 602300 (SYBIL), and the German Federal Ministry of Education and Research (BMBF) within the project "Detection and Individualized Management of Early Onset Osteoporosis (DIMEOS)". We are grateful to the patient and his family members whose cooperation made this study possible.

Authors' roles: Study design: AH, HPH, UK. Study conduct: AH, RO, UK; Data collection: AFH, AH, NS, SB, SG, TR, UR; Data analysis: AFH, AH, AK, JZ, MA, RO, TR, UK, UR; Data interpretation: AH, HPH, TR, UK; Writing manuscript: AFH, AH, HPH, TR, UK; Revising manuscript content: AH, MA, RO, TR, UK; Approving final version of manuscript: AFH, AH, AK, HPH, JZ, MA, NS, RO, SB, SG, TR, UK, UR; The following individuals take responsibility for the integrity of the data analysis: HPH, RO, UK.

The URLs for data presented herein are as follows: Ensembl Genome Browser (http://www.emsembl.org), Mutation Taster (http://www.mutationtaster.org/), Online Mendelian Inheritance in Man (OMIM) (http://www.ncbi.nlm.nih.gov/omim), Human Splicing Finder (http://www.umd.be/HSF3/HSF.shtml); Geneious (https://www.geneious.com/), and The Protein Model Portal (https://www.proteinmodelportal.org).

## References


1. Nishimura G, Kozlowski K. Osteosclerotic metaphyseal dysplasia. Pediatr Radiol. 1993;23(6):450–2.
2. Guo L, Girisha KM, Iida A, et al. Identification of a novel LRRK1 mutation in a family with osteosclerotic metaphyseal dysplasia. J Hum Genet. 2017;62(3):437–41.
3. Iida A, Xing W, Docx MK, et al. Identification of biallelic LRRK1 mutations in osteosclerotic metaphyseal dysplasia and evidence for locus heterogeneity. J Med Genet. 2016;53(8):568–74.
4. Miryounesi M, Nikfar A, Changi-Ashtiani M, et al. A novel homozygous LRRK1 stop gain mutation in a patient suspected with osteosclerotic metaphyseal dysplasia. Ann Hum Genet. 2019;84:102–6.
5. Bosgraaf L, Van Haastert PJ. Roc, a Ras/GTPase domain in complex proteins. Biochim Biophys Acta. 2003;1643(1–3):5–10.
6. Marin I. The Parkinson disease gene LRRK2: evolutionary and structural insights. Mol Biol Evol. 2006;23(12):2423–33.
7. Xing W, Liu J, Cheng S, Vogel P, Mohan S, Brommage R. Targeted disruption of leucine-rich repeat kinase 1 but not leucine-rich repeat kinase 2 in mice causes severe osteopetrosis. J Bone Mineral Res. 2013;28(9):1962–74.
8. Si M, Goodluck H, Zeng C, et al. LRRK1 regulation of actin assembly in osteoclasts involves serine 5 phosphorylation of L-plastin. J Cell Biochem. 2018;119(12):10351–7.
9. Zeng C, Goodluck H, Qin X, Liu B, Mohan S, Xing W. Leucine-rich repeat kinase-1 regulates osteoclast function by modulating RAC1/Cdc42 small GTPase phosphorylation and activation. Am J Physiol Endocrinol Metab. 2016;311(4):E772–80.
10. Edwards BJ, Gounder M, McKoy JM, et al. Pharmacovigilance and reporting oversight in US FDA fast-track process: bisphosphonates and osteonecrosis of the jaw. Lancet Oncol. 2008;9(12):1166–72.
11. Hoff AO, Toth BB, Altundag K, et al. Frequency and risk factors associated with osteonecrosis of the jaw in cancer patients treated with intravenous bisphosphonates. J Bone Mineral Res. 2008;23(6):826–36.
12. Zervas K, Verrou E, Teleioudis Z, et al. Incidence, risk factors and management of osteonecrosis of the jaw in patients with multiple myeloma: a single-centre experience in 303 patients. Br J Haematol. 2006;134(6):620–3.
13. Infante-Cossio P, Gonzalez-Perez LM, Martinez-de-Fuentes R, Infante-Cossio M, Castano-Seiquer A, Jimenez-Castellanos E. Maxillomandibular osteomyelitis associated with osteopetrosis. J Craniofac Surg. 2014;25(1):e79–82.
14. Khullar SM, Tvedt D, Chapman K, Herlofson BB. Sixty cases of extreme osteonecrosis and osteomyelitis of the mandible and maxilla in a West African population. Int J Oral Maxillofac Surg. 2012;41(8):978–85.
15. Dempster DW, Compston JE, Drezner MK, et al. Standardized nomenclature, symbols, and units for bone histomorphometry: a 2012 update of the report of the ASBMR Histomorphometry Nomenclature Committee. J Bone Miner Res. 2013;28(1):2–17.
16. Butscheidt S, Rolvien T, Kornak U, et al. Clinical significance of DXA and HR-pQCT in autosomal dominant osteopetrosis (ADO II). Calcif Tissue Int. 2018;102(1):41–52.
17. Koehne T, Vettorazzi E, Kusters N, et al. Trends in trabecular architecture and bone mineral density distribution in 152 individuals aged 30-90 years. Bone. 2014;66:31–8.
18. Rolvien T, Koehne T, Kornak U, et al. A novel ANO5 mutation causing gnathodiaphyseal dysplasia with high bone turnover osteosclerosis. J Bone Miner Res. 2017;32(2):277–84.
19. Li H, Durbin R. Fast and accurate short read alignment with Burrows-Wheeler transform. Bioinformatics. 2009;25(14):1754–60.
20. McKenna A, Hanna M, Banks E, et al. The Genome Analysis Toolkit: a MapReduce framework for analyzing next-generation DNA sequencing data. Genome Res. 2010;20(9):1297–303.
21. Heinrich V, Kamphans T, Stange J, et al. Estimating exome genotyping accuracy by comparing to data from large scale sequencing projects. Genome Med. 2013;5(7):69.
22. Wang K, Li M, Hakonarson H. ANNOVAR: functional annotation of genetic variants from high-throughput sequencing data. Nucleic Acids Res. 2010;38(16):e164.
23. Kamphans T, Krawitz PM. GeneTalk: an expert exchange platform for assessing rare sequence variants in personal genomes. Bioinformatics. 2012;28(19):2515–6.
24. Schwarz JM, Cooper DN, Schuelke M, Seelow D. MutationTaster2: mutation prediction for the deep-sequencing age. Nat Methods. 2014;11(4):361–2.
25. Lek M, Karczewski KJ, Minikel EV, et al. Analysis of protein-coding genetic variation in 60,706 humans. Nature. 2016;536(7616):285–91.
26. Reinke S, Dienelt A, Blankenstein A, Duda GN, Geissler S. Qualifying stem cell sources: how to overcome potential pitfalls in regenerative medicine? J Tissue Eng Regen Med. 2016;10(1):3–10.
27. Schoon J, Geissler S, Traeger J, et al. Multi-elemental nanoparticle exposure after tantalum component failure in hip arthroplasty: in-depth analysis of a single case. Nanomedicine. 2017;13(8):2415–23.
28. Dominici M, Le Blanc K, Mueller I, et al. Minimal criteria for defining multipotent mesenchymal stem cells. The International Society for Cellular Therapy position statement. Cytotherapy. 2006;8(4):315–7.
29. Geissler S, Textor M, Schmidt-Bleek K, et al. In serum veritas-in serum sanitas? Cell non-autonomous aging compromises differentiation and survival of mesenchymal stem cells via the oxidative stress pathway. Cell Death Dis. 2013;4:e970.
30. Supanchart C, Wartosch L, Schlack C, et al. ClC-7 expression levels critically regulate bone turnover, but not gastric acid secretion. Bone. 2013;58:92–102.
31. Desmet FO, Hamroun D, Lalande M, Collod-Beroud G, Claustres M, Beroud C. Human Splicing Finder: an online bioinformatics tool to predict splicing signals. Nucleic Acids Res. 2009;37(9):e67.
32. Guo L, Bertola DR, Takanohashi A, et al. Bi-allelic CSF1R mutations cause skeletal dysplasia of dysosteosclerosis-Pyle disease spectrum and degenerative encephalopathy with brain malformation. Am J Hum Genet. 2019;104(5):925–35.
33. Guo L, Elcioglu NH, Karalar OK, et al. Dysosteosclerosis is also caused by TNFRSF11A mutation. J Hum Genet. 2018;63(6):769–74.
34. Howaldt A, Nampoothiri S, Quell LM, et al. Sclerosing bone dysplasias with hallmarks of dysosteosclerosis in four patients carrying mutations in SLC29A3 and TCIRG1. Bone. 2019;120:495–503.
35. Sobacchi C, Schulz A, Coxon FP, Villa A, Helfrich MH. Osteopetrosis: genetics, treatment and new insights into osteoclast function. Nat Rev Endocrinol. 2013;9(9):522–36.
36. Sobacchi C, Pangrazio A, Lopez AG, et al. As little as needed: the extraordinary case of a mild recessive osteopetrosis owing to a novel splicing hypomorphic mutation in the TCIRG1 gene. J Bone Miner Res. 2014;29(7):1646–50.

37. Whyte MP, Wenkert D, McAlister WH, et al. Dysosteosclerosis presents as an "osteoclast-poor" form of osteopetrosis: comprehensive investigation of a 3-year-old girl and literature review. J Bone Mineral Res. 2010;25(11):2527–39.

38. Soe K, Hobolt-Pedersen AS, Delaisse JM. The elementary fusion modalities of osteoclasts. Bone. 2015;73:181–9.

39. Weinert S, Jabs S, Supanchart C, et al. Lysosomal pathology and osteopetrosis upon loss of H+-driven lysosomal Cl– accumulation. Science. 2010;328(5984):1401–3.

40. Kantaputra PN, Thawanaphong S, Issarangporn W, et al. Long-term survival in infantile malignant autosomal recessive osteopetrosis secondary to homozygous p.Arg526Gln mutation in CLCN7. Am J Med Genet A. 2012;158A(4):909–16.

41. Si M, Zeng C, Goodluck H, Shen S, Mohan S, Xing W. A small molecular inhibitor of LRRK1 identified by homology modeling and virtual screening suppresses osteoclast function, but not osteoclast differentiation, in vitro. Aging. 2019; 11(10):3250–61.

## Supporting Data

### Supp. Fig. 1

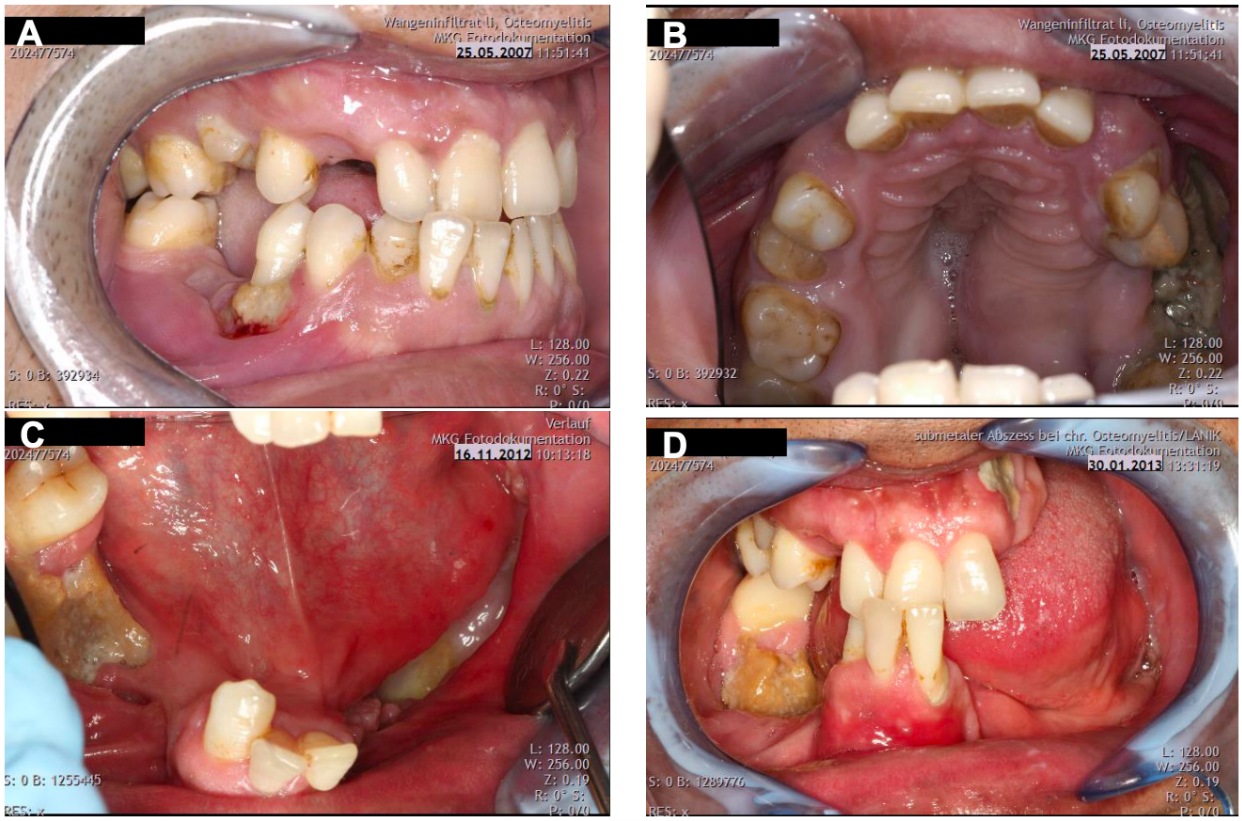


### Supp. Fig. 2

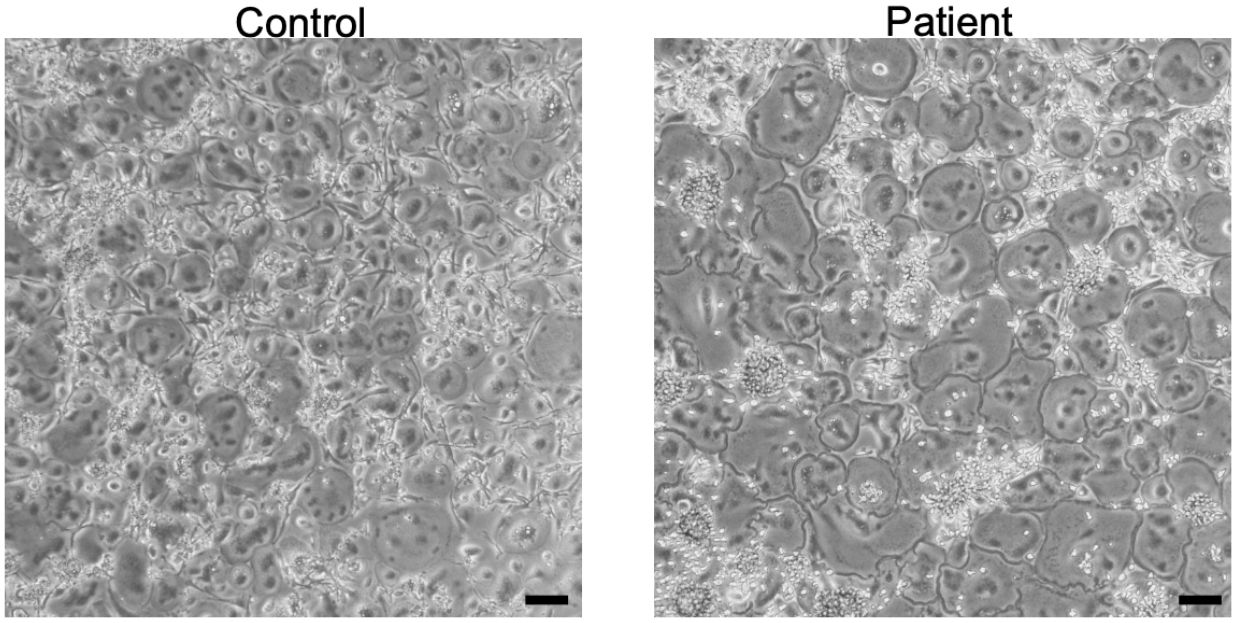

# 13 Curriculum Vitae

Mein Lebenslauf wird aus datenschutzrechtlichen Gründen in der elektronischen Version meiner Arbeit nicht veröffentlicht.

# 14 Publikationsliste

**Publikationen**

***H-index: 1, Zitate insgesamt: 3***

1. Howaldt, A., S. Nampoothiri, L.M. Quell, A. Ozden, B. Fischer-Zirnsak, C. Collet, M.C. de Vernejoul, H. Doneray, H. Kayserili, and U. Kornak, *Sclerosing bone dysplasias with hallmarks of dysosteosclerosis in four patients carrying mutations in SLC29A3 and TCIRG1.* Bone, 2019. 120: p. 495-503. **(Impact factor 2019: 4.31)**
2. Howaldt, A., S. Nampoothiri, D. Yesodharan, S. Udayakumaran, P. Subash, and U. Kornak, *Four novel mutations in EFNB1 in Indian patients with craniofrontonasal syndrome.*, J Hum Genet, 2019. 64(9): p. 867-873. **(Impact factor 2019: 3.46)**
3. Howaldt, A., A.F. Hennig, T. Rolvien, U. Rössler, N. Stelzer, A. Knaus, S. Böttger, J. Zustin, S. Geißler, R. Oheim, M. Amling, H.P. Howaldt, and U. Kornak, *Adult Osteosclerotic Metaphyseal Dysplasia With Progressive Osteonecrosis of the Jaws and Abnormal Bone Resorption Pattern Due to a LRRK1 Splice Site Mutation*. J Bone Miner Res, 2020. 35(7): p. 1322-1332. **(Impact factor 2019: 5.46)**

**Kongresspräsentationen**

1. Howaldt A, Knaus A, Nampoothiri S, Fischer-Zirnsak B, Kornak U, "Compound heterozygous mutation in TCIRG1 causes an intermediate type of autosomal recessive osteopetrosis (ARO)", *European Students Conference,* Berlin, Posterpräsentation, September 2015.
2. Howaldt A, Hennig AF, Rolvien T, Stelzer N, Knaus A, Böttger S, Zustin J, Oheim R, Amling M, Geißler S, Howaldt HP, Kornak U, "Osteopetrosis leading to subtotal loss of the viscerocranial bones", 18th Congress of the International Society of Craniofacial Surgery, Paris, Posterpräsentation, September 2019.
3. Howaldt A, Hennig AF, Rolvien T, Stelzer N, Knaus A, Böttger S, Zustin J, Oheim R, Amling M, Geißler S, Howaldt HP, Kornak U, "Adult osteopetrosis with osteonecrosis of the jaws and abnormal osteoclast resorption due to a LRRK1 splice site mutation", European Human Genetics Virtual Conference (ESHG 2020.2), Posterpräsentation, Juni 2020.
4. Howaldt A, Hennig AF, Rolvien T, Stelzer N, Knaus A, Böttger S, Zustin J, Oheim R, Amling M, Geißler S, Howaldt HP, Kornak U, "Adult osteopetrosis with osteonecrosis of the jaws and abnormal osteoclast resorption due to a LRRK1 splice site mutation", 47th annual meeting of the European Calcified Tissue Society (ECTS 2020 Digital), Posterpräsentation, October 2020.

# 15 Danksagung

Mein außerordentlicher Dank gilt Herrn Prof. Uwe Kornak für die Möglichkeit, diese Arbeit am Institut für Medizinische Genetik und Humangenetik der Charité Universitätsmedizin Berlin durchführen zu können. Für die Betreuung dieser Arbeit, das Überlassen des Themas, die konstruktiven Treffen und das immer offene Ohr möchte ich ihm meinen besonderen Dank aussprechen. Ich bin ganz besonders dankbar für alles, was ich in der Zeit der Promotion bei ihm und vom ihm lernen durfte.

Weiterhin möchte ich mich bei Herrn Dr. Björn Fischer-Zirnsak bedanken, von dem ich etliche Methoden der Humangenetik habe lernen können. Insbesondere das Anlernen der Arbeit in der Zellkultur, die Kultur von embryonalen Mausstammzellen, das Präpieren von Mäusen, die Anfertigung von Western Blot, die Färbung von Osteoklasten und deren Auswertung mittels Immunfluoreszenzmikroskopie sowie die Auswertung von NGS Daten konnte er mir vermitteln. Seine offene, konstruktive Art erlaubte es mir, immerfort Fragen zu stellen und dazuzulernen.

Darüber hinaus möchte ich mich besonders bei meinen Kolleginnen und Co-Autorinnen Frau Uta Rösler und Frau Anna Floriane Hennig bedanken für das Anlernen von Methoden und die dauerhafte und intensive Hilfsbereitschaft im Labor. Ihre Unterstützung bei der Generierung von Daten waren unerlässlich für die hier besprochene Publikation in JBMR. Frau Nina Stelzer möchte ich danken für ihre Unterstützung bei der Generierung von Daten und ihre zuverlässliche Arbeit, welche ebenfalls für die in JBMR publizierte Arbeit besonders wichtig war. Frau Anja Lekaj danke ich herzlichst für die gute Zusammenarbeit im Labor und ihre fortlaufende Unterstützung.

Ein herzlicher Dank gilt auch Herrn Dr. Alexej Knaus, Postdoc am Institut für Genomische Statistik und Bioinformatik der Universität Bonn und Co-Autor eines Papers. Von seinem Wissen in Sachen Bioinformatik konnte ich ab dem ersten Tag meiner Arbeit im Institut profitieren, Tipps und Tricks lernen und mich auch im Laufe der Jahre immer wieder mit ihm austauschen. Sein Beitrag für das hier zitierte JBMR Paper war unerlässlich für den Erfolg der Arbeit.

Den Patient*innen möchte ich danken für das Überlassen der Daten und ihr Einverständnis zur Publikation selbiger.

Ganz besonders möchte ich meinen Eltern danken für ihre unermüdliche Unterstützung in der Zeit der Promotion, meines Studiums und darüber hinaus. Unser Zusammenhalt konnte mich immer stärken.